(2)

NAVAL POSTGRADUATE SCHOOL
Monterey, California

THESIS

THE INFLUENCE OF TEMPERATURE AND COMPOSITION ON THE ACTIVATON ENERGY FOR CREEP IN BINARY ALUMINUM LITHIUM ALLOYS

by

Robert Leonard Seaton

December, 1990

Thesis Advisor: Terry R. McNelley
Co-Advisor: Peter N. Kalu

Unclassified
SECURITY CLASSIFICATION OF THIS PAGE

REPORT DOCUMENTATION PAGE

Form Approved
OMB No. 0704-0188

1a REPORT SECURITY CLASSIFICATION: Unclassified	1b RESTRICTIVE MARKINGS
2a SECURITY CLASSIFICATION AUTHORITY	3 DISTRIBUTION / AVAILABILITY OF REPORT: Approved for public release; distribution is unlimited
2b DECLASSIFICATION / DOWNGRADING SCHEDULE	
4 PERFORMING ORGANIZATION REPORT NUMBER(S)	5 MONITORING ORGANIZATION REPORT NUMBER(S)
6a NAME OF PERFORMING ORGANIZATION: Naval Postgraduate School; 6b OFFICE SYMBOL (If applicable): 34	7a NAME OF MONITORING ORGANIZATION: Naval Postgraduate School
6c ADDRESS (City, State, and ZIP Code): Monterey, CA 93943-5000	7b ADDRESS (City, State, and ZIP Code): Monterey, CA 93943-5000
8a NAME OF FUNDING / SPONSORING ORGANIZATION; 8b OFFICE SYMBOL (If applicable)	9 PROCUREMENT INSTRUMENT IDENTIFICATION NUMBER
8c ADDRESS (City, State, and ZIP Code)	10 SOURCE OF FUNDING NUMBERS: PROGRAM ELEMENT NO; PROJECT NO; TASK NO; WORK UNIT ACCESSION NO

11 TITLE (Include Security Classification)
THE INFLUENCE OF TEMPERATURE AND COMPOSITION ON THE ACTIVATION ENERGY FOR CREEP IN BINARY ALUMINUM LITHIUM ALLOYS

12 PERSONAL AUTHOR(S)
Robert L. Seaton

13a TYPE OF REPORT	13b TIME COVERED	14 DATE OF REPORT (Year, Month, Day)	15 PAGE COUNT
Master's Thesis	FROM _____ TO _____	1990, December, 20	98

16 SUPPLEMENTARY NOTATION The views expressed in this thesis are those of the author and do not reflect the offical policy or position of the Department of Defense or the U.S. Government

17 COSATI CODES		
FIELD	GROUP	SUB-GROUP

18 SUBJECT TERMS (Continue on reverse if necessary and identify by block number)
temperature, composition, activation energy, creep binary aluminum lithium alloys

19 ABSTRACT (Continue on reverse if necessary and identify by block number)

An investigation was conducted to determine the temperature and composition dependence on the activation energy for creep of Al-0.5wt.pct.Li, Al-1.0wt.pct.Li, and Al-2.0wt.pct.Li alloys. A series of isothermal tests was conducted to extend previous data. Temperature cycling measurements were conducted utilizing constant true stress creep tests, with nominal temperatures ranging from 300°C to 500°C. Temperature cycling tests involved a range of 10°C for each test. Experimental results indicate all three alloys behave as a class II alloy (pure metal class) with a stress exponent, n, approximately equal to 5. In addition, subgrain formation was observed in association with the primary stage of creep. The activation energy for creep of the Al-0.5wt.pct.Li and Al-1.0wt.pct.Li alloys was observed to be essentially the same as that for pure Aluminum.

20 DISTRIBUTION / AVAILABILITY OF ABSTRACT: ☒ UNCLASSIFIED/UNLIMITED ☐ SAME AS RPT ☐ DTIC USERS	21 ABSTRACT SECURITY CLASSIFICATION: Unclassified
22a NAME OF RESPONSIBLE INDIVIDUAL: Terry R. McNelley	22b TELEPHONE (Include Area Code): (408) 646-2586; 22c OFFICE SYMBOL: ME/MC

DD Form 1473, JUN 86 *Previous editions are obsolete.* SECURITY CLASSIFICATION OF THIS PAGE

S/N 0102-LF-014-6603 Unclassified

Approved for public release; distribution is unlimited.

The Influence of Temperature and Composition on the Activation Energy for Creep in Binary Aluminum Lithium Alloys

by

Robert L. Seaton
Lieutenant Commander, United States Navy
B.A., Potsdam College, 1976
M.B.A., Duke University, 1983

Submitted in partial fulfillment
of the requirements for the degree of

MASTER OF SCIENCE IN MECHANICAL ENGINEERING

from the

NAVAL POSTGRADUATE SCHOOL
December 1990

Author: _____
Robert L. Seaton

Approved by: _____
Terry R. McNelley

Co-Advisor: _____
Peter N. Kalu

_____
Anthony J. Healey, Chairman
Department of Mechanical Engineering

ABSTRACT

An investigation was conducted to determine the temperature and composition dependence on the activation energy for creep of Al-0.5wt.pct.Li, Al-1.0wt.pct.Li, and Al-2.0wt.pct.Li alloys. A series of isothermal tests was conducted to extend previous data. Temperature cycling measurements were conducted utilizing constant true stress creep tests, with nominal temperatures ranging from 300°C to 500°C. Temperature cycling tests involved a range of 10°C for each test. Experimental results indicate all three alloys behave as a class II alloy (pure metal class) with a stress exponent, n, approximately equal to 5. In addition, subgrain formation was observed in association with the primary stage of creep. The activation energy for creep of the Al-0.5wt.pct.Li and Al-1.0wt.pct.Li alloys was observed to be essentially the same as that for pure Aluminum.

TABLE OF CONTENTS

I. INTRODUCTION 1

II. BACKGROUND 3

A. THE STRUCTURE OF THE AL-LI SYSTEM 3

B. CREEP AND CREEP MECHANISMS 4

1. The Dependence of Creep on Temperature . . . 5

2. Dependence of Creep on Stress 6

3. Solid Solutions and Creep Rate 7

4. Previous Work at NPS 8

III. EXPERIMENTAL PROCEDURE 10

A. MATERIAL PROCESSING AND FABRICATION 10

B. CREEP TESTING 11

1. Creep Testing Apparatus 11

2. Cam Calibration 15

3. Software used for Constant Stress Tests . . 17

4. Constant Temperature Testing 17

5. Temperature Cycling Tests 20

6. Optical Microscopy 20

IV. RESULTS AND DISCUSSION 22

A. INITIAL MICROSTRUCTURE 22

B. CONSTANT STRESS, ISOTHERMAL TESTS 22

1. Strain-Rate Dependence of Stress 23

2. Strength Dependence on Lithium Concentration 27

3. Microstructural Evolution During Creep . . . 31

C. TEMPERATURE CYCLING TESTS 36
1. Activation Energy 37
D. DISCUSSION 46

V. CONCLUSIONS 48

APPENDIX A. CREEP AND CREEP RATE CURVES FOR Al-0.5%Li . 49

APPENDIX B. CREEP AND CREEP RATE CURVES FOR Al-1.0%Li . 68

APPENDIX C. CREEP AND CREEP RATE CURVES FOR Al-2.0%Li . 83

APPENDIX D. DATA FROM PREVIOUS WORK AT NPS 87

LIST OF REFERENCES 89

INITIAL DISTRIBUTION LIST 91

I. INTRODUCTION

With the fast pace of technology in the aerospace industry today there are ever increasing demands for higher strength and stiffness in structural materials but with reduced weight and improved formability. Aluminum alloys have been widely used in the construction of aerospace vehicles for many years because of their high strength to weight ratio, forming characteristics and corrosion resistance. It should be kept in mind that the specific application determines selection of the particular strength- or stiffness-to-weight ratio that should be utilized. For structures in uniaxial tension a ratio of E/ρ should be maximized for best design. Here E is Young's modulus and ρ is the density. Those structures to be loaded in bending should utilize a ratio of $E^{1/2}/\rho$ and in design of plates subjected to distributed loads, a ratio of $E^{1/3}/\rho$ is best [Ref. 1].

Each weight percent Lithium added to aluminum reduces the density, ρ, of the alloy by approximately three percent and increases the elastic modulus, E, by six percent. Lithium is the only potential alloy addition to Aluminum that affects The density and modulus in such a manner [Ref. 2]. Thus Lithium additions to Aluminum provide improvements in both modulus and density for a wide range of potential applications and therefore provide attractive benefits to designers. However, without other alloying elements such as Copper or Magnesium, Al-Li alloys exhibit poor fracture toughness.

Due to the positive effects of Lithium addition to Aluminum there is currently substantial research and development of Al-Li alloys in progress for service at ambient

temperatures. However, Al-Li alloys are not viewed as high temperature materials there is presently no accepted limit on the operating temperatures for these alloys. Many components in today's aerospace vehicles must withstand elevated temperatures while maintaining good strength properties.

The determination of acceptable operating temperatures for Al-Li alloys will require understanding of the essential role of Lithium in Aluminum at elevated temperatures. The purpose of this research is to expand the current data on Al-0.5wt.pct.Li, Al-1.0wt.pct.Li and Al-2.0wt.pct.Li alloys in the 300-500°C range. A series of constant stress creep tests between 300-500°C was conducted to determine the stress and temperature dependence of creep in the three Al-Li alloys described above. An additional series of constant stress temperature cycling tests was used to evaluate the temperature dependence through activation energy in the same temperature range.

II. BACKGROUND

A. THE STRUCTURE OF THE AL-LI SYSTEM

The Al-Li equilibrium phase diagram pictured in Figure 1 is that developed by McAlister and published in 1982.[Ref. 3] The solid solubility of Lithium in Aluminum is less than 0.5 weight percent at ambient temperature, 1.5 weight percent at 300°C and reaches a maximum of 4.2 weight percent at 600°C.

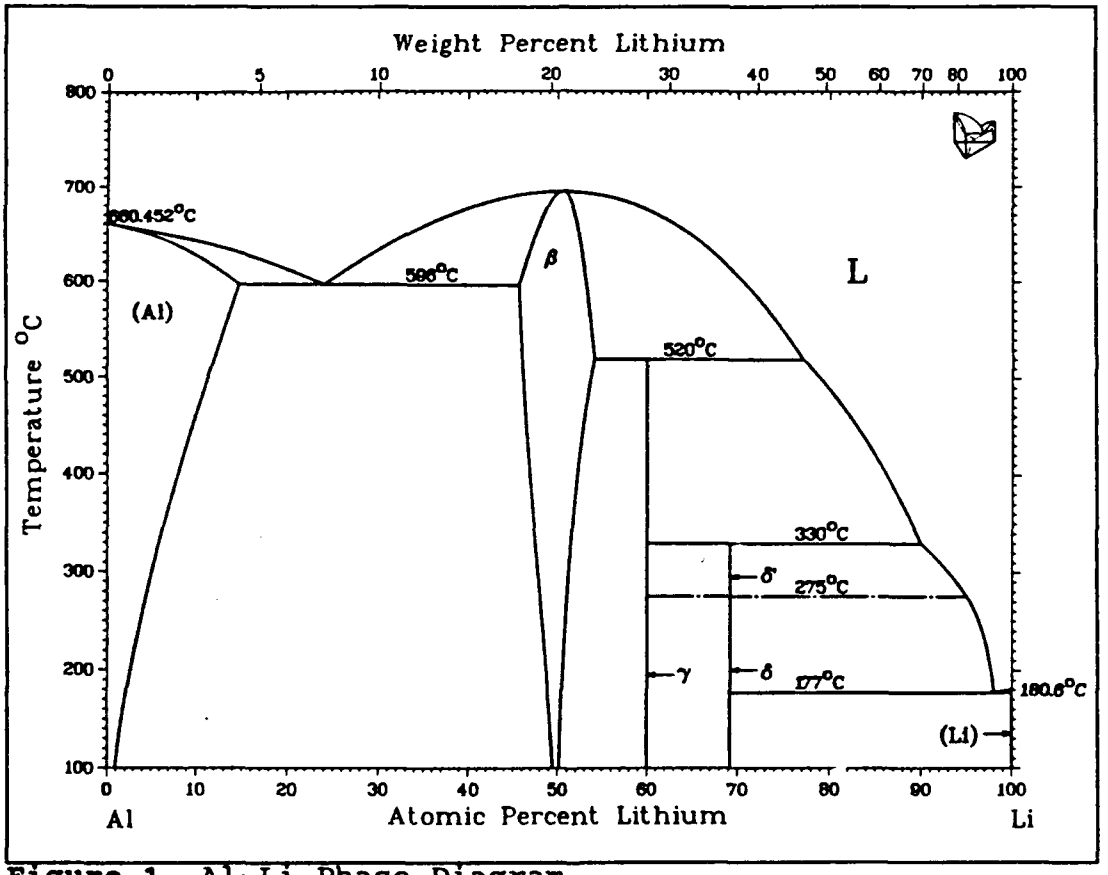

Figure 1. Al-Li Phase Diagram.

Again, the major focus of this research is the Al-0.5wt.pct.Li and Al-1.0wt.pct.Li in the 300-500°C range. Both of these alloys are within the solid solution region of the phase diagram and thus should not be influenced by precipitation.

The increase in the ambient temperature elastic modulus due to the addition of Lithium has been studied by Fox and Fisher [Ref. 4] in alloys containing between 1.33 and 2.14 weight percent Lithium. The addition of Lithium results in an increase in the electron charge density between nearest neighbor Aluminum and Lithium atoms. This increase in the electron charge density results in an increased force between atoms and an increase in the modulus of elasticity.

Radmilovic, Fox, and Thomas [Ref. 5] have shown that ordered δ' Al_3-Li precipitates develop within the disordered matrix in Al-Li alloys due to spinodal decomposition of the solid solution. This spinodal reaction occurs by increasing the Lithium content of Lithium enriched regions in the alloy. These Lithium enriched regions are ordered and apparently exist at temperatures above the δ' (and δ) solvus temperatures. The existence of this ordering phenomenon explains why it is so difficult to suppress the formation of δ' precipitates in alloys containing greater than 1.6 weight percent Lithium. Both the increase in the modulus of elasticity and the presence of ordering in the solid solution are indications that Aluminum and Lithium atoms will tend to bond.

The modulus of elasticity and the stacking fault energy are two factors that are known to exert an influence on the creep of metals and alloys and thus one could expect the creep response of Al-Li alloys to reflect these factors [Ref. 6]

B. CREEP AND CREEP MECHANISMS

Creep is the inelastic, time-dependent response of a material. At elevated temperatures creep imposes limits on stress and lifetimes of engineering components. Subjected to

a constant tensile load, a mechanical component will elongate from creep. Under constant load, the decrease in area results in an increase in stress and failure occurs following the initiation of necking. The temperature regime particularly important for creep is $0.5T_m<T<T_m$, the range in which diffusion is an important factor [Ref. 7]

1. The Dependence of Creep on Temperature

At sufficiently high temperatures atom mobility may be high enough to permit diffusion-controlled dislocation movement to be the rate controlling process. If the creep process is dependent upon dislocation climb then we would expect that the steady state creep rate would be proportional to the diffusion coefficient of atoms:

$$\dot{\epsilon} \alpha D \qquad (1)$$

and there currently exists ample evidence for the correlation between $\dot{\epsilon}$ and D. Since the creep rate is proportional to the diffusion coefficient one would expect that the activation energy for creep of pure metals should be about equal to the activation energy for self diffusion.[Ref. 6]

This suggests that the creep rate can be described by an Arrhenius type of equation:

$$\dot{\epsilon} \alpha \exp\left(-\frac{Q_c}{RT}\right) \qquad (2)$$

where Q_c is the activation energy for creep, R is the gas constant and T is the absolute temperature. The activation energy for creep, Q_c, can be calculated if the creep rate is known at two temperatures:

where T_1 and T_2 are the absolute temperatures at which creep rates $\dot{\epsilon}_1$ and $\dot{\epsilon}_2$ were determined.[Ref. 6] Again , if diffusion

$$Q_c = -R \frac{\ln\left(\frac{\dot{\epsilon}_1}{\dot{\epsilon}_2}\right)}{\left(\frac{1}{T_2} - \frac{1}{T_1}\right)} \quad (3)$$

is the sole temperature dependent process involved then it is expected that $Q_c = Q_D$

2. Dependence of Creep on Stress

Creep is also stress dependent. Sherby and Burke [Ref. 6], have demonstrated that:

$$\dot{\epsilon} \alpha D f(\sigma) \quad (4)$$

thus:

$$\frac{\dot{\epsilon}}{D} \alpha f(\sigma) \quad (5)$$

and several regimes have been identified.

Sherby and Burke [Ref. 6] have determined that there are three ranges with three different relationships between the steady state creep rate and the stress. In the low stress range (I), at constant temperature, where ϵ/D is around 10^2 cm^{-2} the creep rate follows:

$$\dot{\epsilon} \alpha \sigma^1 \quad (6)$$

In the intermediate range (II), at constant temperature with ϵ/D between 10^2 and 10^9 cm^{-2} the creep rate follows:

$$\dot{\epsilon} \alpha \sigma^n \quad (7)$$

with n being approximately 5 for pure metals. In range III, at constant temperature with creep rates above 10^9 cm^{-2} the creep rate is:

$$\dot{\epsilon} \alpha e^{B\sigma} \tag{8}$$

Different types of mechanical behavior are observed in the three ranges and since creep can occur by any one of several independent processes the fastest process will usually be the rate controlling one.[Ref. 6]

3. Solid Solutions and Creep Rate

Sherby and Burke [Ref. 6] have also noted that solid solution alloys with $\dot{\epsilon}/d$ between 10^2 and 10^9 cm^{-2}, can be divided into two classes (I and II). Class I alloys follow the microcreep law:

$$\dot{\epsilon} = BD_s\left(\frac{\sigma}{E}\right)^3 \tag{9}$$

where $\dot{\epsilon}$ is the strain rate, D_s the diffusion coefficient of the solute, σ the stress, E the modulus of elasticity and B a physical constant. This theory is based on dislocation glide where the rate is determined by the velocity which solute atoms can be dragged along with a moving dislocation line. These class I alloys often do not exhibit a primary creep stage which limits the effect of subgrain formation and stacking fault energy on the creep rate.

Class II alloys follow a dislocation climb law of the form:

$$\dot{\epsilon} = AD_l\gamma^3\left(\frac{\sigma}{E}\right)^5 \tag{10}$$

where γ is the stacking fault energy, D_l is lattice diffusion coefficient, E is the modulus of elasticity, and A is a physical constant. In this class of alloy the controlling mechanism for creep is dislocation climb, which is related to

subgrain formation, stacking fault energy and the elastic modulus. Class II alloys also exhibit a distinct primary creep phase similar to pure metals. Equation 10 reduces to the form of equation 2 for constant stress and reduces to equation 7 at constant temperature. Furthermore, if stacking fault energy or modulus become temperature dependent equation 10 predicts that the observed value of Q_c may differ from Q_D.

Following Goodson [Ref. 10]:

$$Q_c = -R\frac{\partial lnD}{\partial(\frac{1}{T})} + 5R\frac{\partial lnE}{\partial(\frac{1}{T})} - 3R\frac{\partial ln\gamma}{\partial(\frac{1}{T})} \qquad (11)$$

In the expression it is seen that if either E or γ become strongly temperature dependent this will result in an additional factor in the activation energy.

4. Previous Work at NPS

Initial isothermal studies conducted by Ellison [Ref. 9] over a range of temperatures and stresses and it was determined that the Al-2.0wt.pct.Li exhibited a stress exponent of n = 5 but that Q_c was anomalously high, well in excess of that for pure Aluminum. In similar work by Taylor [Ref. 8] on Al-0.5.wt.pct.Li and Al-1.0wt.pct.Li alloys the stress exponent was also found to be similar to that for pure metals, that is n = 5.

Subsequent studies by Goodson [Ref. 10] on the Al-2.0wt.pct.Li, utilizing temperature cycling methods, also concluded that the 2.0 wt.pct. Lithium alloy exhibited anomalously high activation energy. This result was attributed to ordering of Lithium at elevated temperatures and the effects of ordering on temperature dependence and the modulus of elasticity. This study extends the research on all three alloys and provides additional data on the activation

energy for the Al-0.5.wt.pct.Li and Al-1.0wt.pct.Li alloys utilizing a temperature cycling technique.

III. EXPERIMENTAL PROCEDURE

A. MATERIAL PROCESSING AND FABRICATION

The alloys used in the conduct of this investigation were cast by the Naval Surface Weapons Center in White Oak, Maryland utilizing 99.99 percent pure Aluminum alloyed with 99.99 percent pure Lithium. The three alloys studied were of nominal compositions Al-0.5wt.pct.Li, Al-1.0wt.pct.Li and Al-2.0wt.pct.Li. The material was received in the form of tapered cylindrical ingots 200 mm (8.0 in.) in length and approximately 76 mm (3.0 in.) in diameter. Transverse sections 25 mm (1.0 in.) thick and 76 mm (3.0 in.) in diameter were solution treated at 540°C for 12 hours. The homogenized billets were rolled between 400 and 450°C to a final thickness of 2 mm (0.08 in.) in most cases and 1.4 mm (0.055 in.), in one case, in accordance with the rolling schedule developed by Goodson [Ref. 10].

The rolled sheets of both thicknesses (2.0 mm and 1.4 mm) were machined so that the tensile axis was parallel to the rolling direction. The sample geometry is shown in Figure 2. A special device to hold the material was utilized due to the softness and ductility of the material. Five specimens were machined at one time using a cutting plan that would ensure the maximum number of samples possible were cut from each sheet. The finished samples were examined and surface/machining imperfections were removed with a jewelers file. Prior to testing all samples were annealed for 15 minutes at 500°C. [Ref. 8]

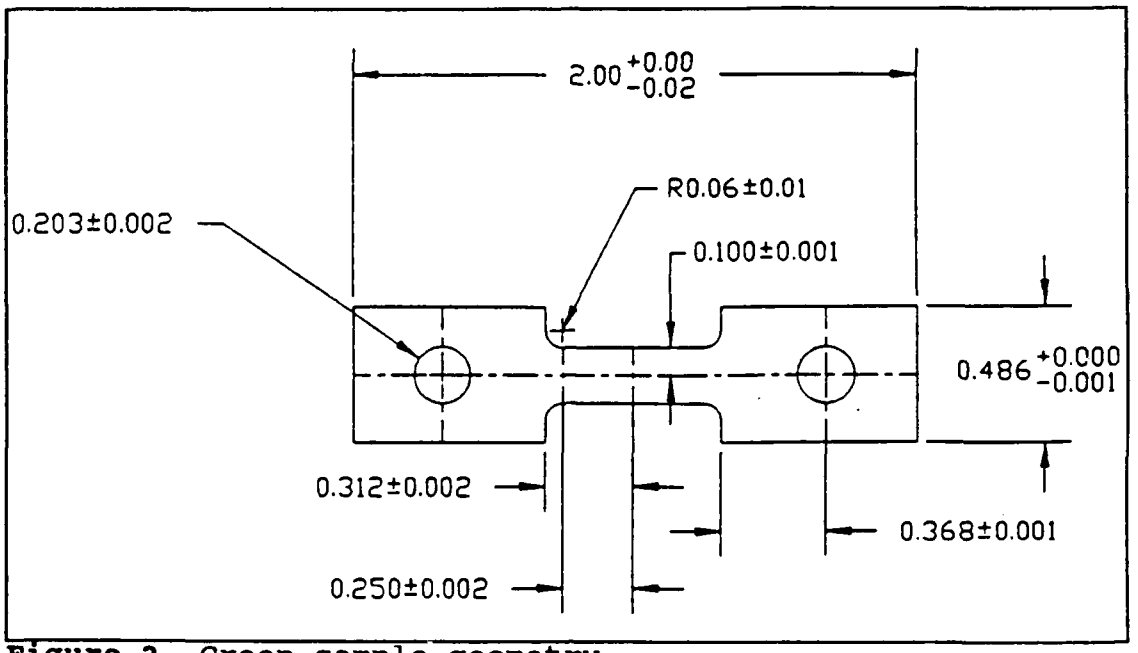

Figure 2. Creep sample geometry.

B. CREEP TESTING

1. Creep Testing Apparatus

The two creep testers shown in Figure 3 were specially designed to transmit loads between 1.5 and 222.5 Newtons (0.3 to 50 lbs.) at strains as high as 300 percent. These machines were designed at NPS and patterned after a machine built by Barrett and later modified by Matlock [Ref. 11]. The constant stress is obtained by means of an Andrade-Chalmers lever arm [Ref. 12]. The rotation of the contoured lever arm during elongation of the specimen decreases the effective lever arm in proportion to the decrease in cross sectional area of the specimen. This proportional decrease in applied load to specimen cross section allows a constant true stress to be maintained. The design of the arm is based on the assumption that the load train is rigid and the linkage displacement is taken up uniformly. The contour of the lever arm was designed using AUTOCAD software in conjunction with a graphical technique developed by Coghlan [Ref. 13]. The design was

based on the effective specimen gauge length of 12.7 mm (0.5 in.) and utilized an initial lever ratio of 10:1. The lever arm was constructed of 6.4 mm (0.25 in.) thick 2024-T6 aluminum and is attached to one end of a shaft which rotates on a set of precision bearings. An adjustable counter balance is attached to the opposite end of the shaft which allows the arm to be balanced so that the applied force on the sample is due only to the weight suspended from the contoured arm. A fixed counter balance, W1 in Figure 3, was attached inboard of the adjustable counter balance to counter act the weight of the load train. [Ref. 9]

In the original design a flexible steel strap, 9.5 mm (0.375 in.) wide by 0.51 mm (0.02 in.) thick, followed the contour of the lever arm and hung along the vertical tangent to the lever. A second steel strap of the same dimensions was hung tangent to a 51 mm (2.0 in.) radius cylinder centered on the fulcrum point which transmitted the load to the specimen. The steel strap on the lever arm has been replaced by a 9.5 mm (0.375 in.) wide by 0.127 mm (0.005 in.) thick strip of monel which is lighter and provides more flexibility. The steel strap connecting the load train to the cylinder has been replaced by a 51 mm (2.0 in.) wide by 0.254 mm (0.01 in.) thick strap of monel. The cylinder was replaced by a 51 mm (2.0 in.) wide aluminum cylinder of the same radius, 51 mm (2.0 in.). An aluminum block was designed which attaches to the monel strap on top and the universal joint is threaded in on the bottom. The block has attachments on the forward side for the linear variable differential transformer (LVDT) core and on the back side for a counter balance to ensure the tangent to the cylinder is maintained.

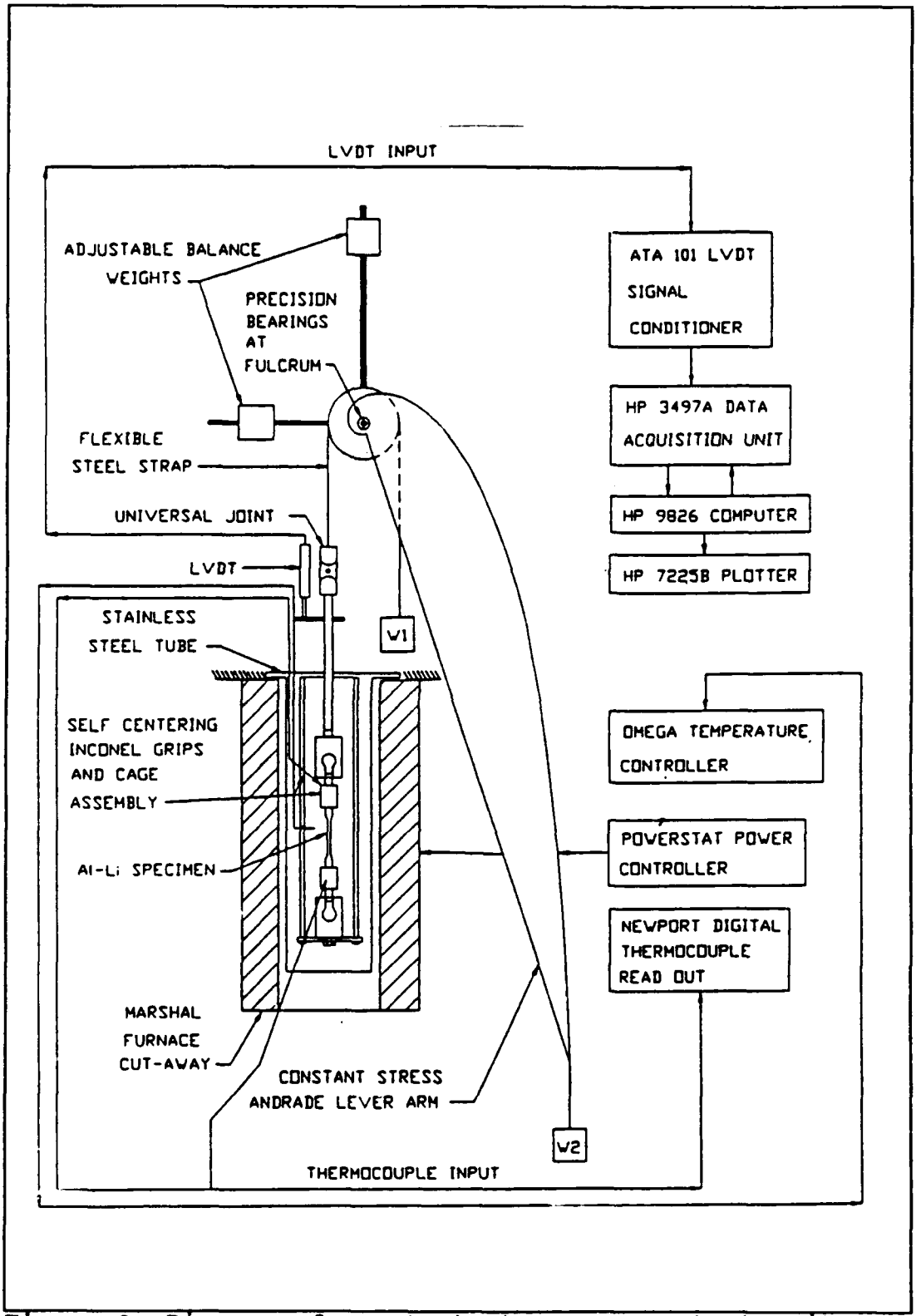

Figure 3. Diagram of constant stress creep test unit.

Sample elongation was measured using a Schaevitz LVDT with a 25.4 mm (1.0 in.) displacement. The core was attached to the aluminum block in the load train above the universal joint. A 2.866 mV/V output signal from the LVDT is conditioned by a Schaevitz ATA 101 Analog Transducer Amplifier. The amplifier voltage was measured using a Hewlett Packard (HP) 3497A Data Acquisition unit controlled by a HP 9826 computer.

Marshall tubular furnaces, capable of attaining 1200°C, were used to maintain required temperatures in conjunction with Eurotherm 808 digital temperature controllers. A temperature gradient of less than 2°C was established along the gauge length by installing external shunts and temperature was continuously monitored using "K" type chromel-alumel thermocouples.

Special self aligning grips, manufactured with Inconel Alloy 625, were designed to hold the creep specimens (Figure 4). These grips were made by the Collins Instrument Company, Freeport, Texas using a wire electro-discharge machining (EMD) process to control tolerances. The tapered shank connected to the button head provides self alignment and facilitates rapid installation and removal to minimize heat loss while changing samples [Ref. 9]. At lower stresses the weight of the lower grip assembly accounts for a significant addition of stress to the specimen. This was taken into account in performing calculations when feasible. However, future testing should incorporate some type of spring loading in the lower grip to offset the additional stress when experimenting at levels of reduced stress.

2. Cam Calibration

Extensive cam calibration was conducted subsequent to the equipment modifications described in the preceding section. A 50 lbf capacity Interface load cell was rigidly attached to the frame of the creep unit and then aligned in the load train at the same position as a tensile sample. The load cell was connected to the load train using a threaded steel rod and nuts. The 2.866 mV/V output signal from the load cell was conditioned using an HP 6216A constant current DC power supply at a setting of 10 V prior to processing by the HP 3497A Data Acquisition unit.

A weight was suspended from the monel strap at the end of the contoured lever arm. The LVDT and load voltages were read and the steel rod was measured from the load cell to a pre-set mark on the rod using a digital caliper. The lower

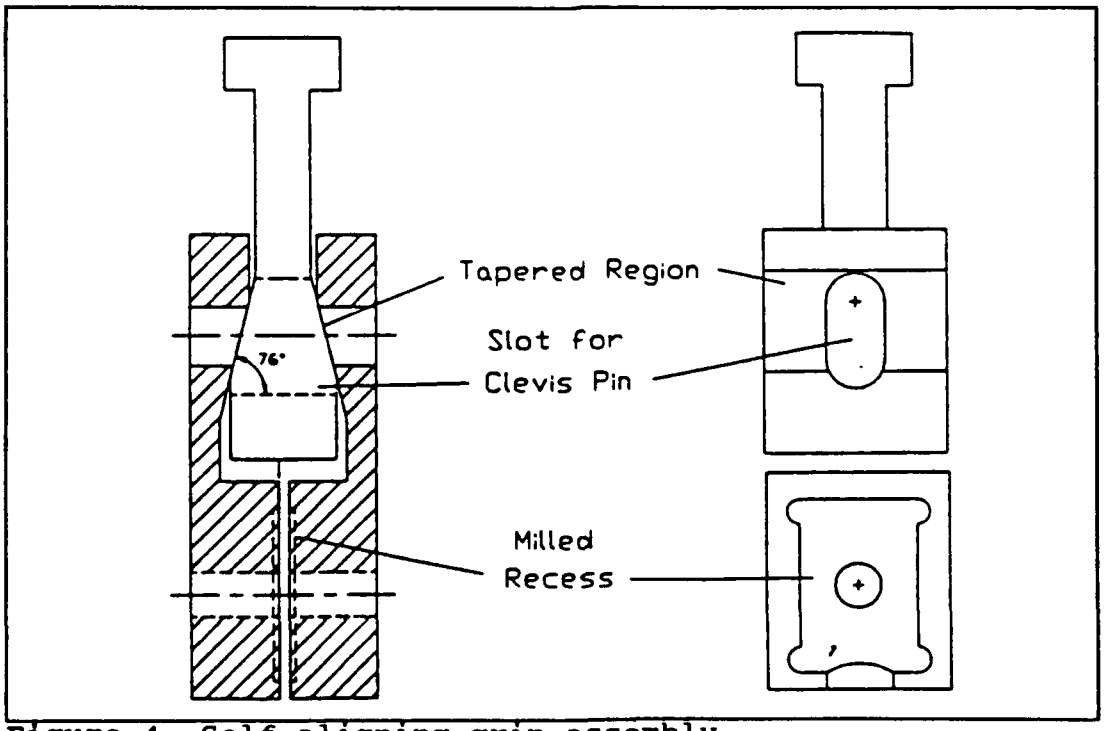

Figure 4. Self aligning grip assembly.

nuts on the steel rod were adjusted to allow the moment arm to decrease. The LVDT and load cell voltages were read and recorded and the distance the steel rod "elongated" was then measured. This was repeated in intervals of 1.3 mm to 1.8 mm (0.05-0.07 in.) until an elongation of approximately 11.5 mm (0.45 in.) was achieved. This corresponded to the maximum expected ductility of the specimen. The expected variation in load with deflection can be calculated using the definition of constant true stress and assuming constant volume of the material:

$$\sigma = \frac{P}{A} \tag{12}$$

and:

$$V = constant = Al = A_0 l_0 \tag{13}$$

where σ is the stress, P the load, A the area, A_0 the initial area, l_0 the initial length and $l = l_0 + \Delta l$, where Δl is the deflection. Equations 12 and 13 can be combined to show:

$$P = \frac{\sigma_0 A_0 l_0}{l_0 + \Delta l} \tag{14}$$

This procedure was repeated for various applied weights ranging from 0.29 to 5.4 lb. The difference between theoretical and experimental results from each test were compared with error ranging from 0.98 to 4.18 percent, the greatest error being at the lightest loads. Figures 5 and 6 represent applied force, both calculated and experimental, plotted as a function of elongation.

During the course of the test phase 16 of 65 tests were discarded. On several occasions the grip became

entangled with a thermocouple creating unusable data. At the lowest stress levels the weight of the lower grip assembly accounted for a significant additional stress which in turn introduced variability in results. This was taken into account by calculating the additional stress associated with the grip and adjusting calculations for applied weight or stress if a test had already been run.

3. Software used for Constant Stress Tests

The software developed for the creep testing is written in HP Basic 2.0 and was last modified by Goodson [Ref. 10]. The software is designed to control both creep units simultaneously and provides a graphic display of real time engineering strain vs. time for both tests. Once tests are completed the user can save accumulated data on any of three floppy disk drives. Plots of true strain vs. time and percent elongation vs. time can be plotted on the HP 7275B plotter. A strain rate program was also developed by Goodson [Ref. 10] which plots strain rate versus true strain. Activation energies for the alloys were calculated from temperature cycling tests and graphical differentiation of the creep curves using Goodson's program.

4. Constant Temperature Testing

Once required furnace temperature was attained the furnace was de-energized and lowered. The grip assembly containing the sample was carefully installed into the grip holders and the slack was removed from the load train by a small preload to prevent slippage in the grips. The furnace was raised, re-energized and allowed to stabilize for approximately 35-45 minutes. Both the bottom and the top furnace openings were insulated to minimize any flue effects.

Prior to temperature stabilization the creep program

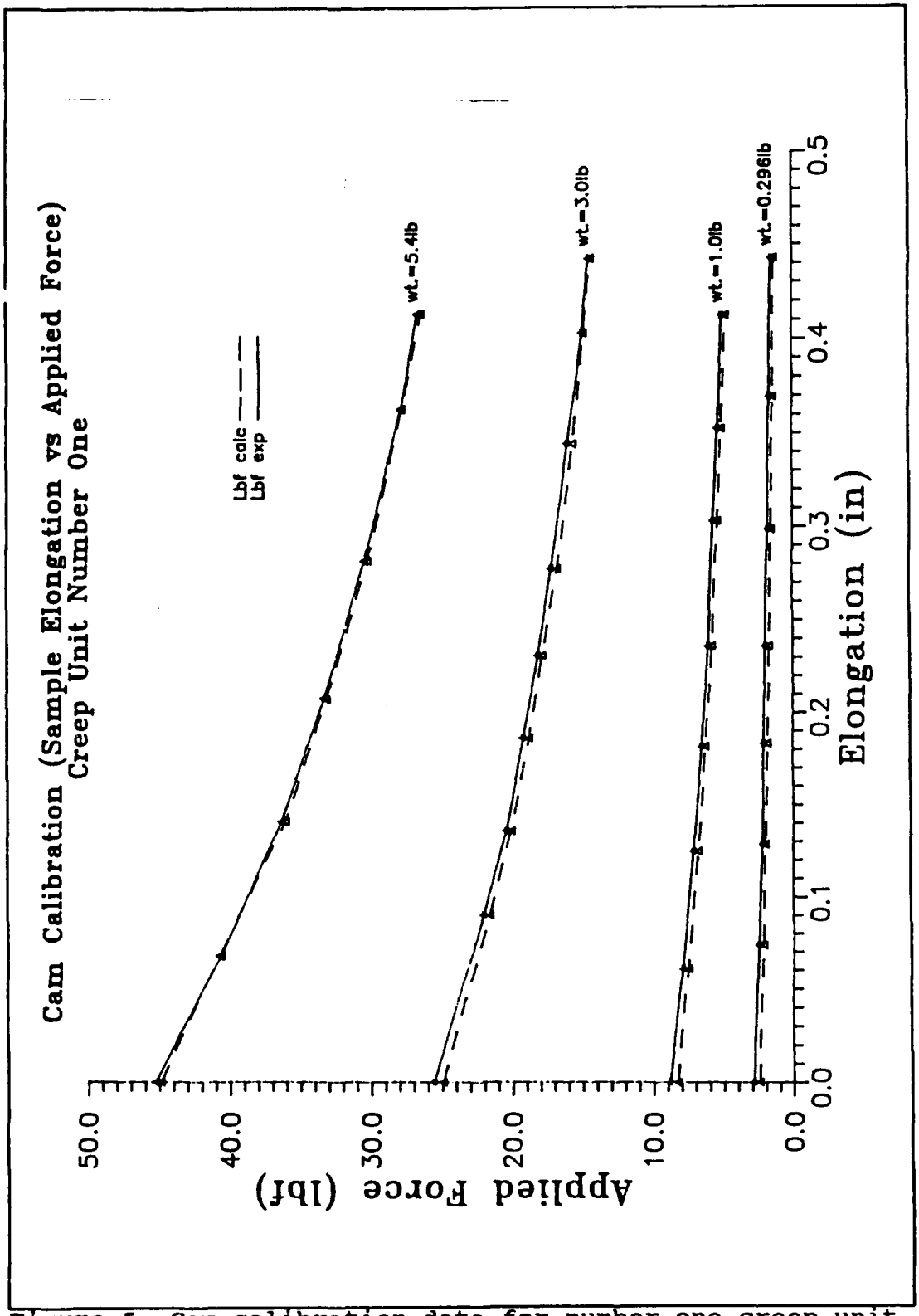

Figure 5. Cam calibration data for number one creep unit.

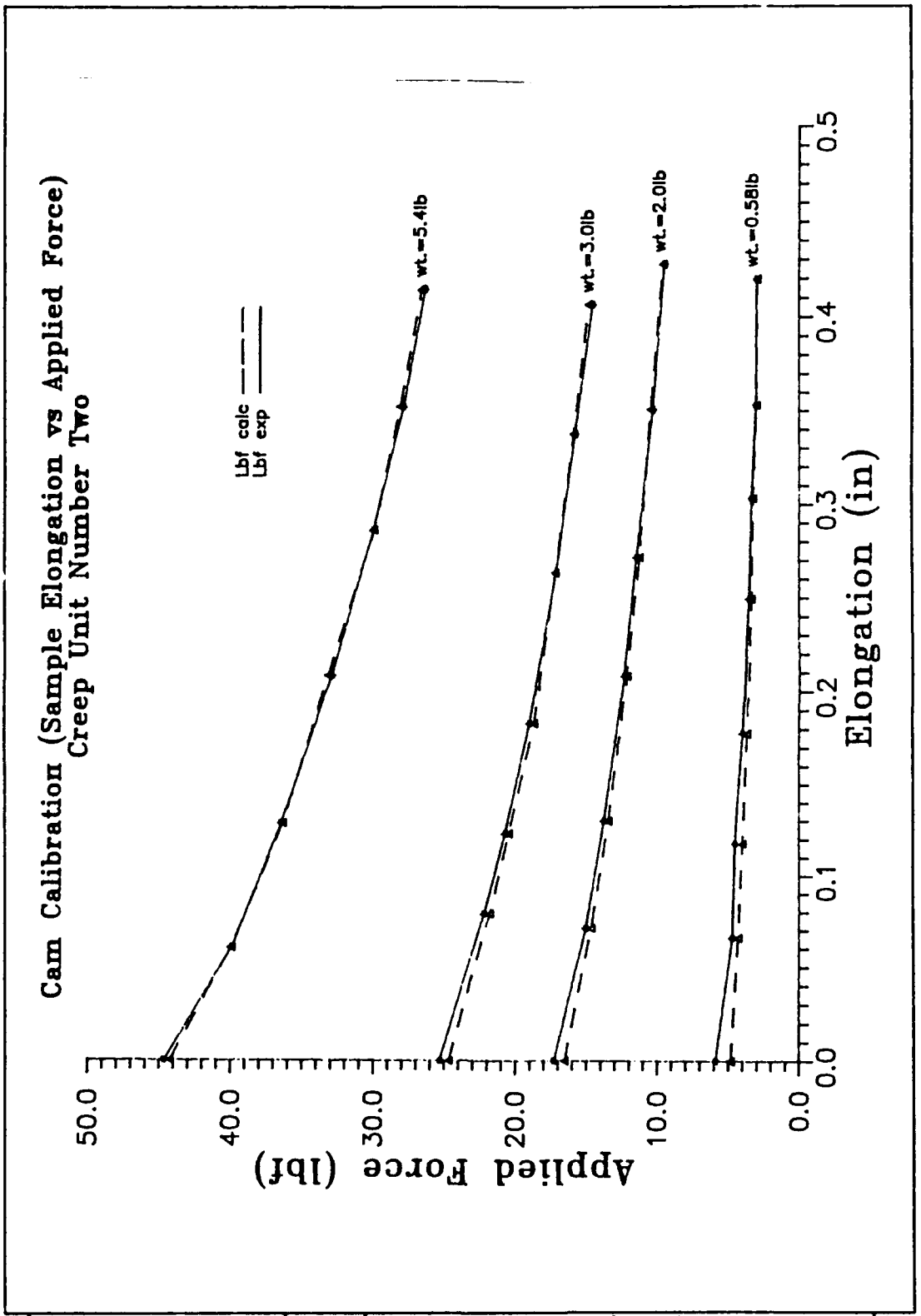

Figure 6. Cam calibration data for number two creep unit.

was started and initial test parameters entered. The weight to be applied was calculated and placed in a modified funnel which centered the lead shot used for the weight. After the temperature had stabilized the weight was carefully suspended from the lever arm by the flexible strap and the program started. The LVDT was zeroed by the data acquisition program as it was started. Each test was allowed to continue to failure.

5. Temperature Cycling Tests

Accurate temperature cycling was achieved using a Eurotherm 808 programmable digital temperature controller which allowed for precise control of temperature ramp, level, and dwell time. Prior to test initiation the temperature controller was programmed so that the temperature difference between levels was 10°C with a dwell time of four hours at each level. The remaining pretest setup is identical to that for a constant temperature test with the exception that the Eurotherm program is set to run prior to applying the load and starting the creep program. The Eurotherm program was set for continuous cycling so that each test would proceed under these conditions until failure.

6. Optical Microscopy

Specimens were cut from as-rolled and annealed, untested samples and from Al-0.5wt.pct.Li and Al-1.0wt.pct.Li materials that were tested at 400°C at a stress of 8.84 MPa. The tests were allowed to continue to the steady state creep stage at which time the furnace was de-energized, lowered and the sample cooled under load to ambient temperature. Specimens were mounted in Buehler fast-cure acrylic, manually ground to 600 grit and polished with 1 μm diamond paste. The samples were subsequently electropolished and etched using a

modified Barker's reagent (HBF_4, 48% solution, 46 cm^3, boric acid 79 cm^3, H_2O 970 cm^3). Examination was done using Zeiss ICM-405 optical microscopes. Both normal illumination and plane-polarized light techniques were employed.

IV. RESULTS AND DISCUSSION

A. INITIAL MICROSTRUCTURE

Ellison [Ref. 9] studied the microstructural development of a Al-2.0wt.pct.Li alloy and found that the as-rolled material was free of inclusions, with elongated columnar grains oriented in the rolling direction. After annealing at 500°C for 15 minutes, a coarse, equiaxed and stable grain structure, free of residual stresses, was produced. Grains were approximately 50 microns (0.05 mm) in size with no evidence of precipitation present.

B. CONSTANT STRESS, ISOTHERMAL TESTS

During this phase of the research specimens of all three alloys, Al-0.5wt.pct.Li, Al-1.0wt.pct.Li, and Al-2.0wt.pct.Li, were tested at various stresses and temperatures in order to determine a minimum creep rate. All tests were conducted at a constant stress and under isothermal conditions until specimen failure. A typical creep curve with true strain plotted versus time is shown in Figure 7.

Examination of the Figure reveals three distinct portions of the creep curve. The primary phase is characterized by a rapid initial strain rate which decreases until a steady state is reached. In the primary phase the decrease in the strain rate reflects substructure changes that increase the overall resistance to dislocation motion. Strain hardening at elevated temperatures involves dislocation generation and subgrain formation associated with the rearrangement of the dislocations. Therefore as creep increases and dislocation motion decreases, the rate of strain hardening decreases.

Examination of the creep curves for all three alloys reveals primary creep in all cases, consistent with pure Aluminum. [Ref. 6]

In the secondary phase a minimum creep rate, corresponding to a steady state rate, becomes apparent. This constant strain rate in the secondary stage indicates a stable substructure and a dynamic balance between the hardening and softening processes. [Ref. 14]

In the tertiary stage the creep rate accelerates until fracture. This accelerating creep rate is dominated by instability in the form of localized necking, microvoid formation and coalescence followed by fracture. In addition, the strain hardening grains may recrystallize and further destroy the balance between material hardening and softening processes.[Ref. 14]

The minimum creep rate was determined from a plot of creep rate versus true strain. Figure 8 is such a creep rate curve corresponding to the creep curve shown in Figure 7. The jagged appearance of the curve is the result of quantization errors in the data acquisition equipment. Alternatively, the creep curve itself could be used to determine the creep rate by graphical calculation of the Δ(strain)/Δ(time), which is easily accomplished with a well pronounced steady state region.

1. Strain-Rate Dependence of Stress

The data of Table I summarize the results of the constant stress isothermal tests which were utilized to expand on the work of Taylor [Ref. 8] and Goodson [Ref. 10] in compiling a more comprehensive body of data. Sherby and Burke [Ref. 6] note that for an intermediate stress range the relationship between strain rate and stress at constant

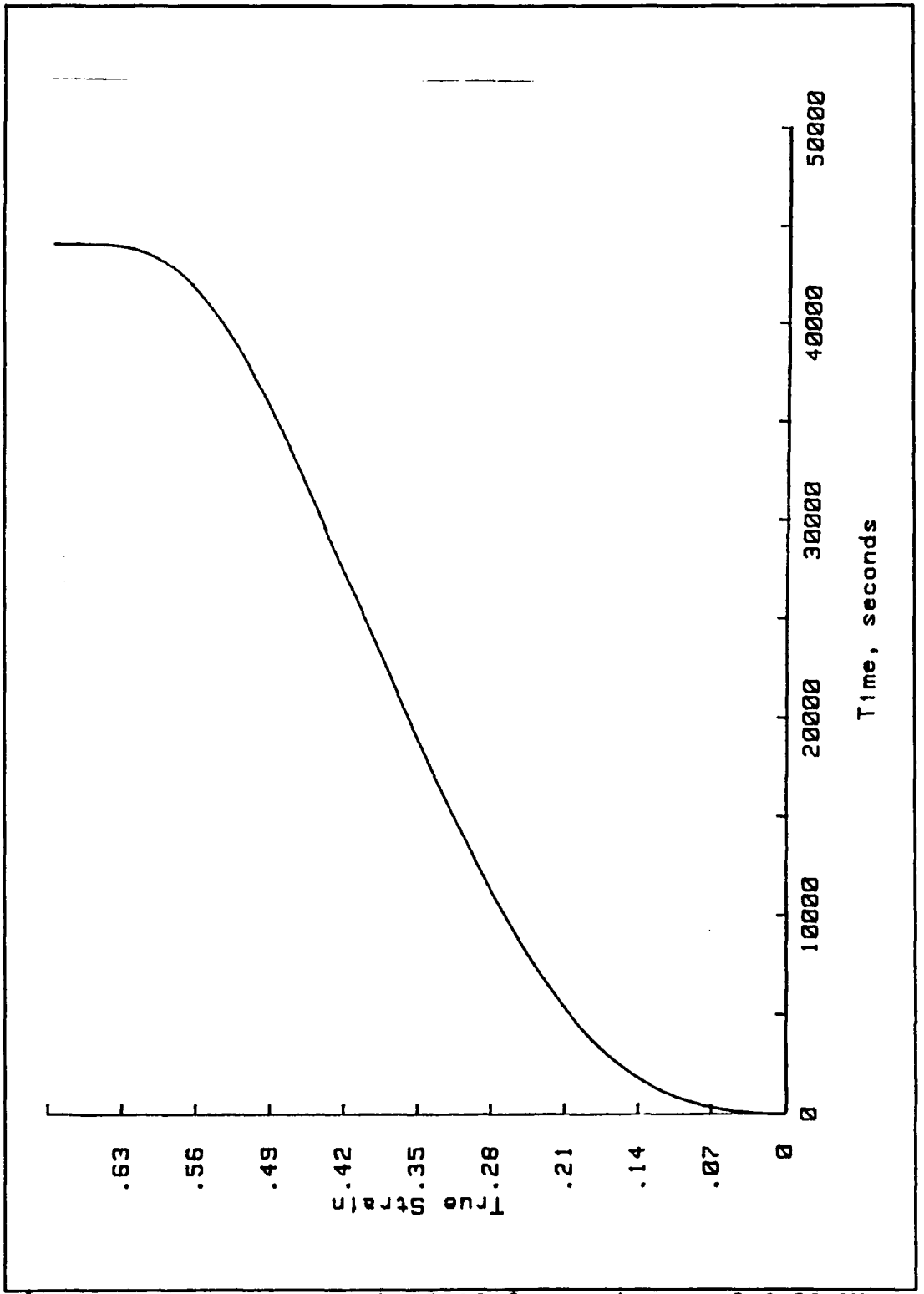

Figure 7. Creep Curve at 350°C for a stress of 6.28 MPa: $\dot{\epsilon}_{min} = 9.0 \times 10^{-8}$ sec^{-1}

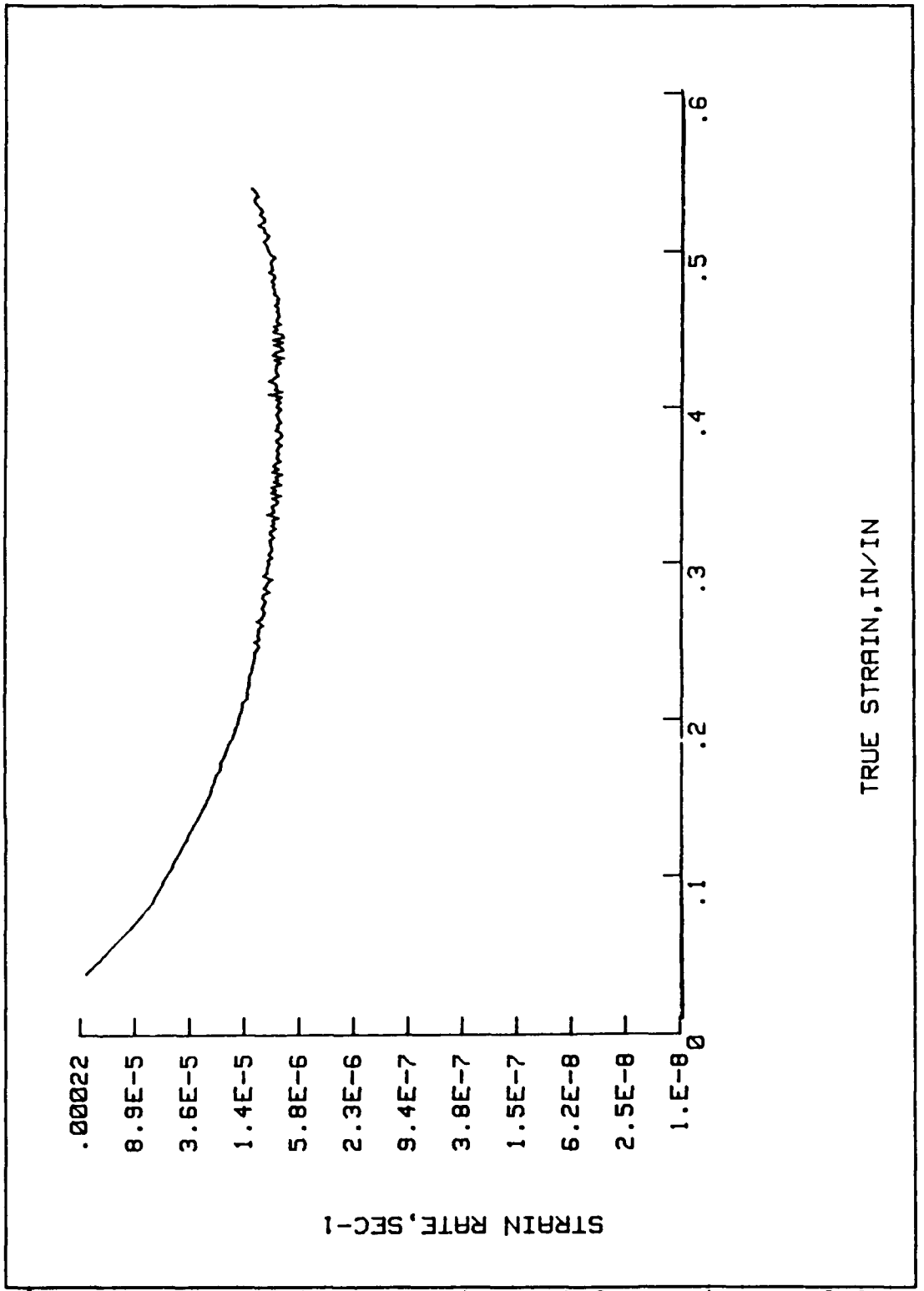

Figure 8. Creep Rate Curve at 350°C for a stress of 6.28 MPa: $\dot{\epsilon}_{min} = 9.0 \times 10^{-6}$ sec^{-1}

Table I. SUMMARY OF ISOTHERMAL CONSTANT STRESS TESTS

%Li	Temp (°C)	$\dot{\epsilon}$ (sec^{-1})	σ(MPa)	log $\dot{\epsilon}$	log σ
0.5	300	4.4×10^{-6}	9.70	-5.36	0.97
	300	1.15×10^{-4}	15.8	-3.95	1.20
	350	8.34×10^{-5}	8.84	-4.08	0.95
	350	9.0×10^{-6}	6.27	-5.06	0.80
	350	3.75×10^{-6}	5.42	-5.43	0.73
	350	2.61×10^{-7}	3.58	-6.58	0.55
	400	1.54×10^{-2}	14.67	-1.81	1.17
	400	9.1×10^{-6}	3.07	-5.04	0.49
	400	4.76×10^{-7}	1.81	-6.32	0.26
	450	1.79×10^{-5}	2.67	-4.75	0.43
	450	1.28×10^{-5}	2.10	-4.91	0.32
	450	1.33×10^{-6}	1.63	-5.88	0.21
	500	2.0×10^{-4}	2.41	-3.70	0.38
1.0	300	8.36×10^{-6}	10.97	-5.07	1.04
	350	1.35×10^{-3}	15.85	-2.87	1.20
	350	1.32×10^{-5}	7.59	-4.88	0.88
	400	3.61×10^{-5}	5.32	-4.44	0.73
	400	1.09×10^{-4}	5.16	-3.96	0.71
	400	5.23×10^{-6}	3.68	-5.28	0.57
	450	2.29×10^{-5}	2.65	-4.64	0.42
2.0	500	6.13×10^{-4}	3.03	-3.21	0.48
	500	8.30×10^{-5}	2.34	-4.08	0.37
	500	9.38×10^{-6}	1.74	-5.03	0.25

temperature can be described by the power law relationship:

$$\dot{\epsilon} = K\sigma^{n} \qquad (15)$$

where values of n for pure metals, Aluminum included, are typically equal to 5. The experimental values of $\dot{\epsilon}_{min}$ were plotted versus σ on log-log axes for each test temperature. Figures 9, 10, and 11 include the results from this research in addition to those obtained by Taylor [Ref. 8] for the Al-0.5wt.pct.Li and Al-1.0wt.pct.Li and that of Goodson [Ref. 10] for the Al-2.0wt.pct.Li alloy. The stress exponents calculated show some temperature dependence in the 300°C and 500°C ranges with values of n at 6.33 and 6.13 at 300°C and 4.31 and 4.29 at 500°C for the Al-0.5wt.pct.Li and Al-1.0wt.pct.Li respectively. These n values based on the above mentioned research were calculated as $n = \Delta\log\dot{\epsilon}/\Delta\log\sigma$ from the data by linear regression and are summarized in Table II. The values of n determined from the combination of previous data and in this research are similar. The most extensive data was collected on the Al-0.5wt.pct.Li and the Al-1.0wt.pct.Li alloys. There are slight differences in some of the n values which can be attributed to refined test procedures and improved accuracy of the equipment. From these n values it is believed that the creep mechanism in these alloys is similar to that of pure Aluminum which deforms by glide and climb of dislocations, with diffusion controlled climb determining the overall rate of straining.

2. Strength Dependence on Lithium Concentration

The curves presented in Figures 13 and 14 are a summary of data collected from work by Taylor [Ref. 8], Goodson [Ref. 10] and this research. Data for all three alloys is shown and grouped together by test temperature. It

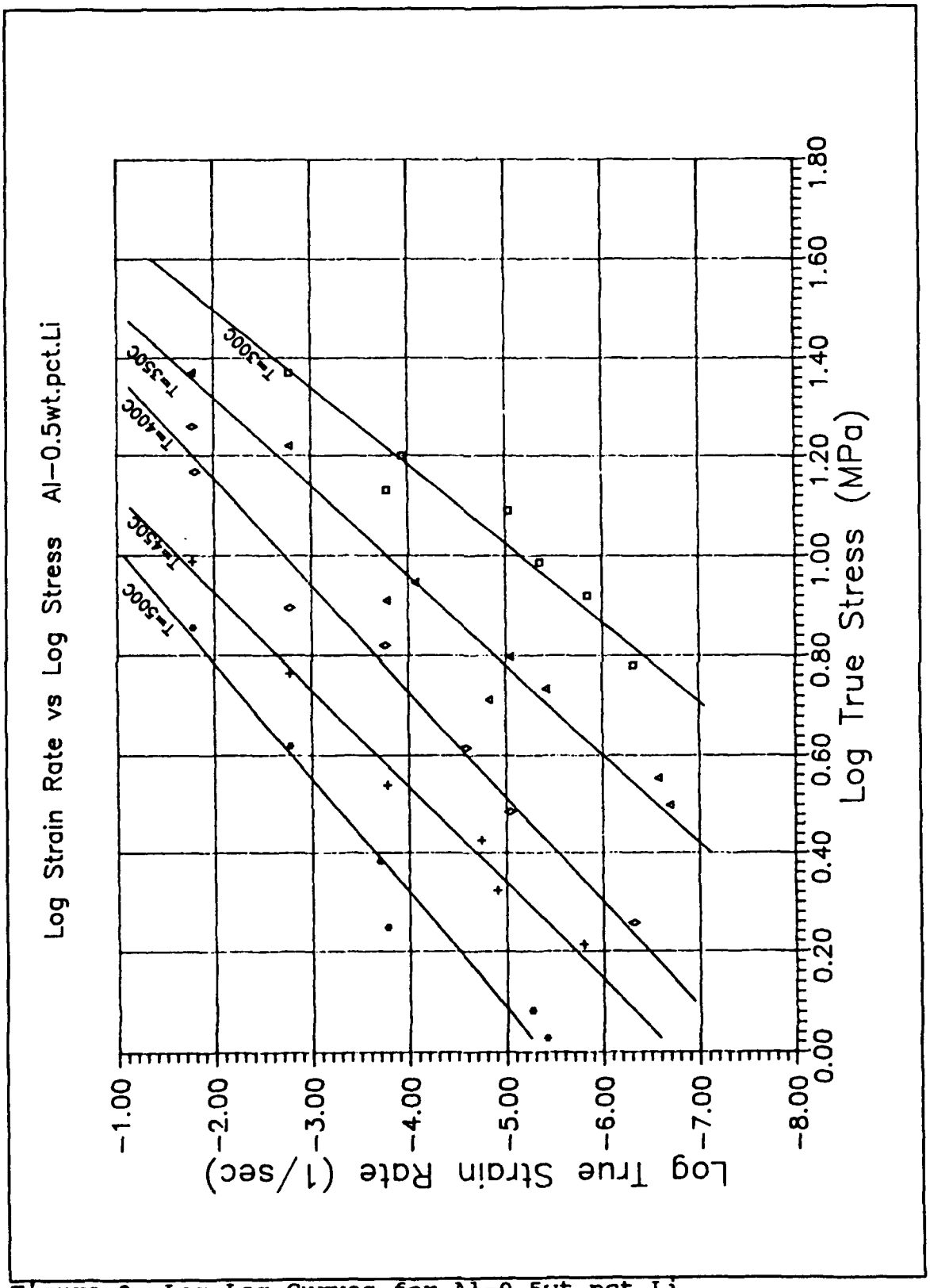

Figure 9. Log-Log Curves for Al-0.5wt.pct.Li

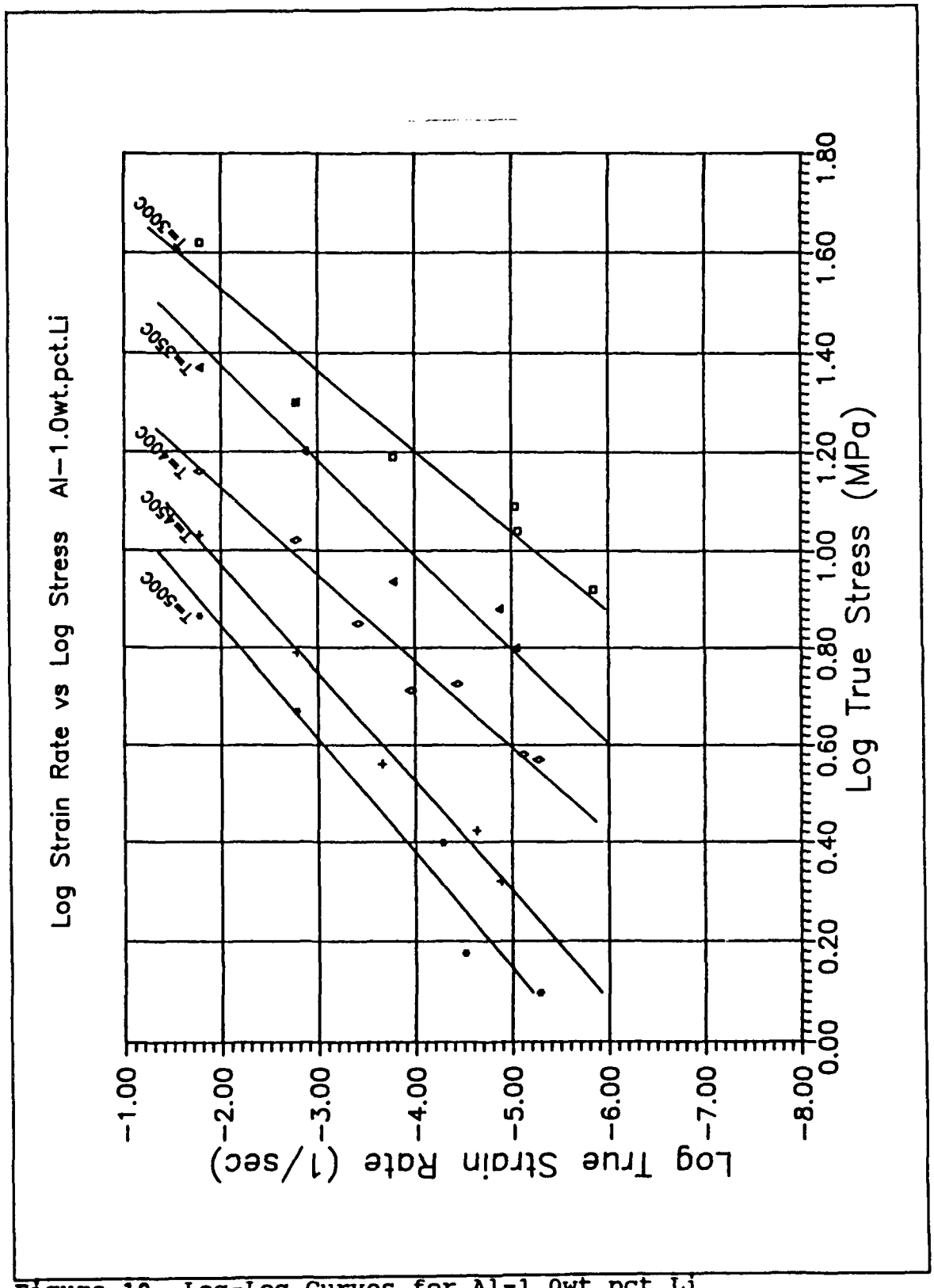

Figure 10. Log-Log Curves for Al-1.0wt.pct.Li

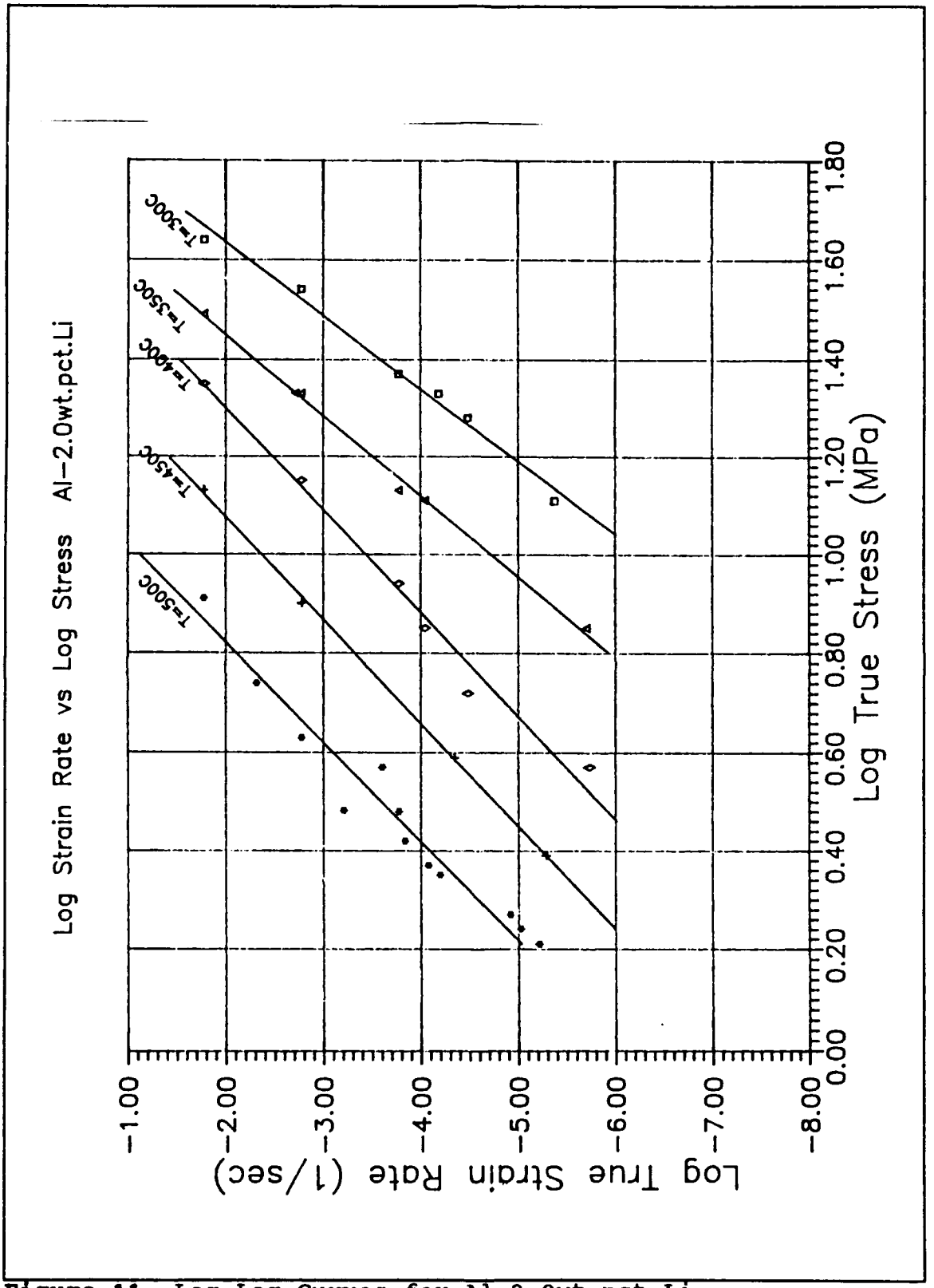

Figure 11. Log-Log Curves for Al-2.0wt.pct.Li

Table II. SUMMARY OF STRESS EXPONENTS

Temp (°C)	Value of n		
	0.5%Li	1.0%Li	2.0%Li
300	6.33	6.13	6.73
350	5.57	5.18	6.06
400	4.69	5.64	4.78
450	5.12	4.50	4.79
500	4.31	4.29	4.96

can easily be discerned that, as the Lithium concentration increases, the necessary applied stress to obtain a given strain rate increases, implying a stronger material under creep. This higher strength with increased Lithium concentration is most pronounced at the lower temperatures. The most notable difference is between the Lithium concentrations of one and two weight percent. With the exception of the 400°C range, the strength of the 0.5 and 1.0 weight percent alloys are within a factor of two. It is also evident that the strength of the 2.0wt.pct.Li increases at a more rapid rate as the temperature decreases than does either the 0.5 or 1.0 weight percent alloys. Up to 1.0 weight percent Lithium the data compares closely to that of pure Aluminum, only slightly stronger.

The strength dependence of Lithium concentration is clearly illustrated in Figure 15 in which each alloy was tested at 400°C and at stresses within 2.7% of each other. There is a slight increase in strength of the 1.0 over the 0.5 weight percent but a very pronounced increase between the 1.0 and 2.0 percent alloys.

3. Microstructural Evolution During Creep

Microstructural analysis of the Al-1.0wt.pct.Li alloy is summarized in Figure 12. The grip section of a sample

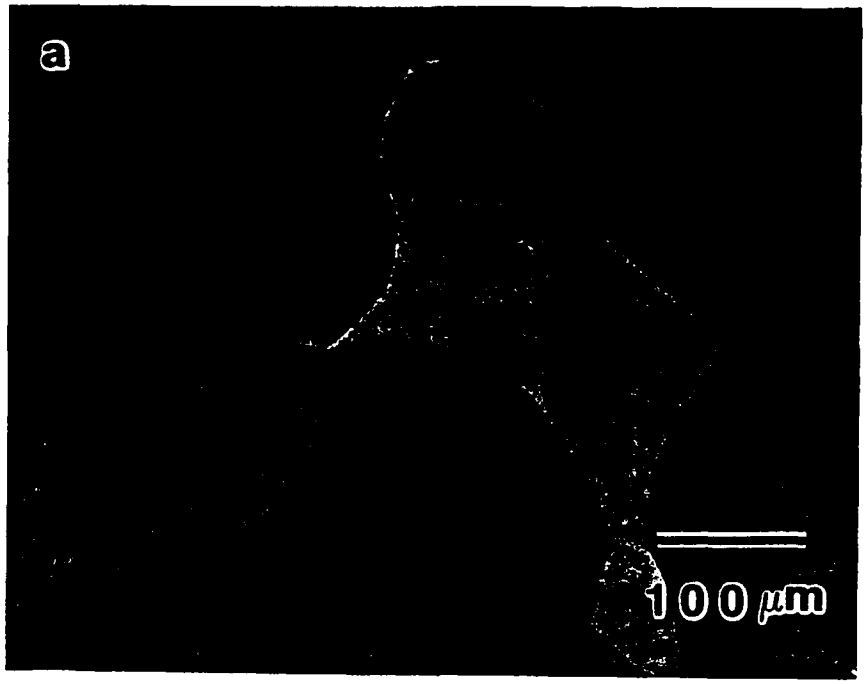

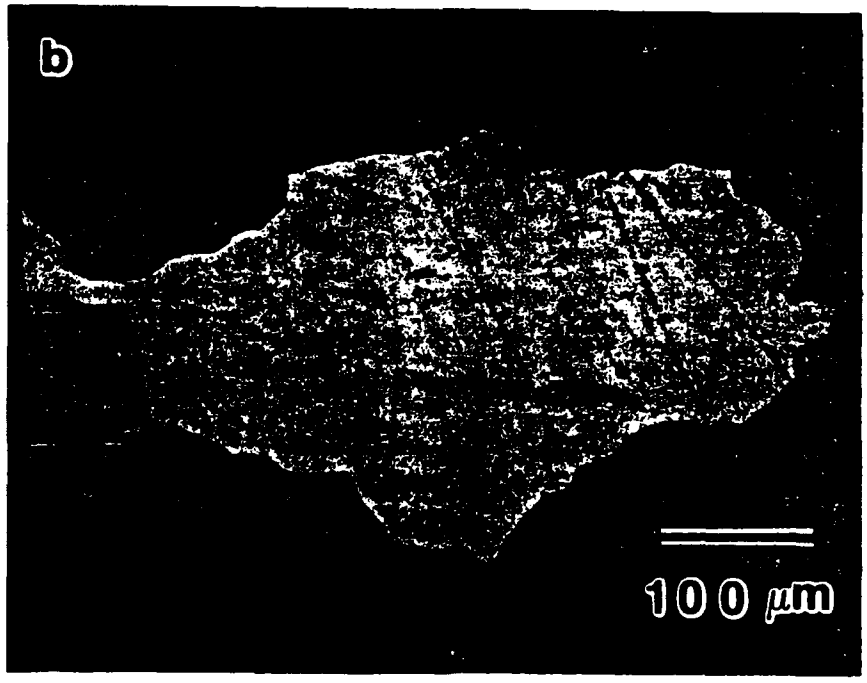

Figure 12. (a) Grip section of Al-1.0%Li at 400°C and a stress of 8.84 MPa. (b) Gage section of Al-1.0%Li at 400°C and a stress of 8.84 MPa. Sample cooled under load.

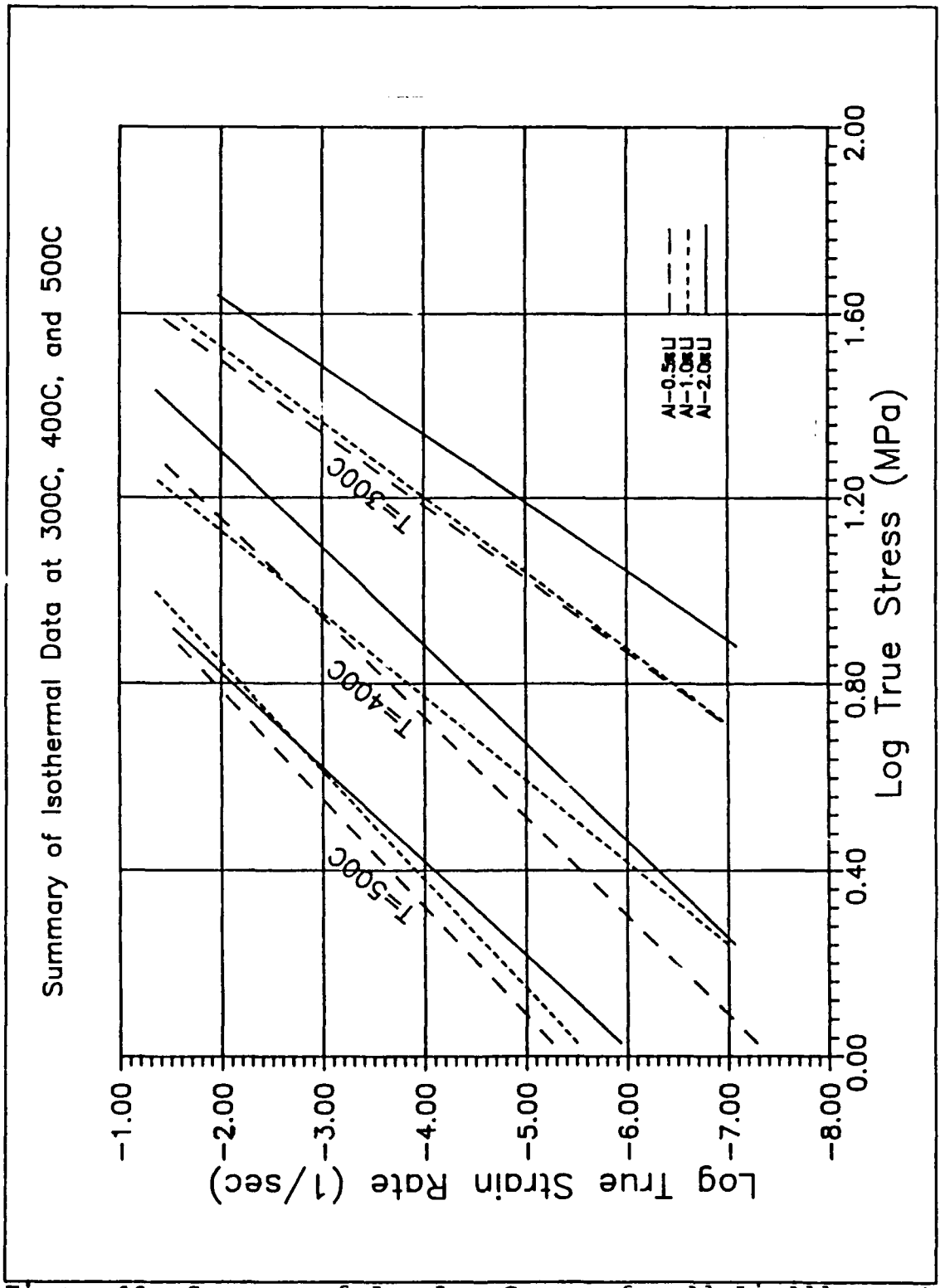

Figure 13. Summary of Log-Log Curves for Al-Li Alloys at 300,400 and 500°C

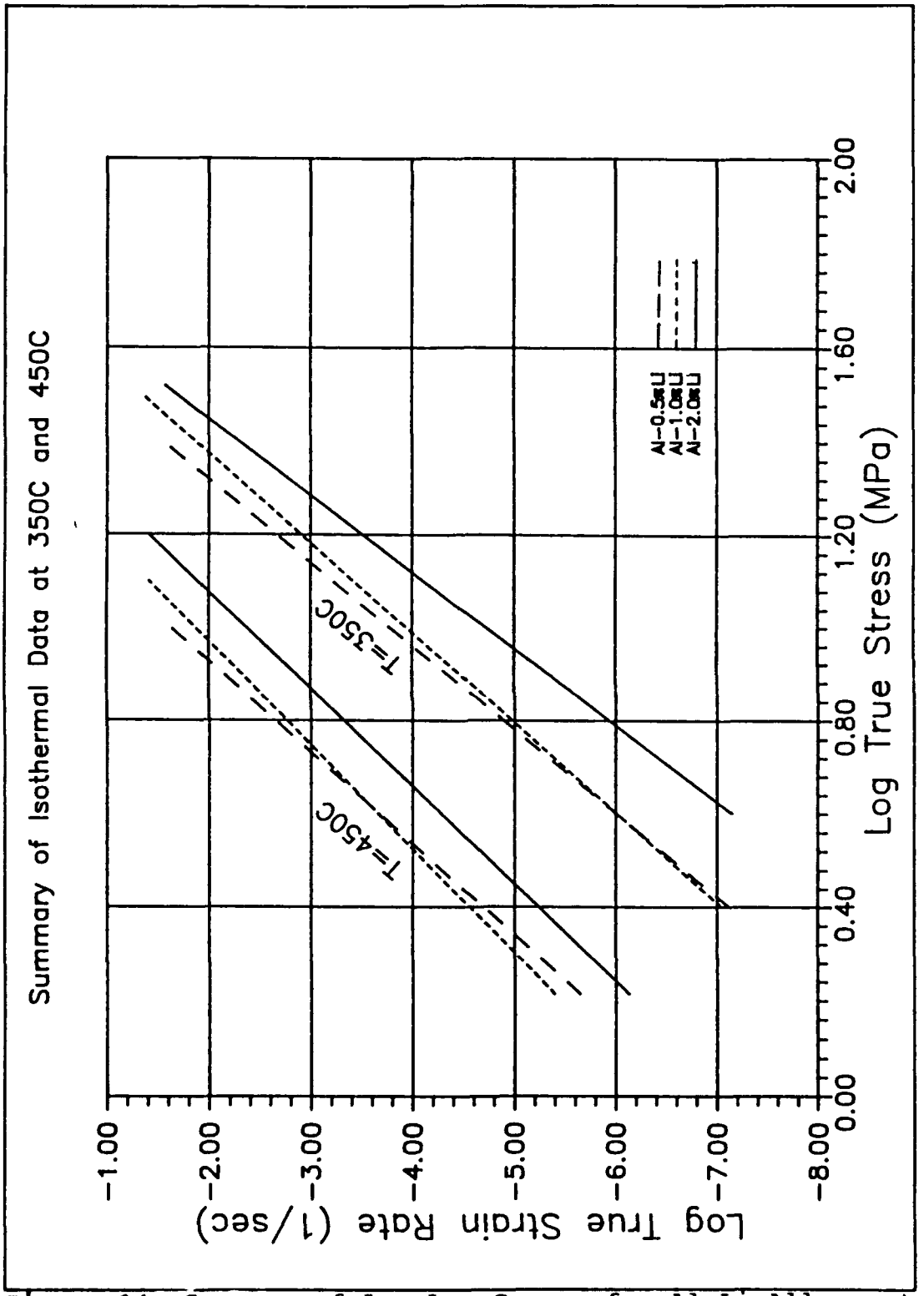

Figure 14. Summary of Log-Log Curves for Al-Li Alloys at 350 and 450°C

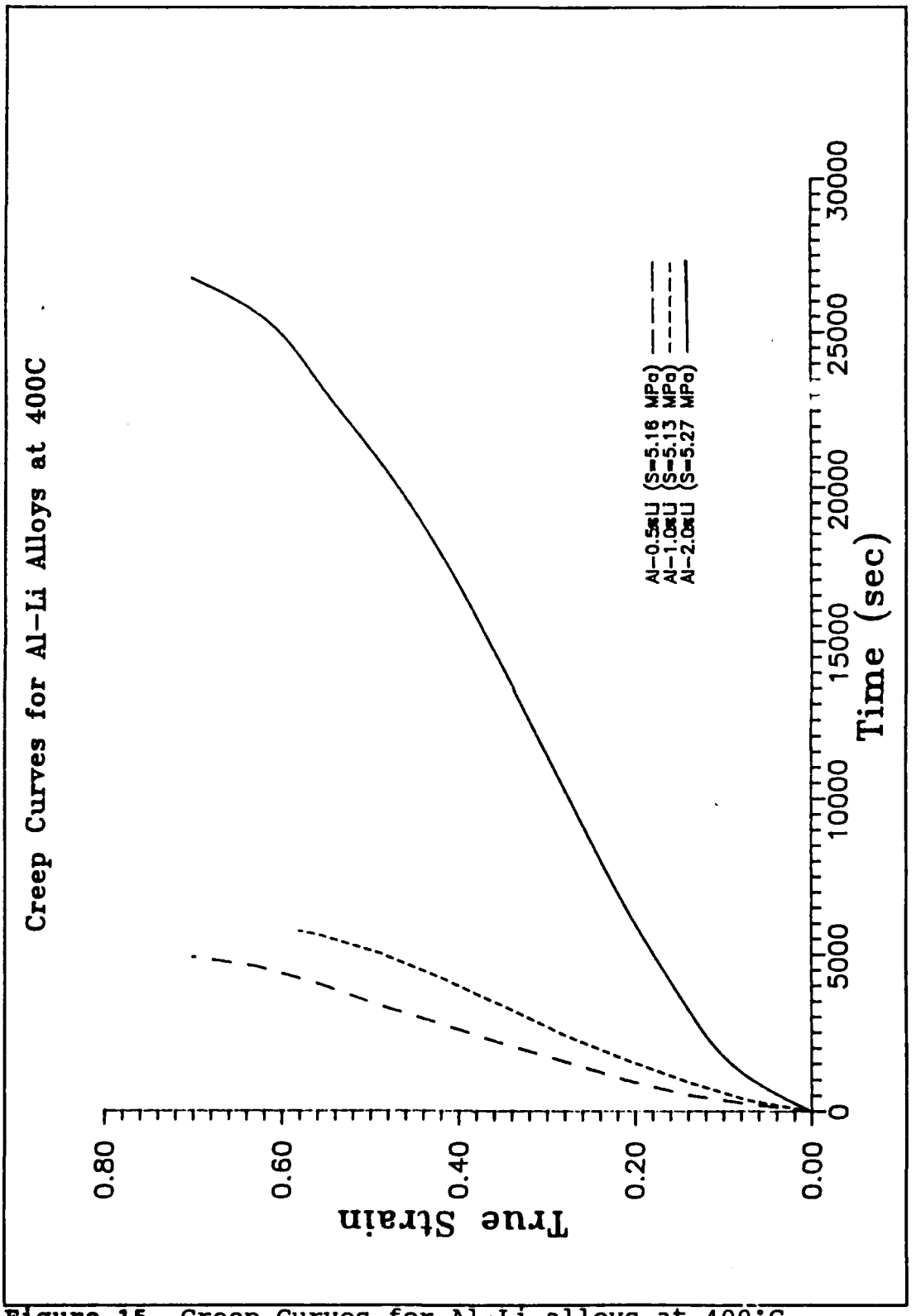

Figure 15. Creep Curves for Al-Li alloys at 400°C

crept at 400°C to a strain of 0.35 (within the steady state regime) is seen (Figure 12a) to exhibit an equiaxed grain structure similar to that reported by Ellison [Ref. 9] at the initiation of testing of the Al-2.0wt.pct.Li alloy and also to be present in the grip section of crept samples of the same Al-2.0wt.pct.Li alloy. The lower micrograph (Figure 12b) was obtained from the deformed gage section of the Al-1.0wt.pct.Li sample and exhibits a microstructural characteristic of subgrain-forming metals. The grain boundaries have become serrated by interaction of the high-angle boundaries with subgrain boundaries in the grain interiors. This serration of the boundaries suggests subgrain formation in association with a stress exponent n = 5 and this leads to the same conclusion reported by Ellison [Ref. 9], that these alloys behave as class II solid solutions.

C. TEMPERATURE CYCLING TESTS

In this phase of the research, identical specimens of the 0.5 and 1.0 weight percent Lithium alloys were crept at a constant stress, σ, while the temperature was varied. The stress was selected from the double log stress versus strain rate plots, shown in Figures 9, 10 and 11, to provide a test duration of approximately one day (80,000-90,000 sec). The test was set up and initiated at temperature T_1, as described in chapter III. After four hours the temperature was rapidly increased to a level $T_2 = T_1 + 10°C$. Temperature T_2 was maintained for four hours as well, after which time the temperature was rapidly decreased to the initial value of T_1. The average time for the 10°C temperature excursion to be completed was 10 minutes. This temperature cycling was repeated through steady state and up to failure.

A typical example of this procedure at 350-360°C is shown in Figure 16, in which true strain, ϵ, is plotted as a function of time. Three phases of creep are evident as in the isothermal curves, and that the duration of the temperature excursion from T_1 to T_2 is nominal when compared to the overall duration of the test. Figure 17 represents a creep rate versus creep strain curve for the temperature cycling test in Figure 16. In examining the creep rate data it can be seen that, after the 10°C temperature increase, the creep rate rapidly attains its new value and that the minimum creep rate after three cycles essentially agrees with the original steady state rate established before the first temperature increase and the creep transient after a temperature change is identical to that of pure Aluminum. [Ref 9]

The creep rate can also be determined from the creep curve itself where the two creep rates are easily discernable. One must be careful to select the steady state region of the curve and not to use an area too close to the primary or tertiary phases. Determination of the two rates is the same as that described for the constant temperature tests.

1. Activation Energy

Assuming that creep is thermally activated and follows an Arrhenius temperature dependence at constant stress, the values for Q_c can be obtained from equation 3. To determine Q_c, the steady state creep rate was evaluated at temperatures T_1 and T_2 for a particular temperature cycling test described previously. The creep rates were determined from the strain rate versus true strain curves as shown in Figure 17. In some instances where the strain rate curve was excessively jagged due to quantization errors in the data acquisition equipment,

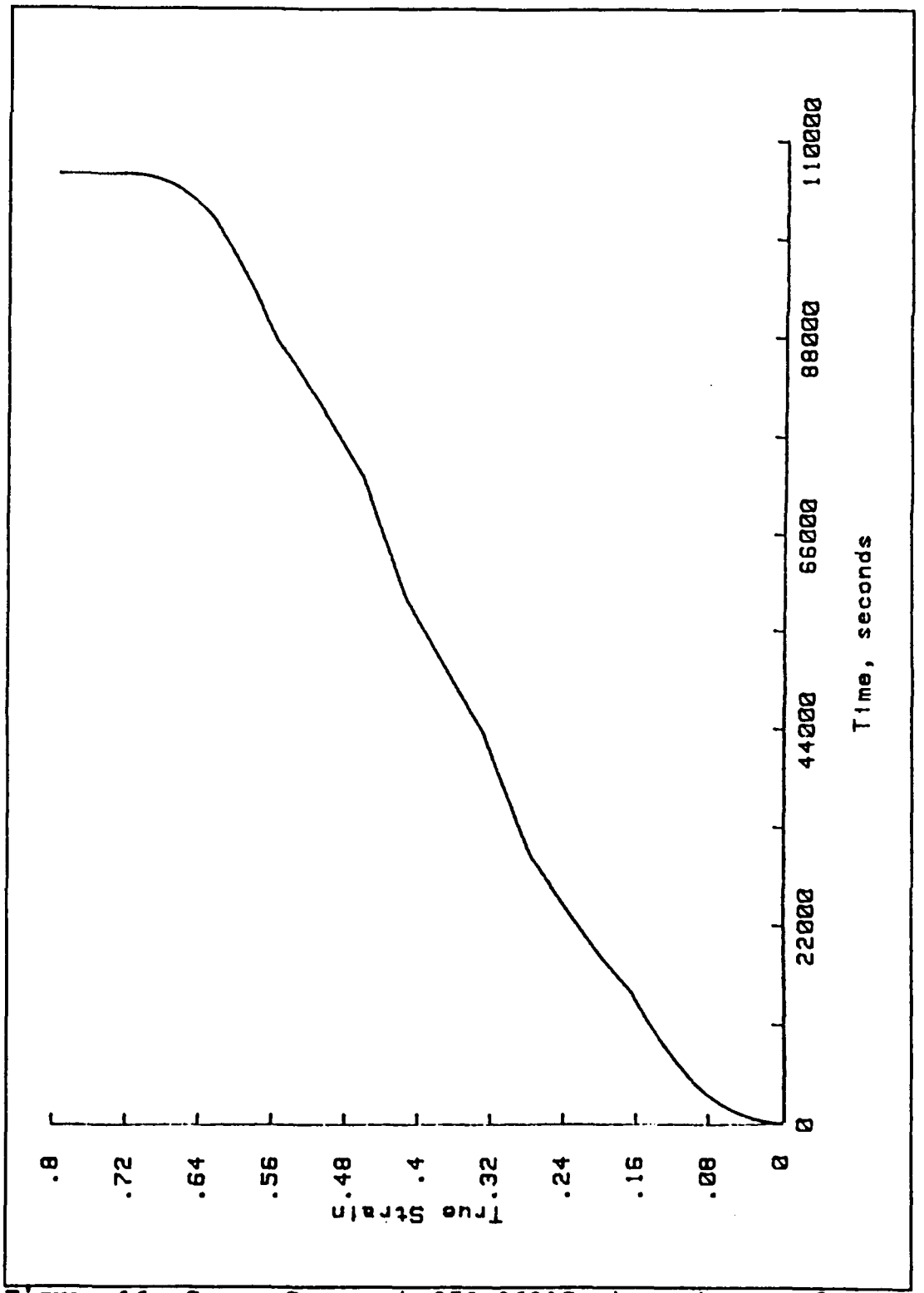

Figure 16. Creep Curve at 350-360°C at a stress of 6.03 MPa: $\dot{\epsilon}_1$ = 6.78 x 10^{-6} sec^{-1} & $\dot{\epsilon}_2$ = 4.23 x 10^{-6} sec^{-1}

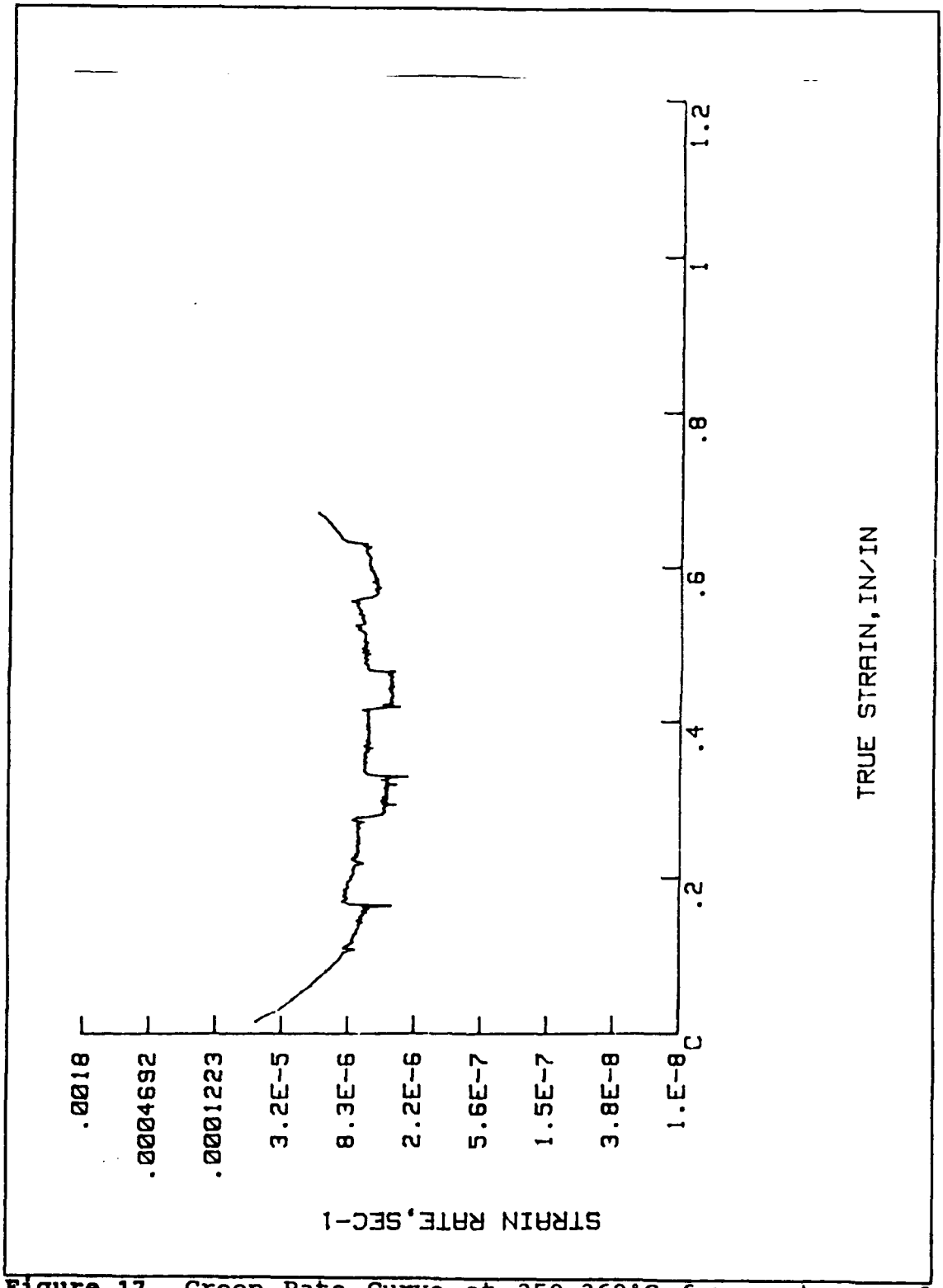

Figure 17. Creep Rate Curve at 350-360°C for a stress of 6.03 MPa: $\dot{\epsilon}_1$ = 6.78 x 10^{-6} sec^{-1} & $\dot{\epsilon}_2$ = 4.23 x 10^{-6} sec^{-1}

Table III. SUMMARY OF ACTIVATION ENERGY FOR TEMPERATURE

%Li	Temp(°C)	$\epsilon_{low}(sec^{-1})$	$\epsilon_{hi}(sec^{-1})$	Q_c (kcal/mole)
0.5	300-310	1.16×10^{-5}	1.95×10^{-5}	34.4
	300-310	3.83×10^{-6}	6.39×10^{-6}	33.8
	350-360	7.44×10^{-6}	1.14×10^{-5}	33.5
	350-360	6.08×10^{-6}	9.30×10^{-6}	33.1
	400-410	6.77×10^{-6}	9.72×10^{-6}	33.0
	400-410	6.03×10^{-6}	8.76×10^{-6}	34.1
	450-460	2.05×10^{-6}	3.04×10^{-6}	41.5
	450-460	1.02×10^{-6}	1.42×10^{-6}	34.3
	450-460	5.03×10^{-6}	7.63×10^{-6}	40.0
	500-510	2.93×10^{-6}	3.95×10^{-6}	35.9
	500-510	4.93×10^{-6}	6.51×10^{-6}	33.3
1.0	300-310	3.75×10^{-6}	6.47×10^{-6}	36.0
	300-310	7.71×10^{-6}	1.32×10^{-6}	35.4
	350-360	4.23×10^{-6}	6.76×10^{-6}	36.7
	350-360	1.81×10^{-5}	1.20×10^{-5}	32.0
	400-410	5.04×10^{-6}	7.26×10^{-6}	33.3
	400-410	1.71×10^{-5}	2.49×10^{-5}	34.3
	400-410	8.44×10^{-6}	1.24×10^{-5}	34.9
	450-460	2.00×10^{-6}	2.79×10^{-6}	35.1
	450-460	3.67×10^{-6}	5.37×10^{-6}	39.8
	500-510	3.45×10^{-6}	4.55×10^{-6}	32.4
	500-510	1.51×10^{-6}	2.00×10^{-6}	33.8

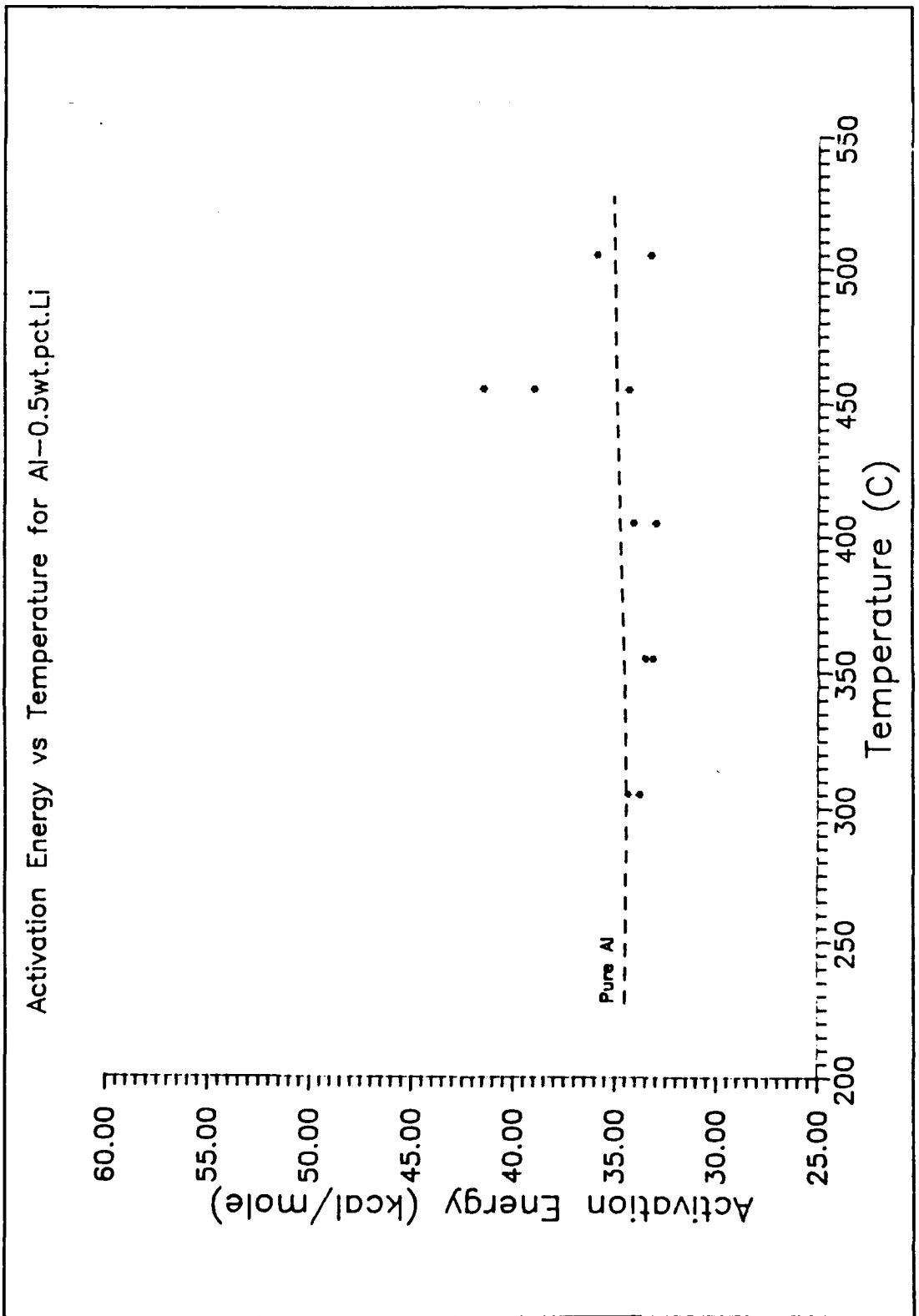

Figure 18. Activation Energy Curve for Al-0.5wt.pct.Li

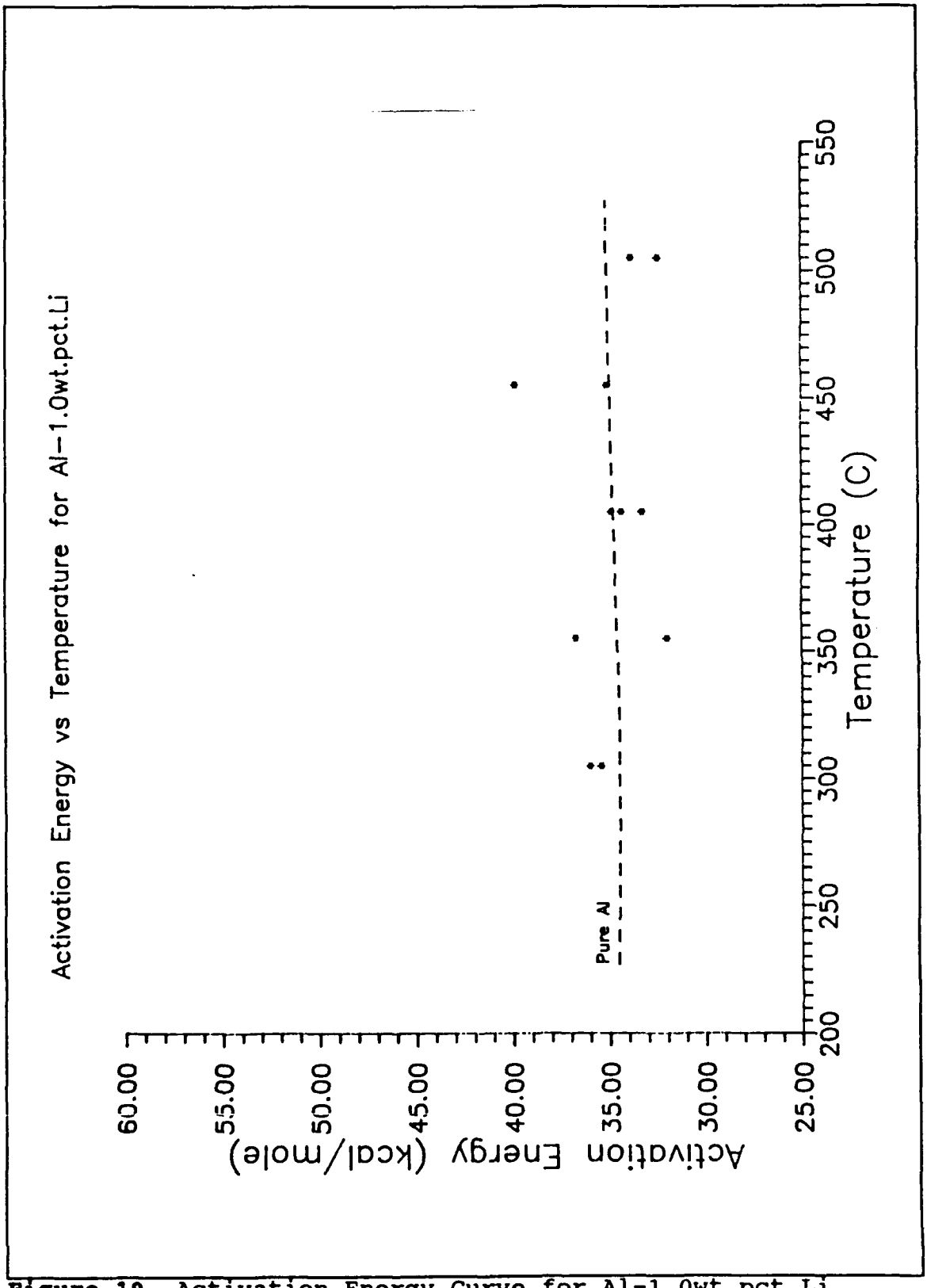

Figure 19. Activation Energy Curve for Al-1.0wt.pct.Li

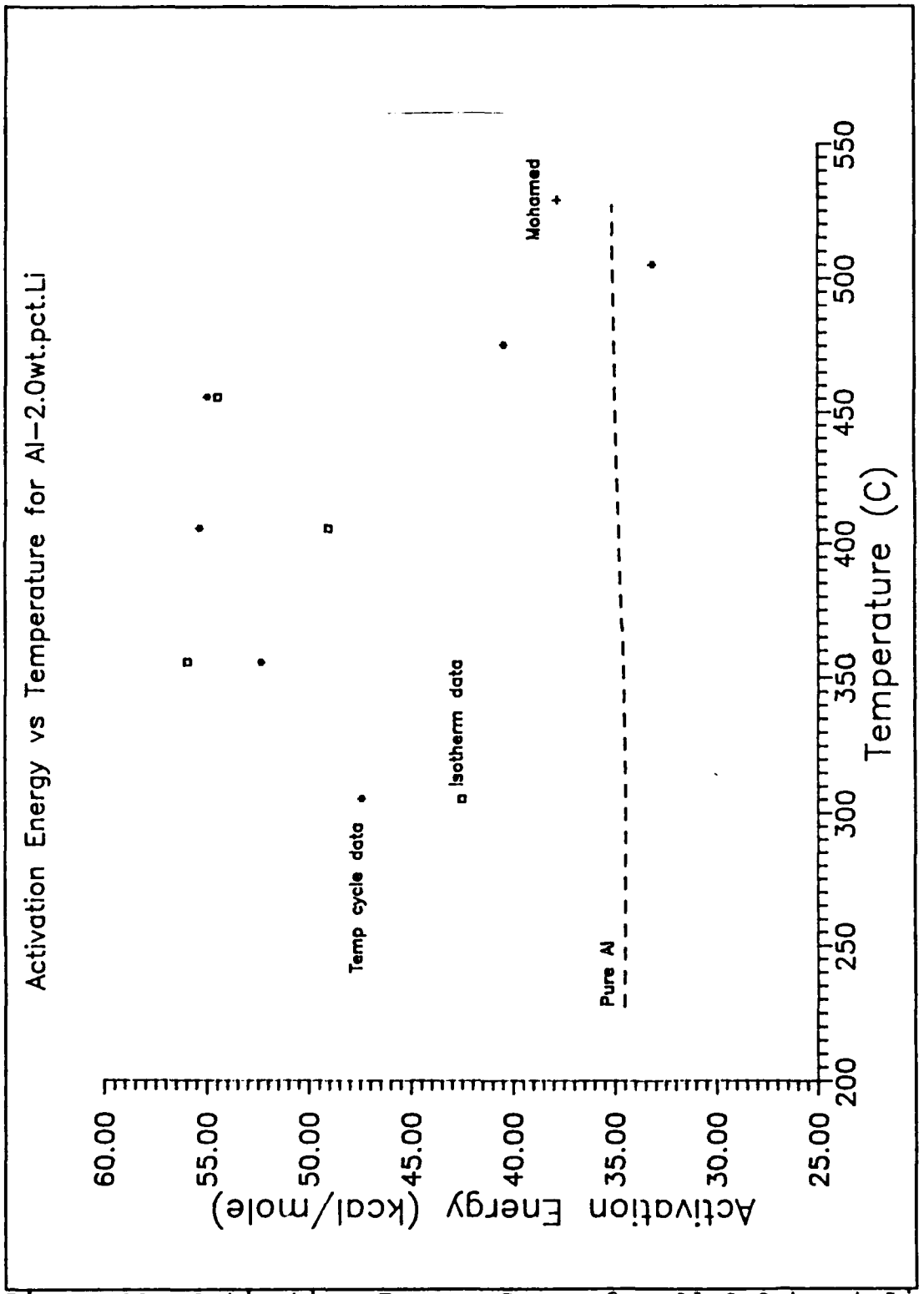

Figure 20. Activation Energy Curve for Al-2.0wt.pct.Li [Ref. 9]

the creep rate was determined from the creep curve as previously described. The mean test temperature [Ref. 15] defined as:

$$\frac{1}{T} = \frac{1}{2}\left(\frac{1}{T_1} + \frac{1}{T_2}\right) \qquad (16)$$

was used in plotting all activation energy results.

The results for the temperature cycling tests on both alloys are summarized in Table III. Data from work by Goodson [Ref. 10] for Al-2.0wt.pct.Li, also determined from temperature cycling tests, and that of Taylor [Ref. 8] for Al-0.5wt.pct.Li and Al-1.0wt.pct.Li from isothermal tests are summarized in Appendix D.

The activation energies are plotted as a function of temperature in Figures 18 and 19. Results from work by Goodson [Ref. 10] are plotted in Figure 20 for comparison purposes. As shown in Figure 18 the activation energy Q_c for Al-0.5wt.pct.Li varies between 33.1 and 35.9 kcal/mole at temperatures of 300,350,400, and 500°C, and in a manner similar to that for pure Aluminum in the same temperature interval. Sherby and Burke [Ref. 6] have shown that the activation energy for pure Aluminum, when determined at constant stress, varies in a gradual manner from 34.5 to 36.4 kcal/mole in the 300-500°C temperature interval. In fact Sherby and Burke [Ref. 6] have shown that the activation energy is constant if this gradual variation is corrected for temperature dependence of the elastic modulus. The exception to this pattern in the present data is at 450°C, where there is an anomalously high Q_c in two of three tests. The activation energy for the Al-1.0wt.pct.Li is also similar to

that for pure Aluminum, ranging from 32 to 39.8 kcal/mole, again the highest value being at the 450°C test point.

Goodson [Ref. 10] reported that the Al-2.0wt.pct.Li exhibits a similar stress dependence and formation of subgrain structure as observed in pure Aluminum. However, the values of Q_c are appreciably higher. He attributed this to a more strongly temperature dependent modulus in this alloy as compared to pure Aluminum, or to a greater temperature dependence in the stacking fault energy.

Goodson [Ref. 10] suggests that the ordering of the Lithium in the solid solution, as proposed by Radmilovic, Fox, and Thomas [Ref. 5], was responsible for the increased temperature dependence of the modulus. Thus upon heating of the alloy at temperatures above the solvus temperature the Al-2.0wt.pct.Li is expected to exhibit a mixture of ordered regions of higher Lithium content and regions depleted in Lithium content. It was further suggested that these ordered regions persisted to temperatures as high as 450°C, at which temperature the structure undergoes an order-disorder transformation. Above this temperature the structure exhibits a random distribution of Lithium in the solid solution. As previously stated, Radmilovic, Fox, and Thomas [Ref. 5] have postulated that such an order-disorder reaction occurs in the as quenched Al-Li alloys containing greater than 1.6 weight percent Lithium, which also corresponds to the solvus for Al-LI at 300°C. Fox and Thomas [Ref.] concluded that Aluminum and Lithium atoms exhibit a strong tendency to bond based on the increased electron charge density between nearest neighbor atoms which is reflected in the increased modulus at room temperature.

Conversely, as pointed out by Goodsor [Ref. 10], for random solid solutions we can anticipate a reduced modulus at temperatures approaching the melting temperature because of the lower value of T_m for the Al-2.0wt.pct.Li alloy as compared to the T_m for pure Aluminum.

In summary, Goodson [Ref. 10] proposed that for the temperature interval over which the ordering reaction occurs the modulus of elasticity will exhibit a stronger temperature dependence than that of pure Aluminum which is reflected in the creep response of the alloy.

Taylor's [Ref. 8] preliminary study of the Al-0.5.wt.pct.Li and Al-1.0wt.pct.Li alloys suggest a similar trend based on limited data. However based on this research it appears that the Lithium content has little effect on the activation energy for creep in the 0.5 and 1.0 weight percent Lithium alloys in the 300-500°C range. In contrast the Al-2.0wt.pct.Li alloy develops a substantially higher activation energy in the 300-450°C range.

D. DISCUSSION

The stress dependence for creep of all three alloys correlates well with that for pure Aluminum. The creep rate appears to follow the power law dependence with the stress exponent equal to approximately 5 for temperatures above 300°C. Also, subgrain formation occurs during primary creep.

The activation energy for the Al-0.5wt.pct.Li and Al-1.0wt.pct.Li alloys determined from this research correlate very well for that of pure Aluminum. The data from the Al-0.5wt.pct.Li and Al-1.0wt.pct.Li suggest that as the Lithium concentration decreases the tendency for ordering diminishes or is eliminated. At high Lithium concentrations it is

difficult to suppress precipitate formation, however at lower Lithium concentrations quenching will suppress the formation of precipitates. By suppressing the precipitate formation through quenching the kinetics have been affected. This would suggest that the modulus of these alloys might exhibit the same temperature dependence as pure Aluminum.

V. CONCLUSIONS

The following conclusions can be drawn concerning the behavior and characteristics of binary Aluminum-Lithium alloys of 0.5, 1.0, and 2.0 weight percent Lithium:

1. The alloys exhibit a creep response consisting of a well defined primary, a secondary, and a tertiary phase. The characteristic shape is similar to that of pure Aluminum.

2. The alloys exhibit a similar stress dependence as that of pure Aluminum ($n \sim 5$), with values of n ranging from 4.3 to 6.3 between 300 and 500°C.

3. Lithium additions of 0.5 and 1.0 weight percent modestly increase the strength of the alloys above that for pure Aluminum, while a 2.0 weight percent addition has a more pronounced effect, particularly as the temperature decreases.

4. Lithium addition of less than 2.0 weight percent has little effect on the activation energy for creep. Alloys in this class exhibit activation energies similar to that of pure Aluminum.

APPENDIX A. CREEP AND CREEP RATE CURVES FOR Al-0.5%Li

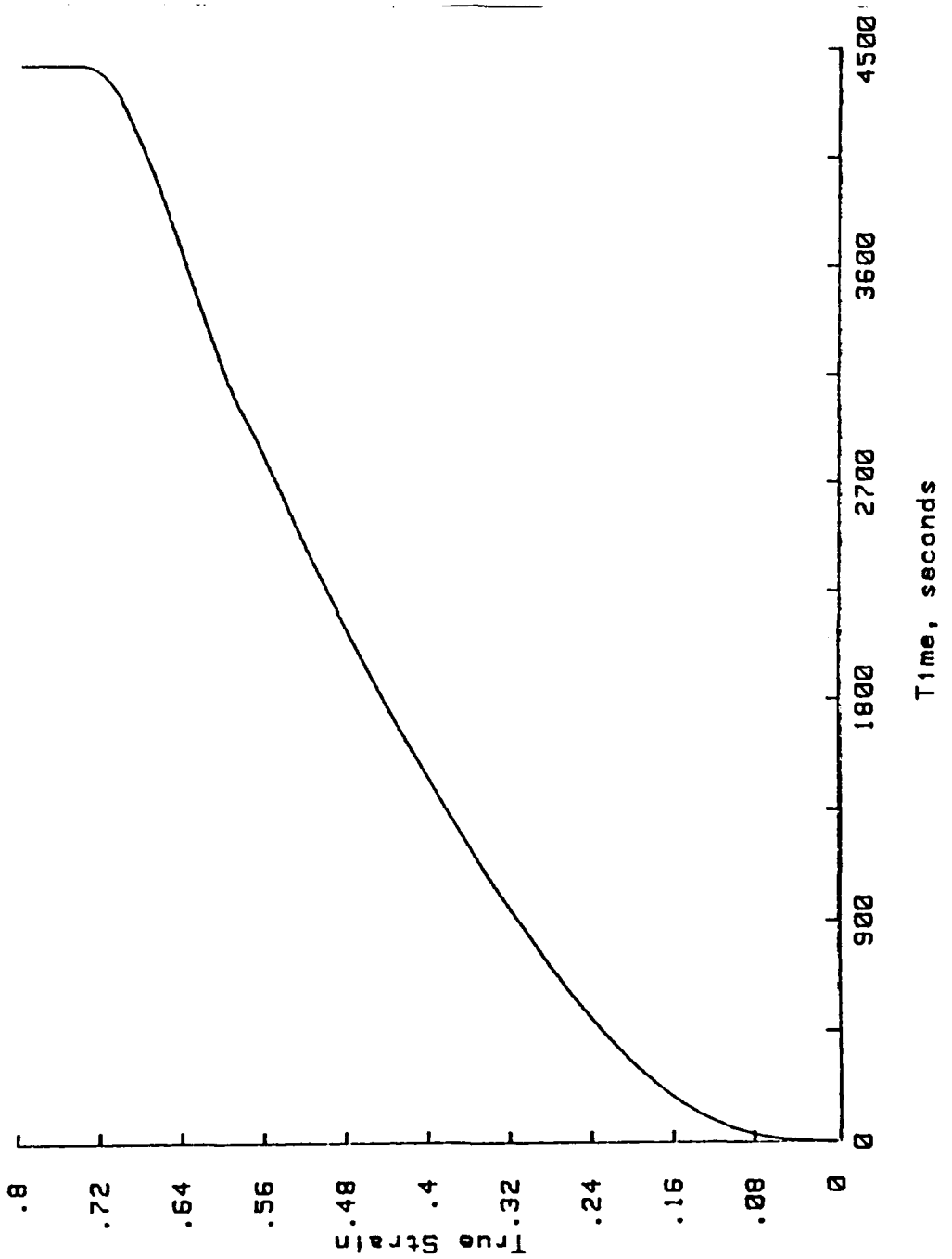

Figure 21. Creep Curve at 300°C for a stress of 15.8 MPa: $\dot{\epsilon}_{min} = 1.15 \times 10^{-4}$ sec^{-1}

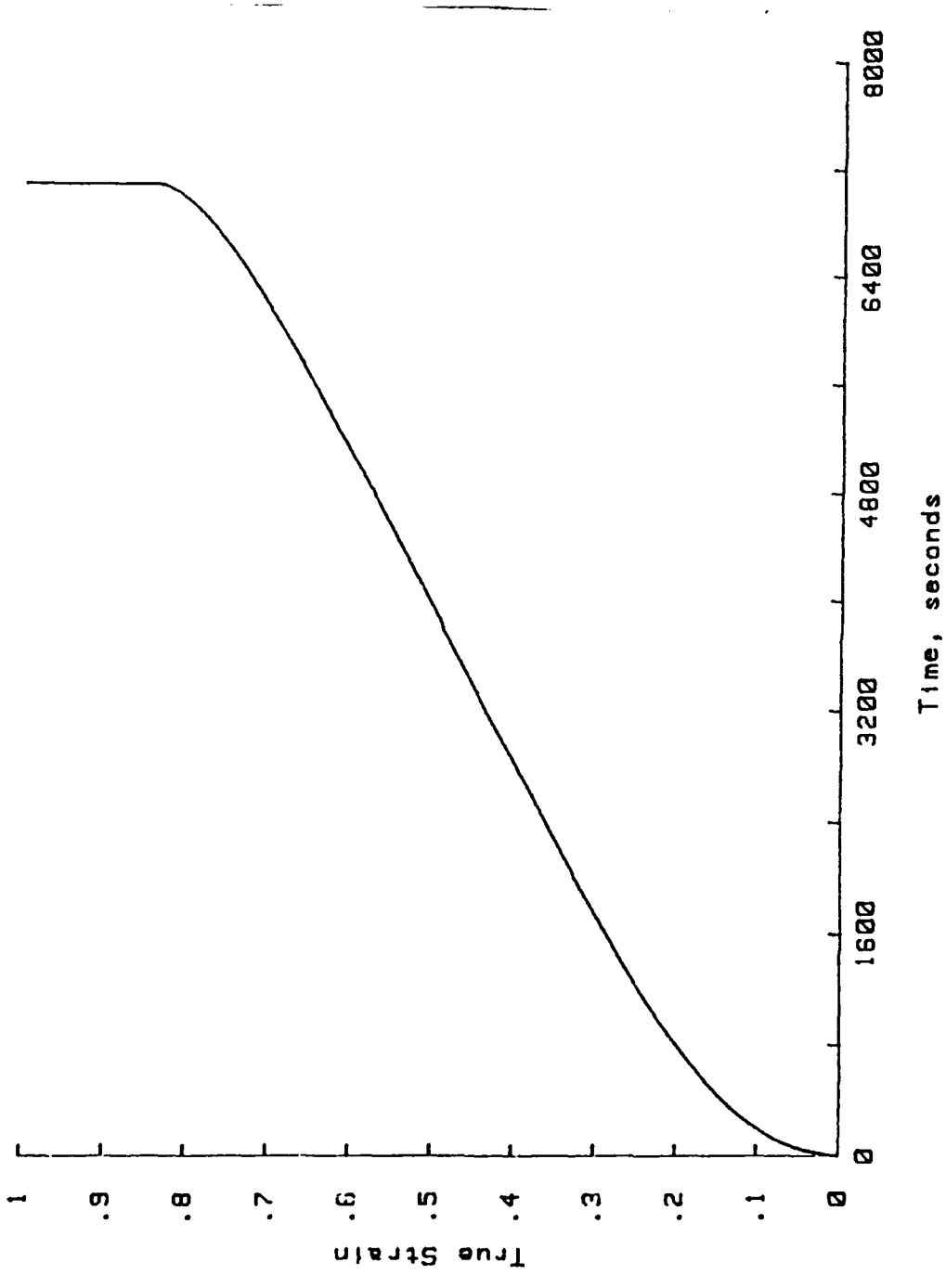

Figure 22. Creep Curve at 350°C for a stress of 8.84 MPa: $\dot{\epsilon}_{min} = 8.34 \times 10^{-5}$ sec^{-1}

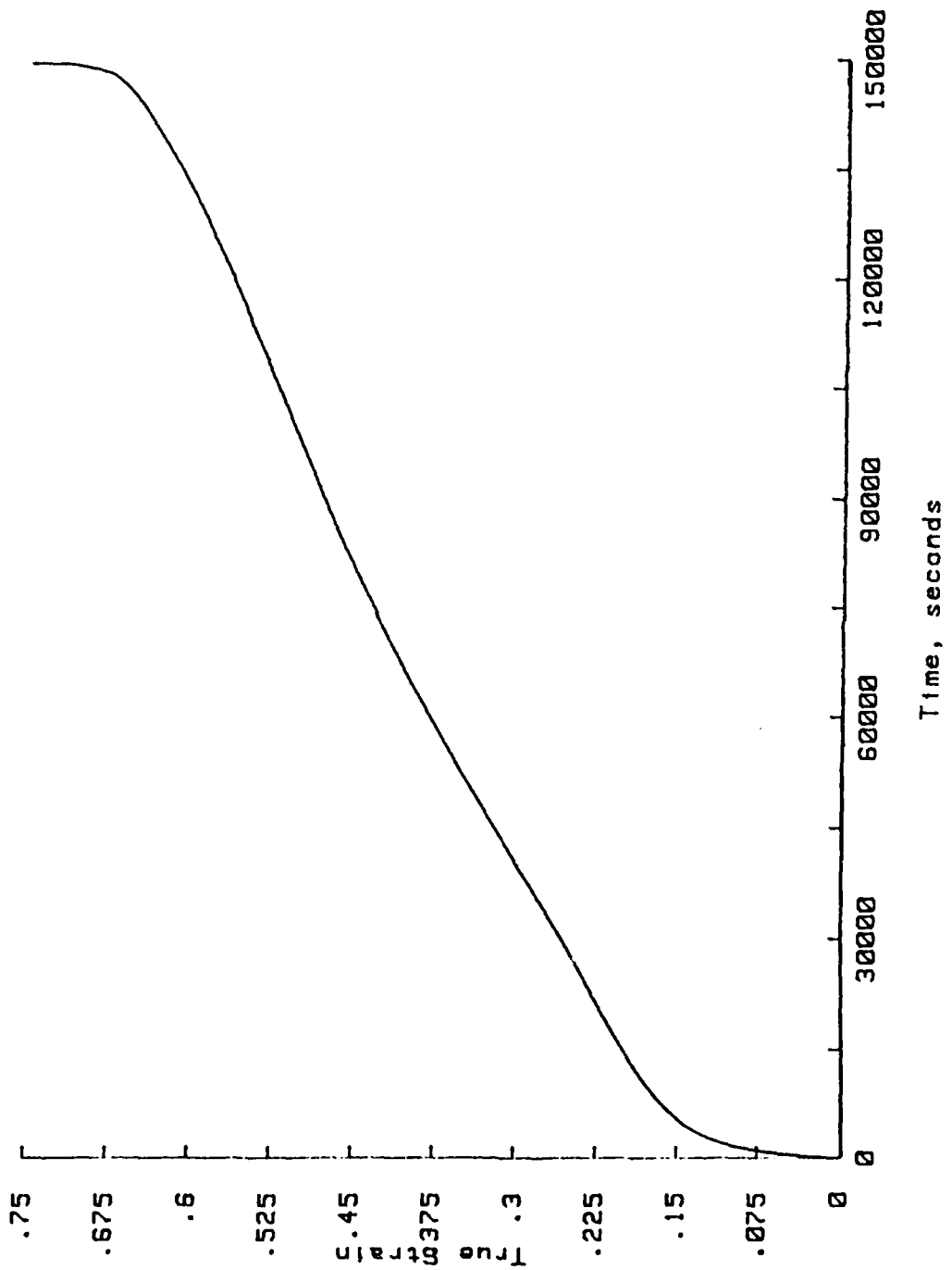

Figure 23. Creep Curve at 350°C for a stress of 5.42 MPa: $\dot{\epsilon}_{min}$ = 3.75 x 10^{-6} sec^{-1}

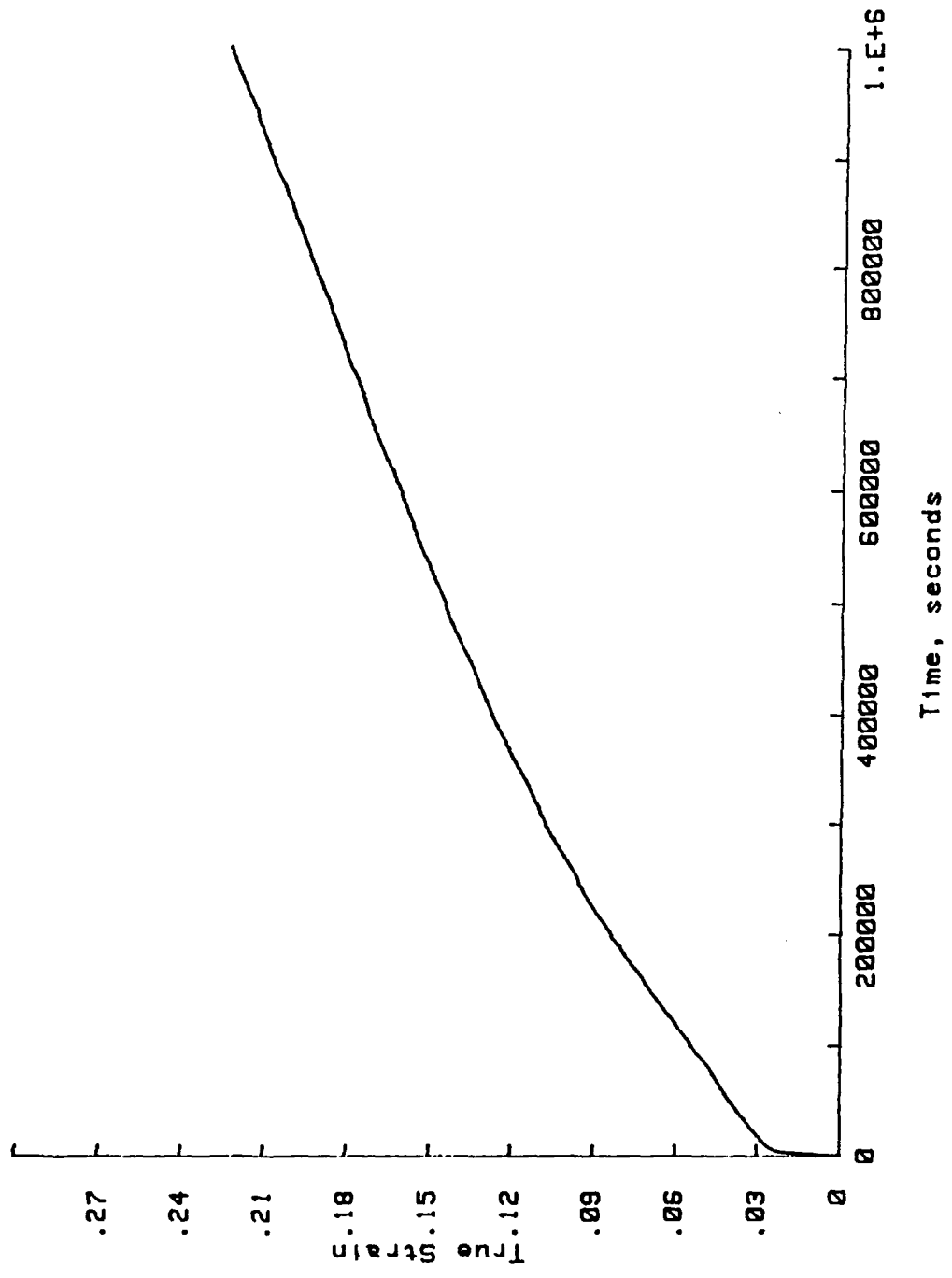

Figure 24. Creep Curve at 350°C for a stress of 3.58 MPa: $\dot{\epsilon}_{min} = 2.61 \times 10^{-7}$ sec^{-1}

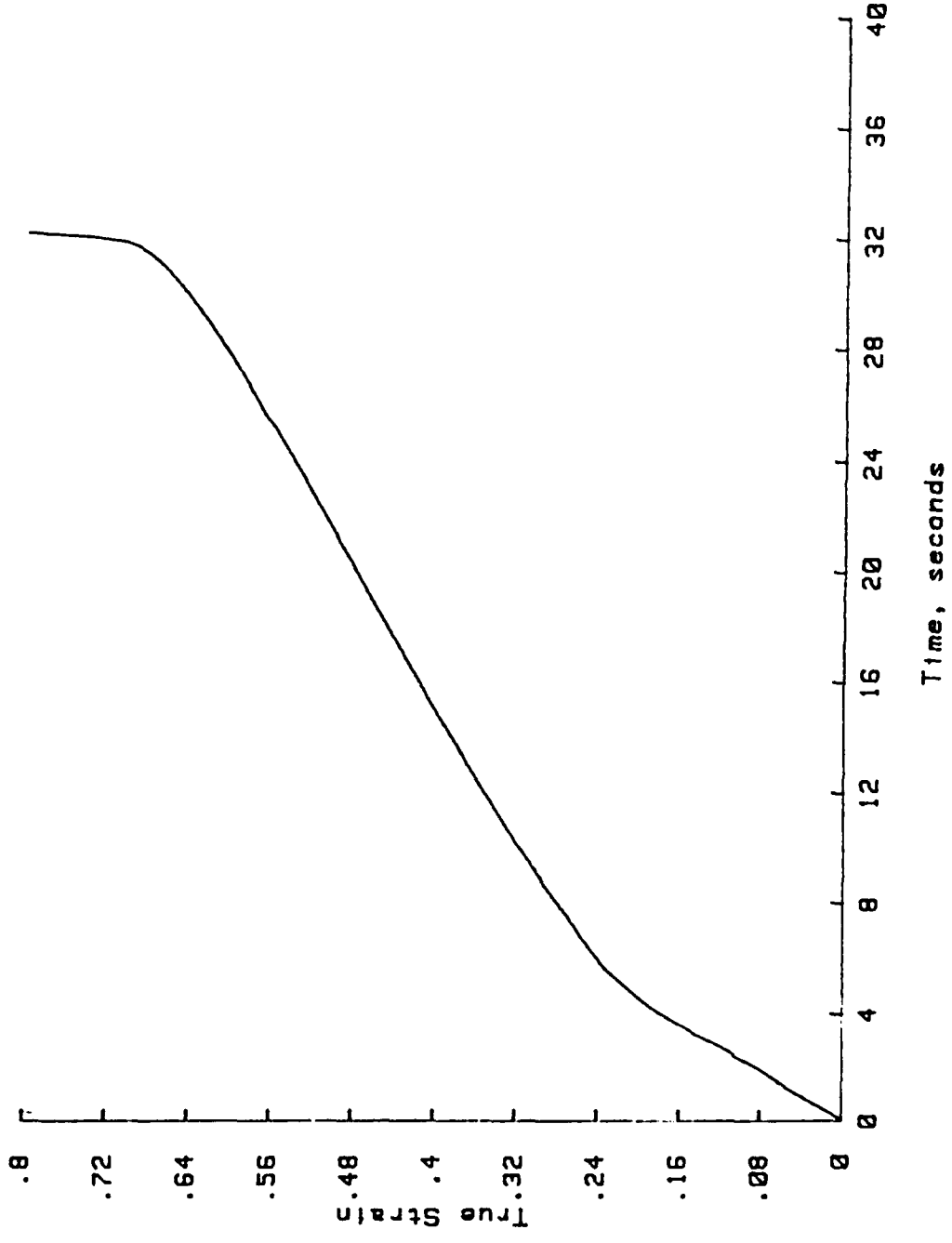

Figure 25. Creep Curve at 400°C for a stress of 14.67 MPa: $\dot{\epsilon}_{min}$ = 1.54 x 10^{-2} sec^{-1}

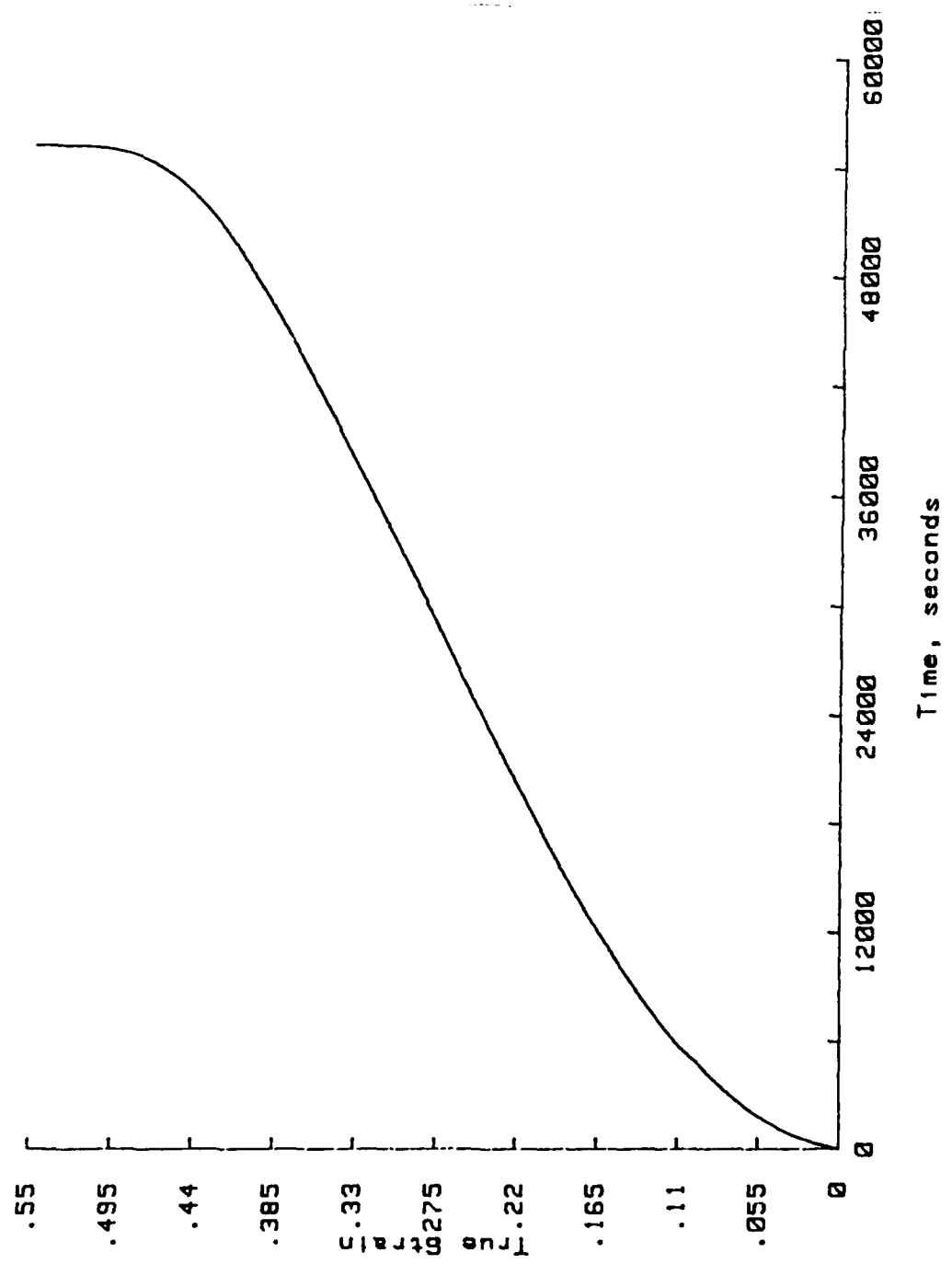

Figure 26. Creep Curve at 400°C for a stress of 3.07 MPa: $\dot{\epsilon}_{min}$ = 9.1 x 10^{-8} sec^{-1}

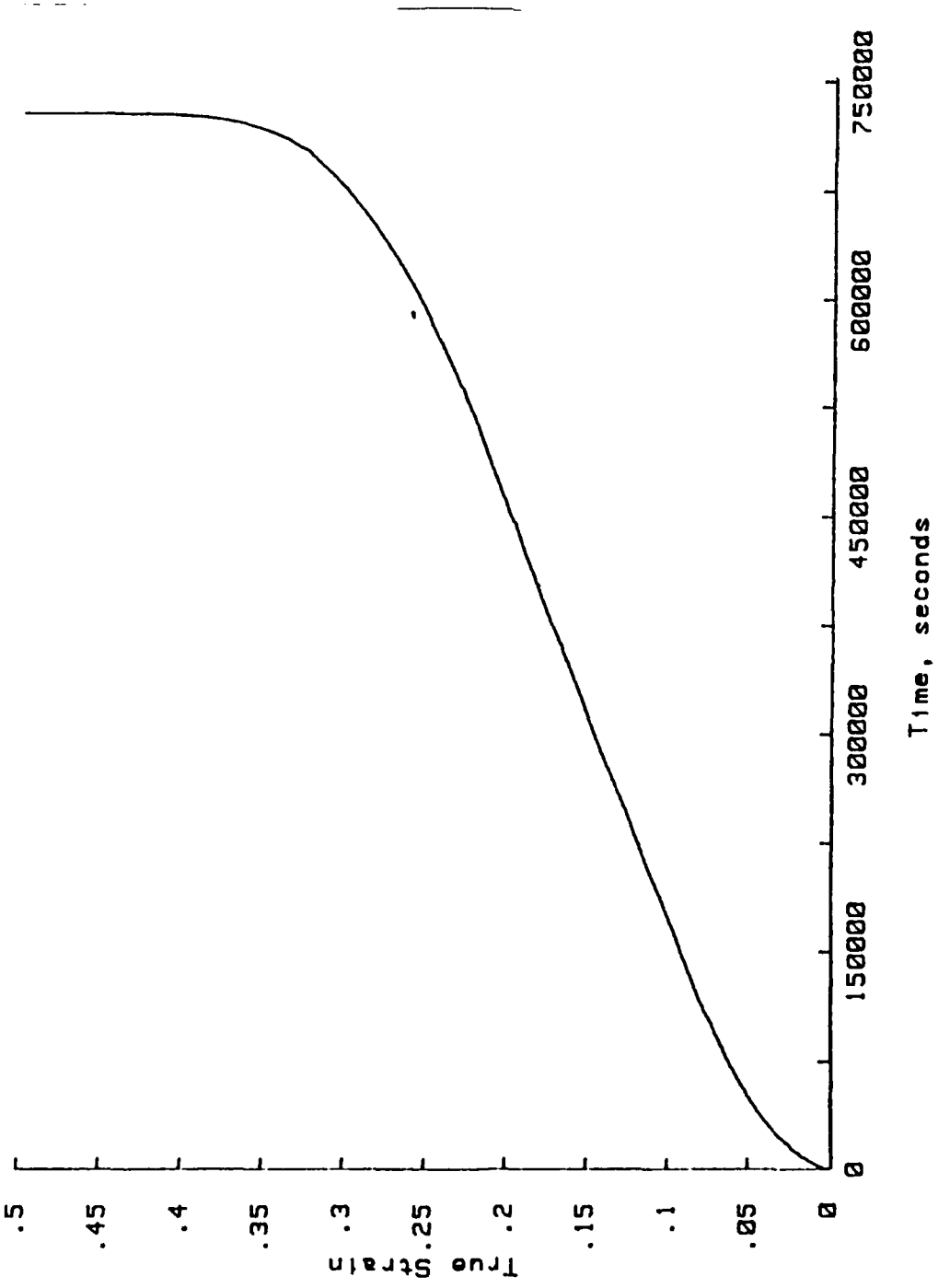

Figure 27. Creep Curve at 400°C for a stress of 1.81 MPa: $\dot{\epsilon}_{min}$ = 4.76 x 10^{-7} sec^{-1}

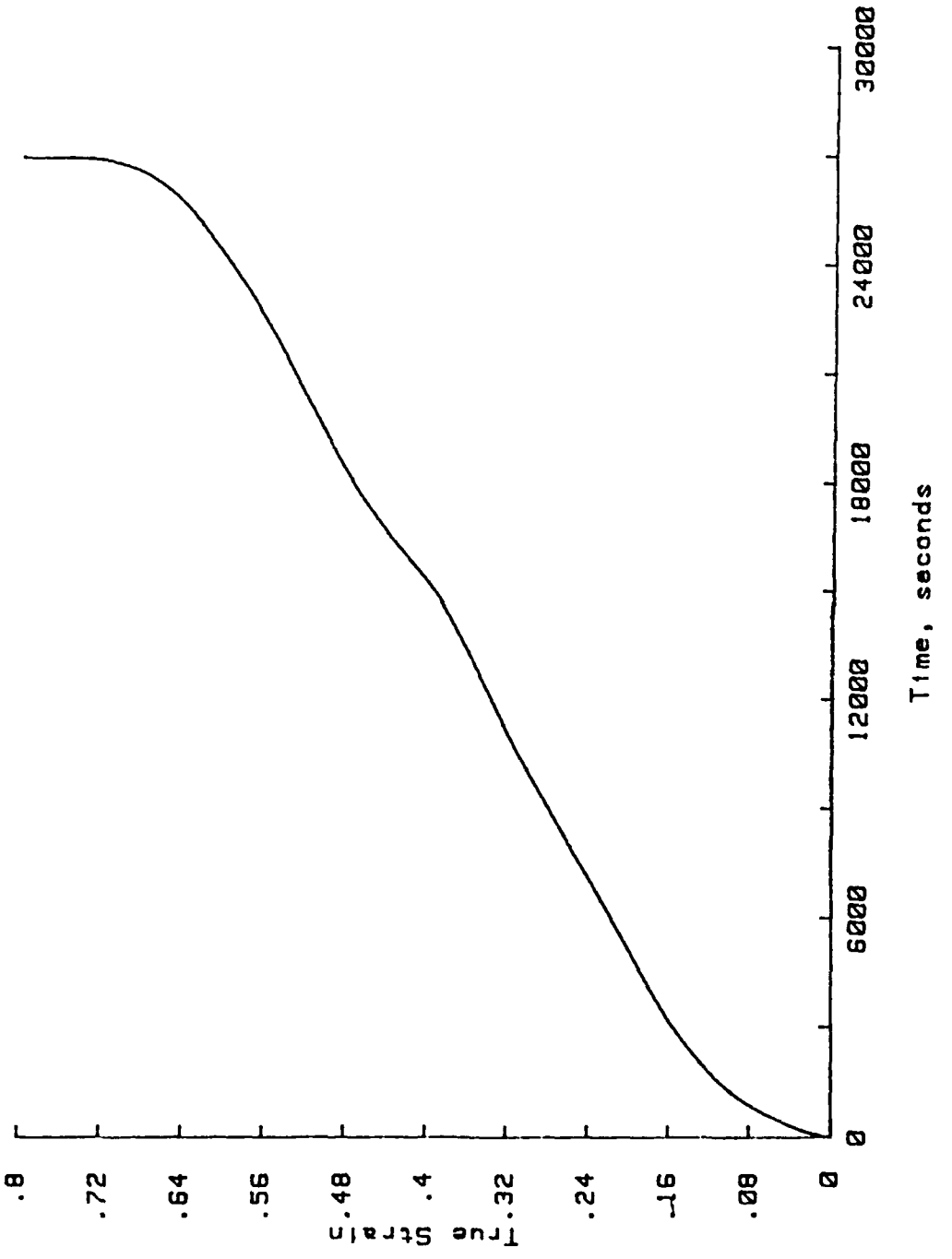

Figure 28. Creep Curve at 450°C for a stress of 2.67 MPa: $\dot{\epsilon}_{min} = 1.79 \times 10^{-8}$ sec^{-1}

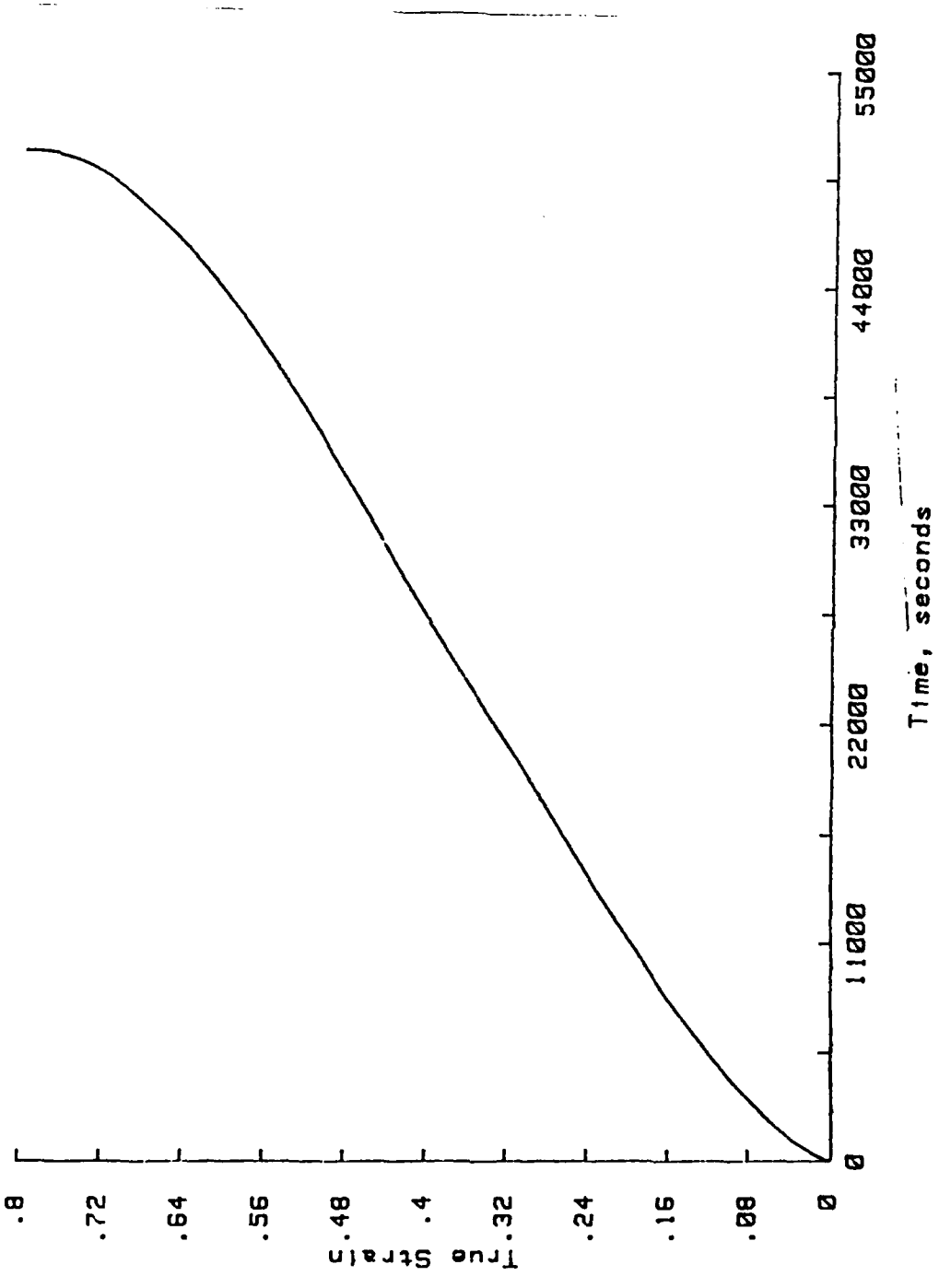

Figure 29. Creep Curve at 450°C for a stress of 2.10 MPa: $\dot{\epsilon}_{min} = 1.28 \times 10^{-5}$ sec^{-1}

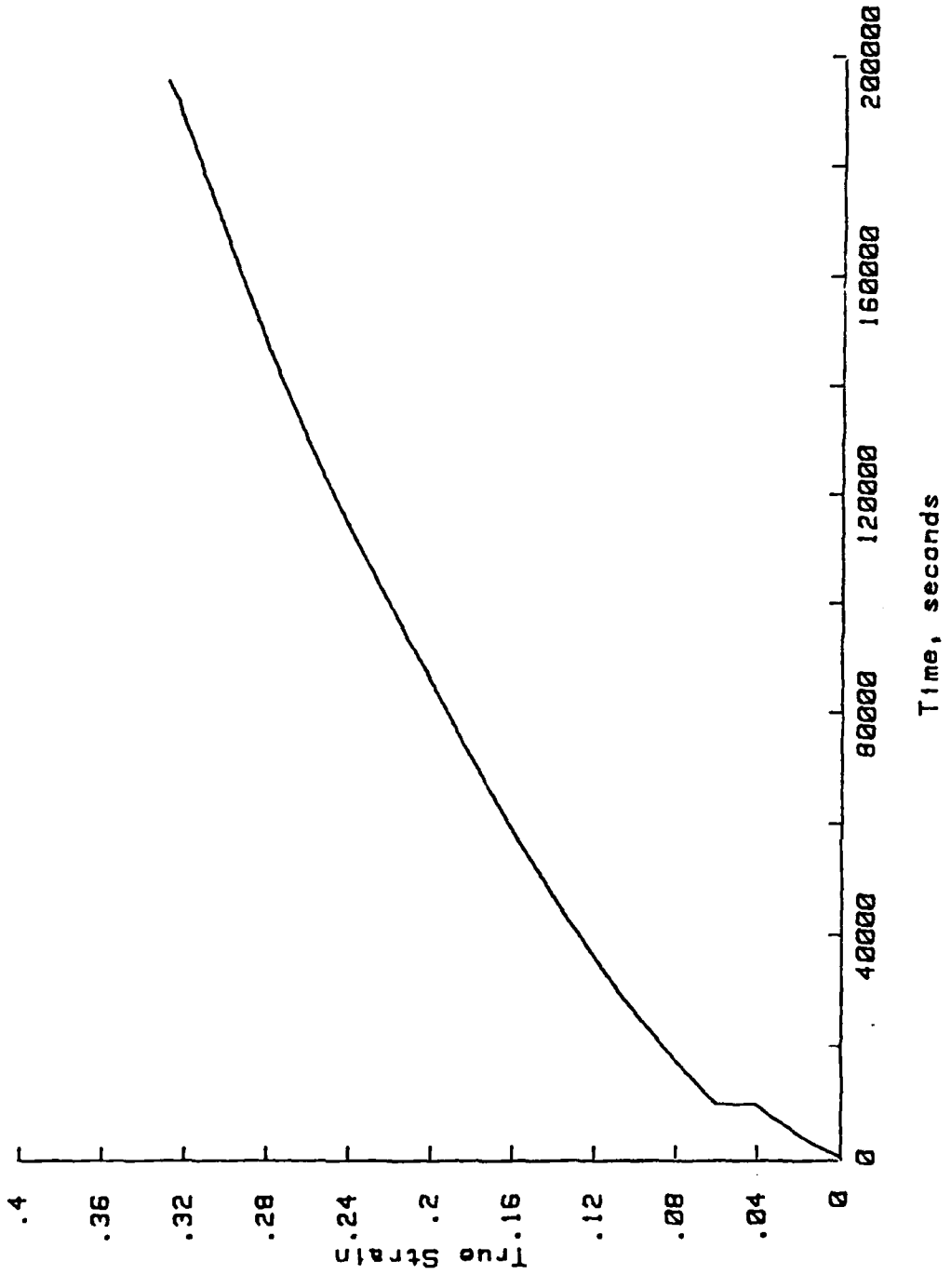

Figure 30. Creep Curve at 450°C for a stress of 1.63 MPa: $\dot{\epsilon}_{min}$ = 1.33 x 10^{-6} sec^{-1}

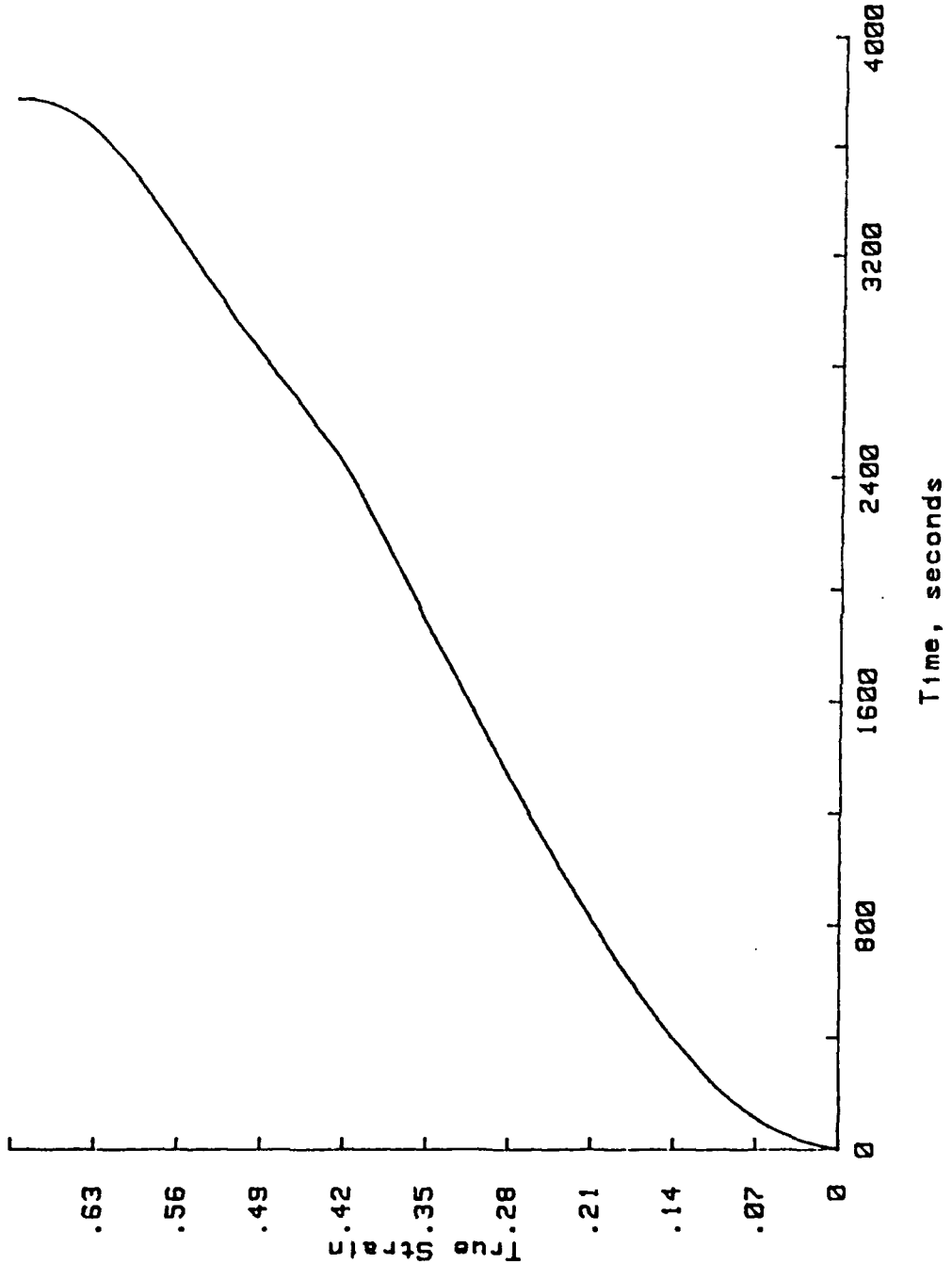

Figure 31. Creep Curve at 500°C for a stress of 2.41 MPa: $\dot{\epsilon}_{min} = 2.0 \times 10^{-4}$ sec^{-1}

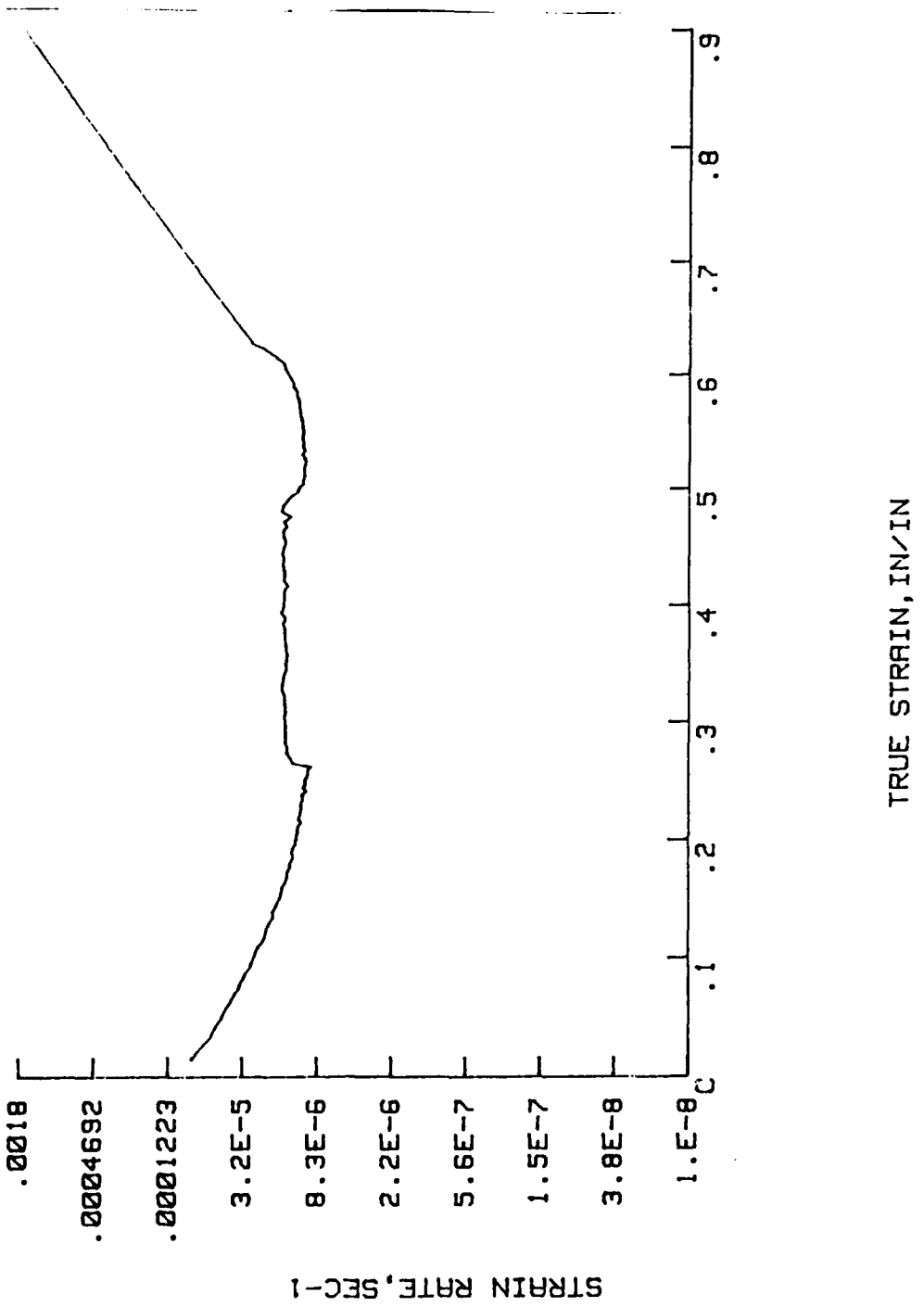

Figure 32. Creep Rate Curve at 300-310°C for a stress of 8.84 MPa: $\dot{\epsilon}_1$ = 1.95 x 10^{-5} sec^{-1} & $\dot{\epsilon}_2$ = 1.16 x 10^{-5} sec^{-1}

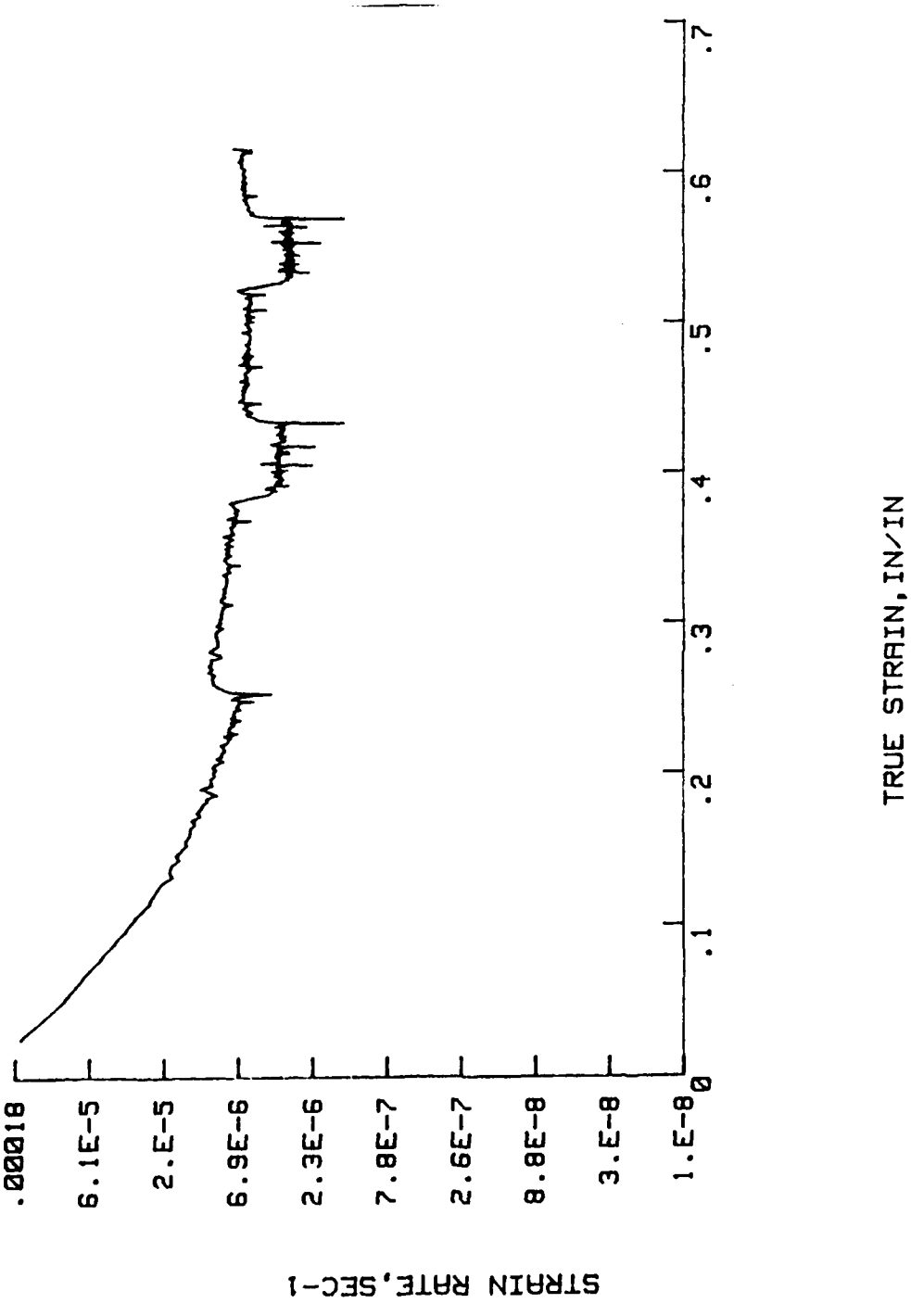

Figure 33. Creep Rate Curve at 300-310°C for a stress of 9.84 MPa: $\dot{\epsilon}_1$ = 6.39 x 10^{-6} sec^{-1} & $\dot{\epsilon}_2$ = 2.83 x 10^{-6} sec^{-1}

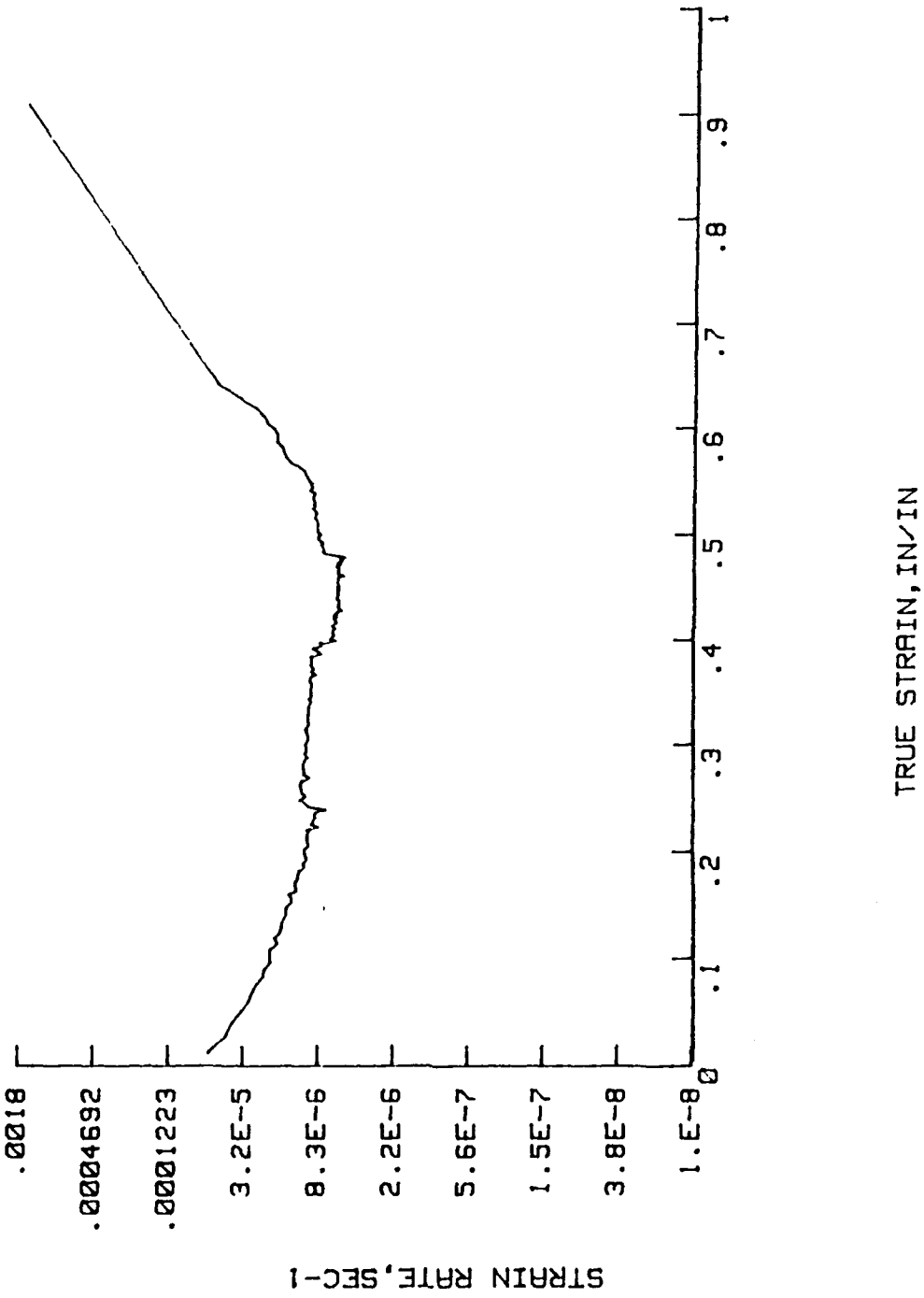

Figure 34. Creep Rate Curve at 350-360°C for a stress of 5.13 MPa: $\dot{\epsilon}_1 = 9.30 \times 10^{-6}$ sec^{-1} & $\dot{\epsilon}_2 = 6.08 \times 10^{-6}$ sec^{-1}

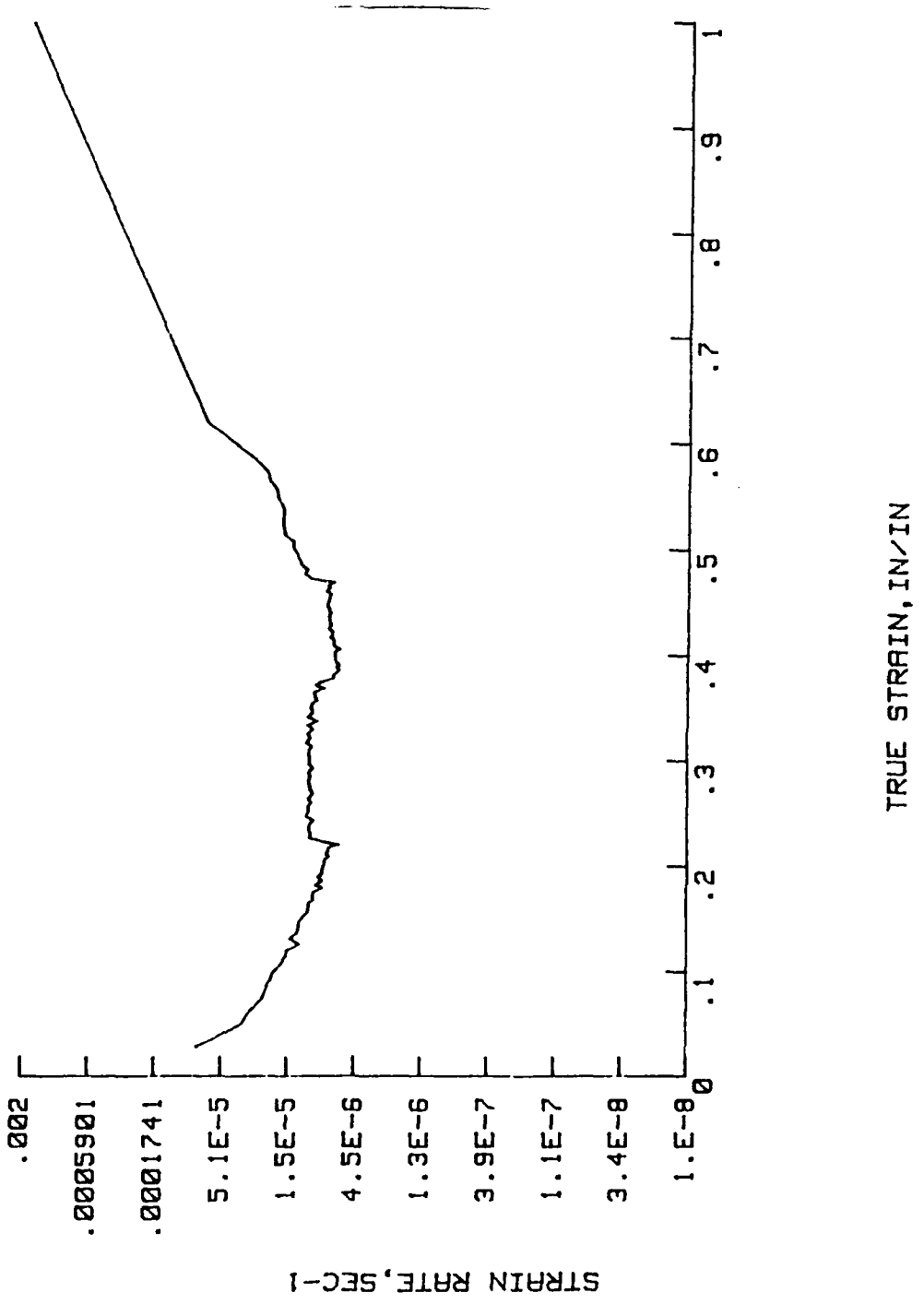

Figure 35. Creep Rate Curve at 350-360°C for a stress of 5.75 MPa: $\dot{\epsilon}_1$ = 1.20 x 10^{-5} sec^{-1} & $\dot{\epsilon}_2$ = 8.13 x 10^{-6} sec^{-1}

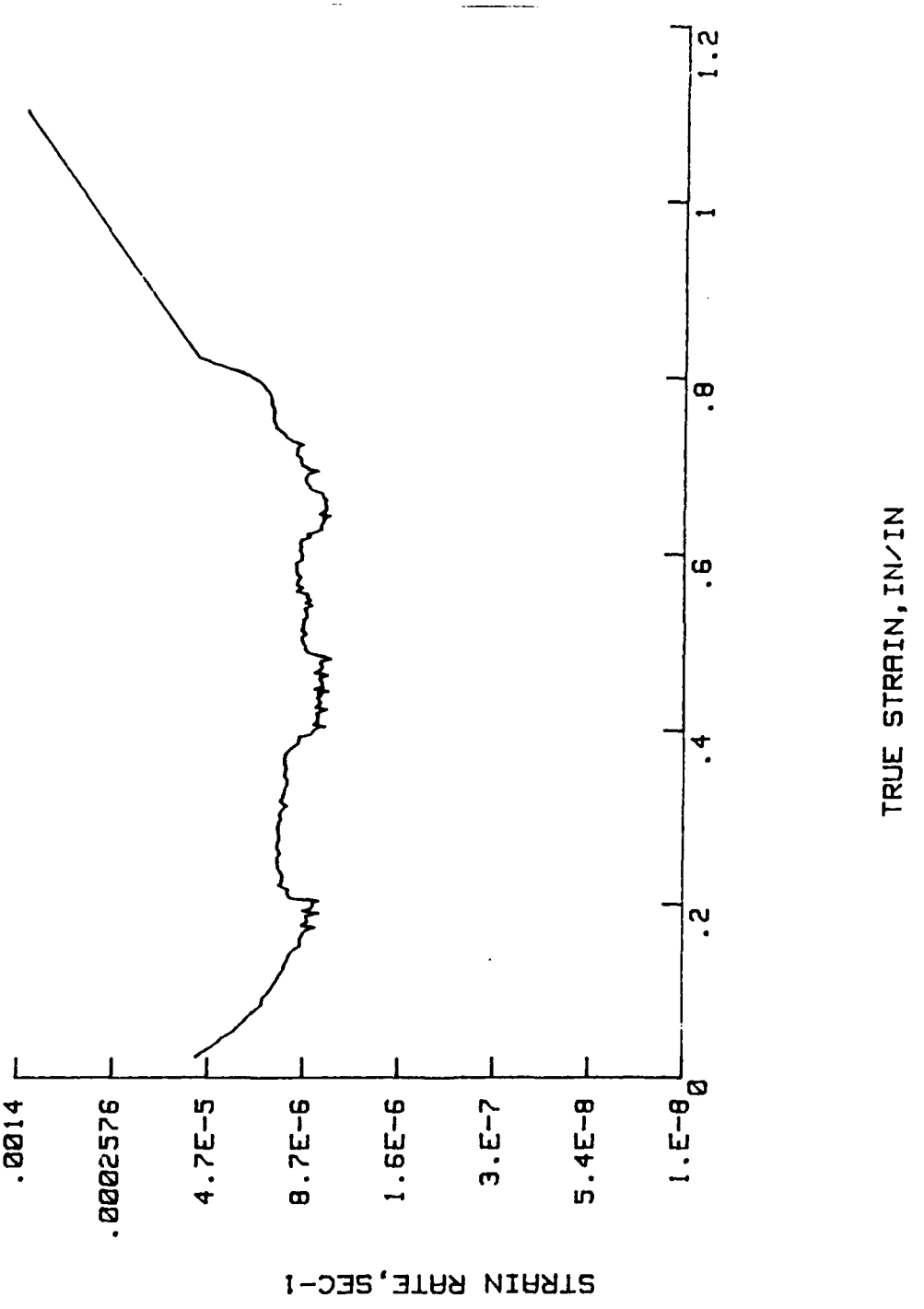

Figure 36. Creep Rate Curve at 400-410°C for a stress of 3.02 Mpa: $\dot{\epsilon}_1$ = 9.72 x 10^{-6} sec^{-1} & $\dot{\epsilon}_2$ = 6.77 x 10^{-6} sec^{-1}

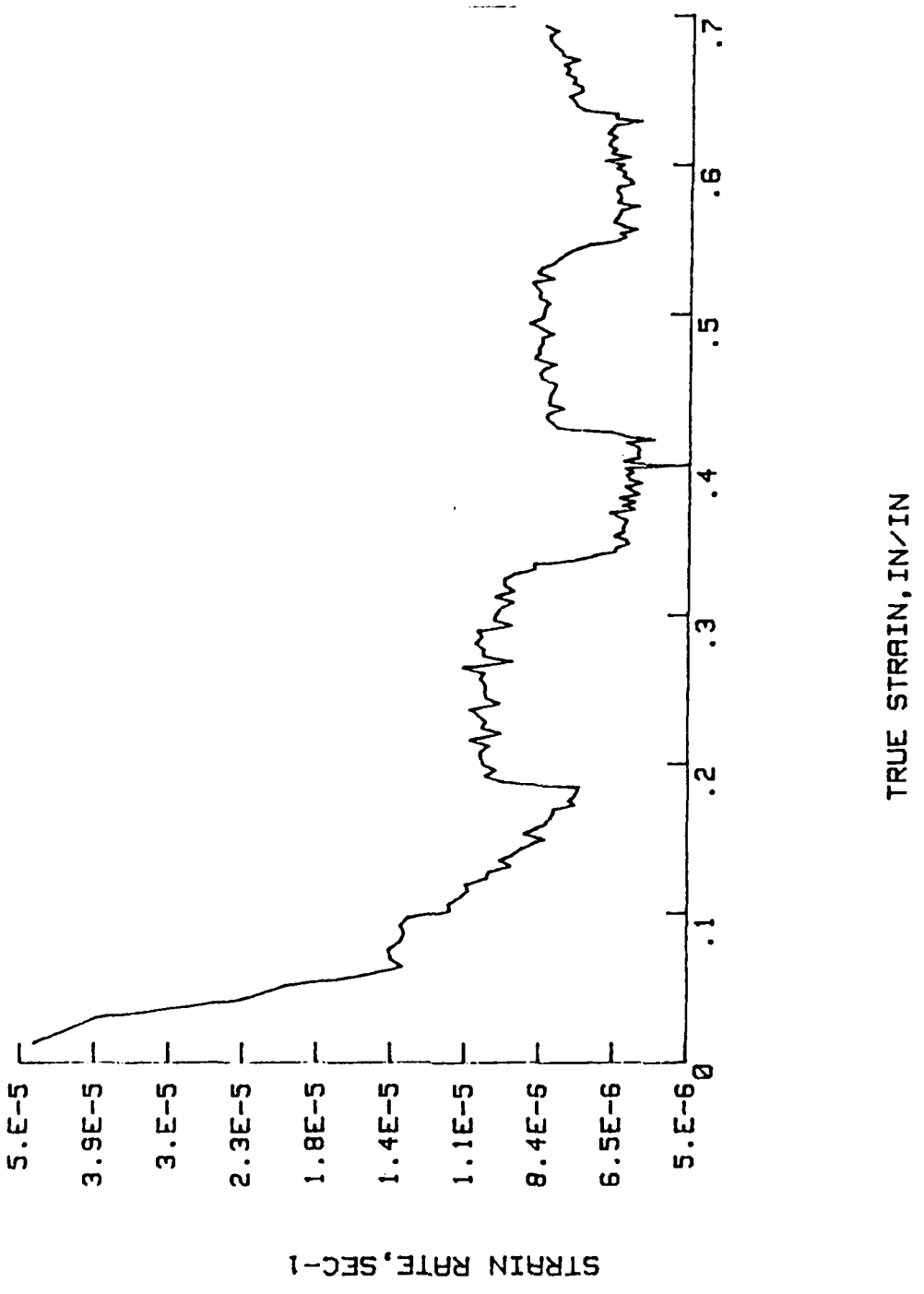

Figure 37. Creep Rate Curve at 400-410°C for a stress of 2.84 MPa: $\dot{\epsilon}_1$ = 8.76 x 10^{-6} sec^{-1} & $\dot{\epsilon}_2$ = 6.03 x 10^{-6} sec^{-1}

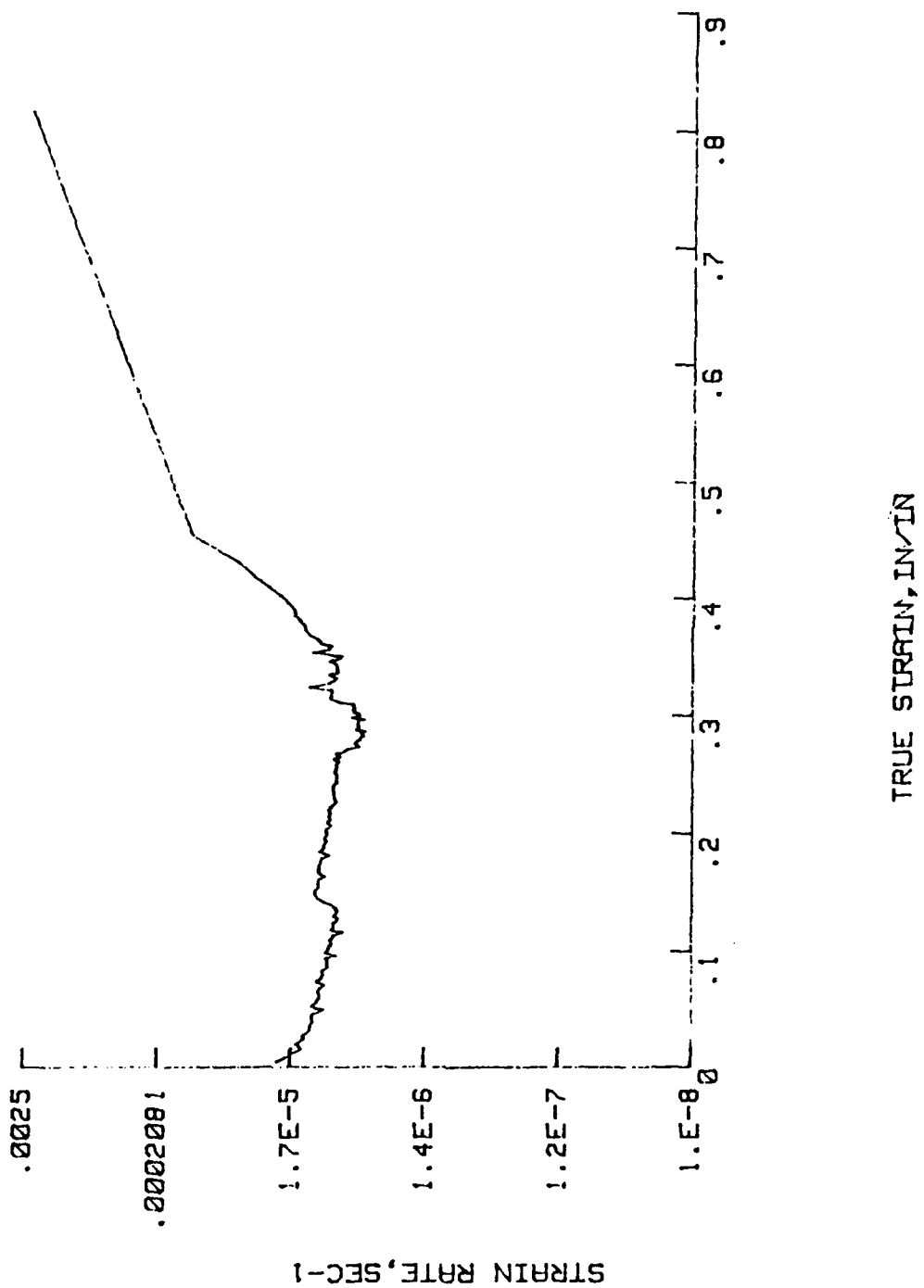

Figure 38. Creep Rate Curve at 450-460°C for a stress of 1.67 MPa: $\dot{\epsilon}_1$ = 7.63 x 10^{-6} sec^{-1} & $\dot{\epsilon}_2$ = 5.26 x 10^{-6} sec^{-1}

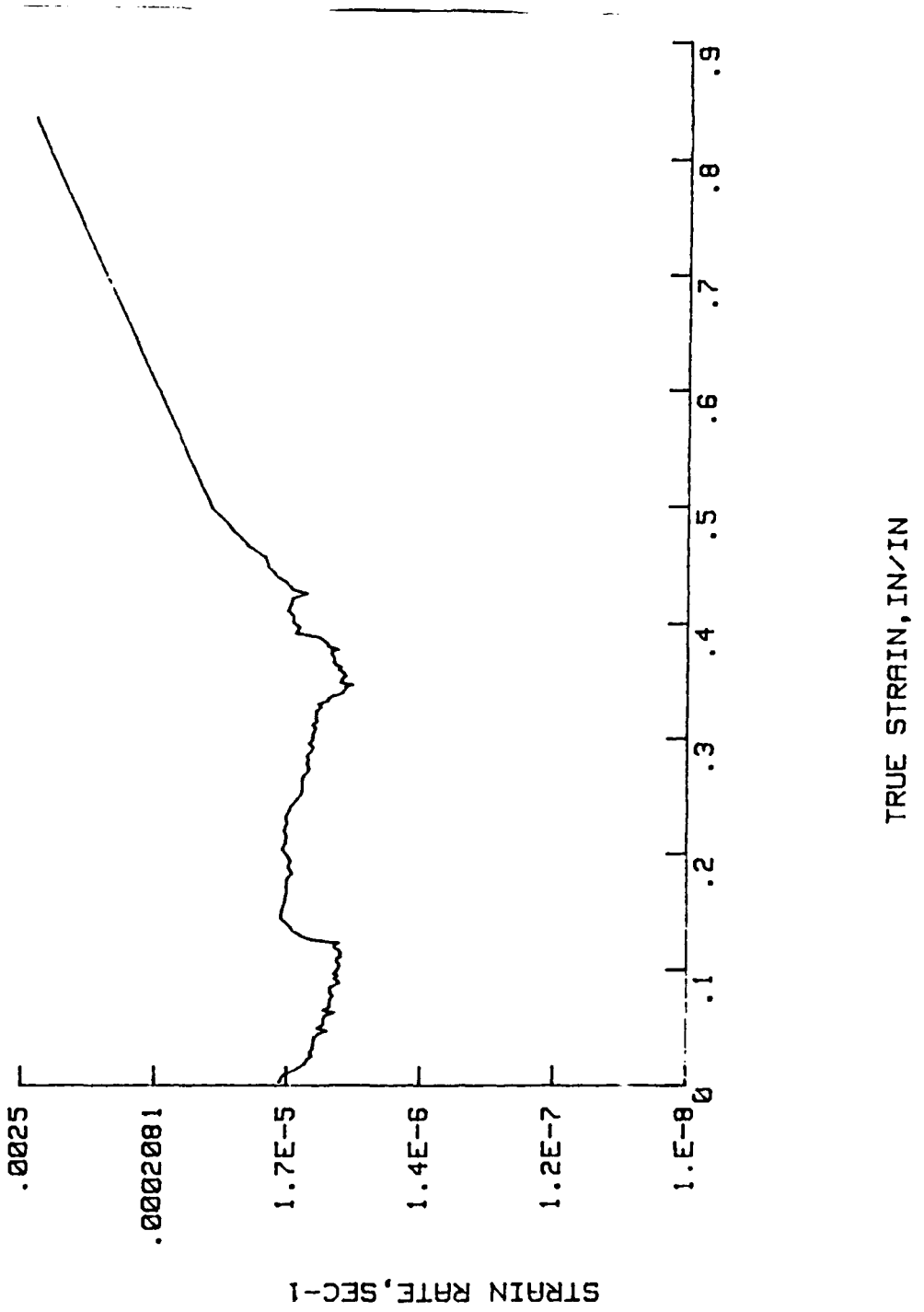

Figure 39. Creep Rate Curve at 450-460°C for a stress of 1.71 MPa: $\dot{\epsilon}_1$ = 1.42 x 10^{-5} sec^{-1} & $\dot{\epsilon}_2$ = 1.02 x 10^{-6} sec^{-1}

APPENDIX B. CREEP AND CREEP RATE CURVES FOR Al-1.0%Li

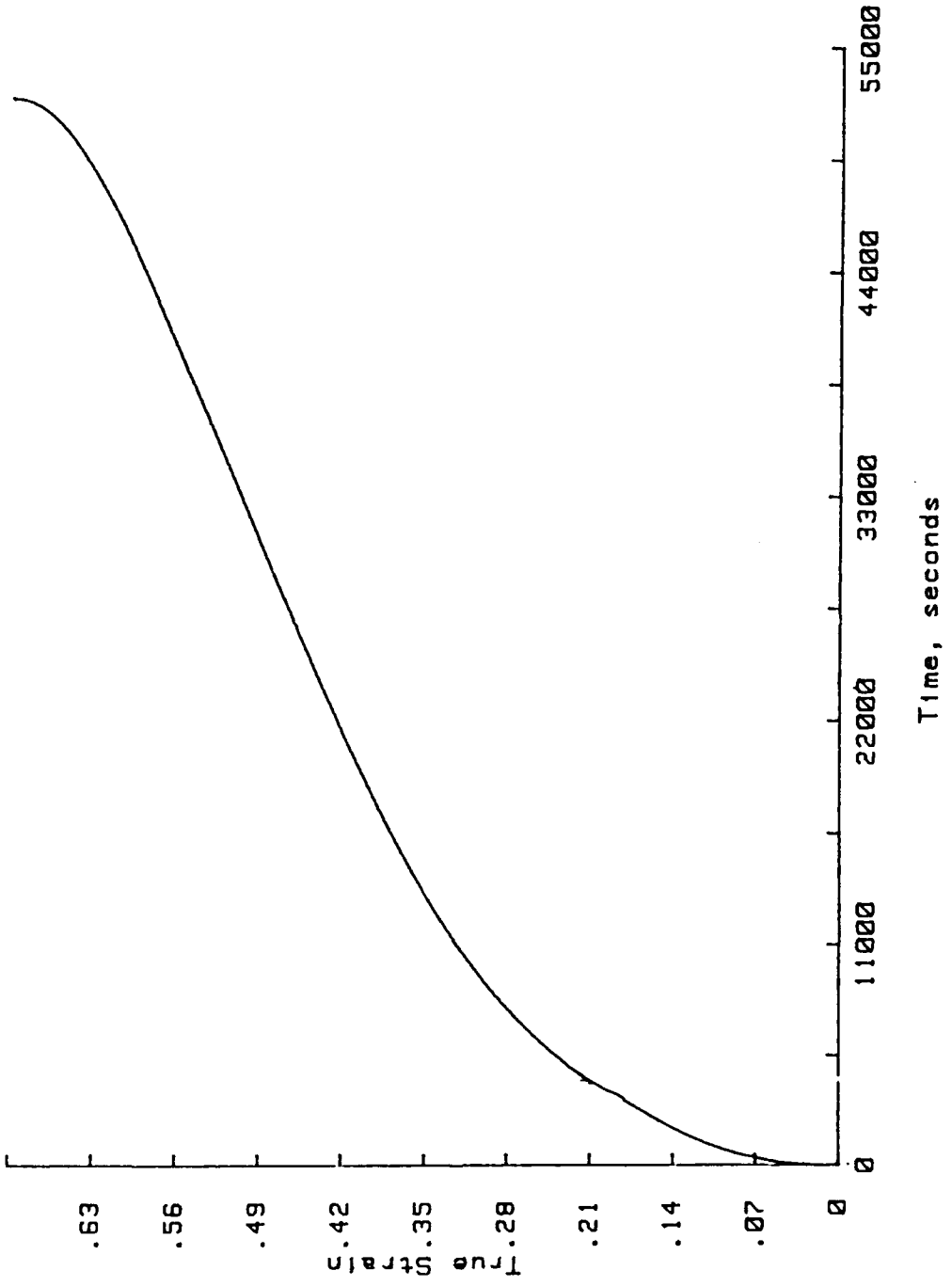

Figure 40. Creep Curve at 300°C for a stress of 10.97 MPa: $\dot{\epsilon}_{min} = 8.36 \times 10^{-6}$ sec^{-1}

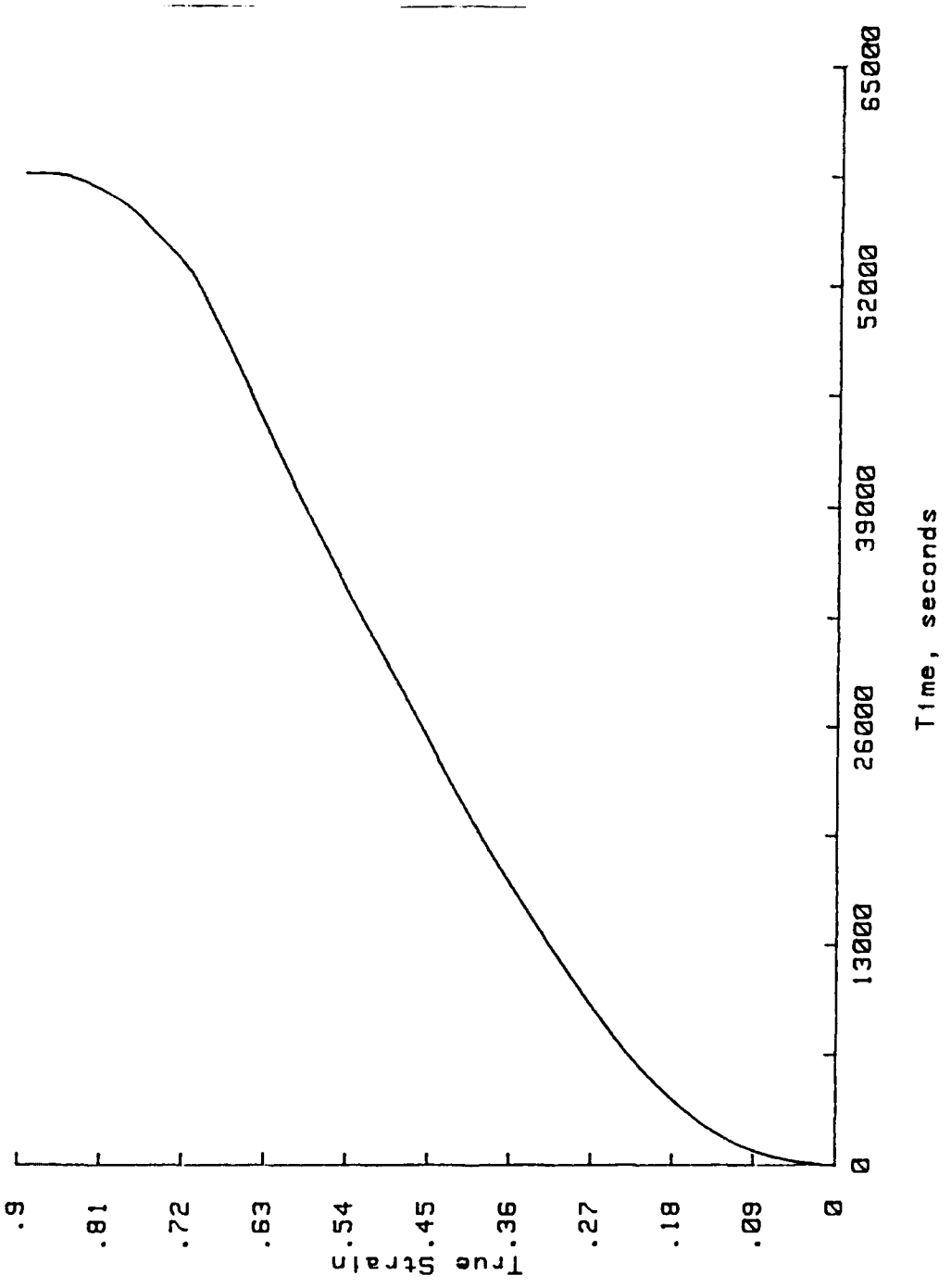

Figure 41. Creep Curve at 350°C for a stress of 7.59 MPa: $\dot{\epsilon}_{min}$ = 1.32 x 10^{-5} sec^{-1}

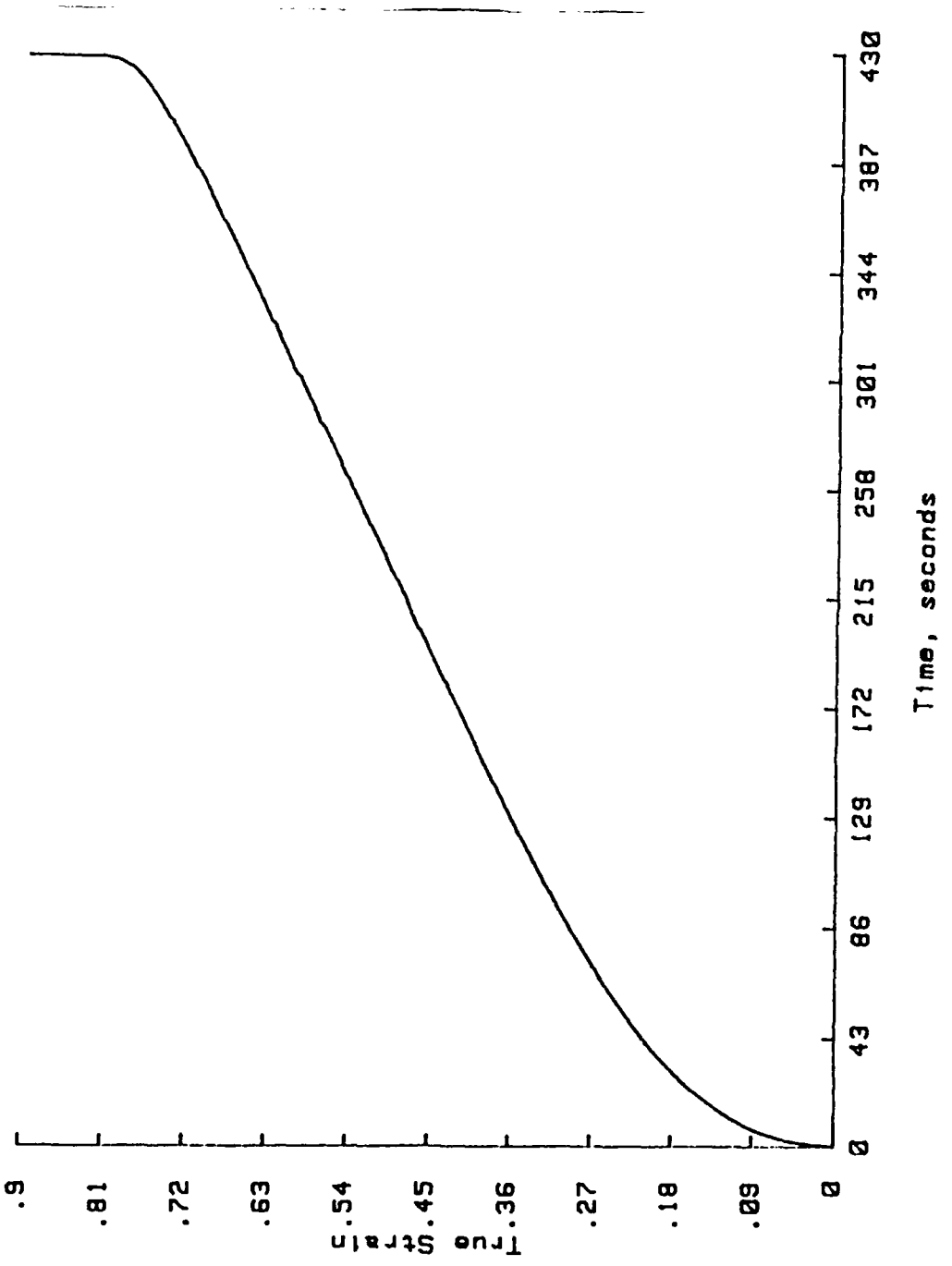

Figure 42. Creep Curve at 350°C for a stress of 15.85 MPa: $\dot{\epsilon}_{min} = 1.35 \times 10^{-3}$ sec^{-1}

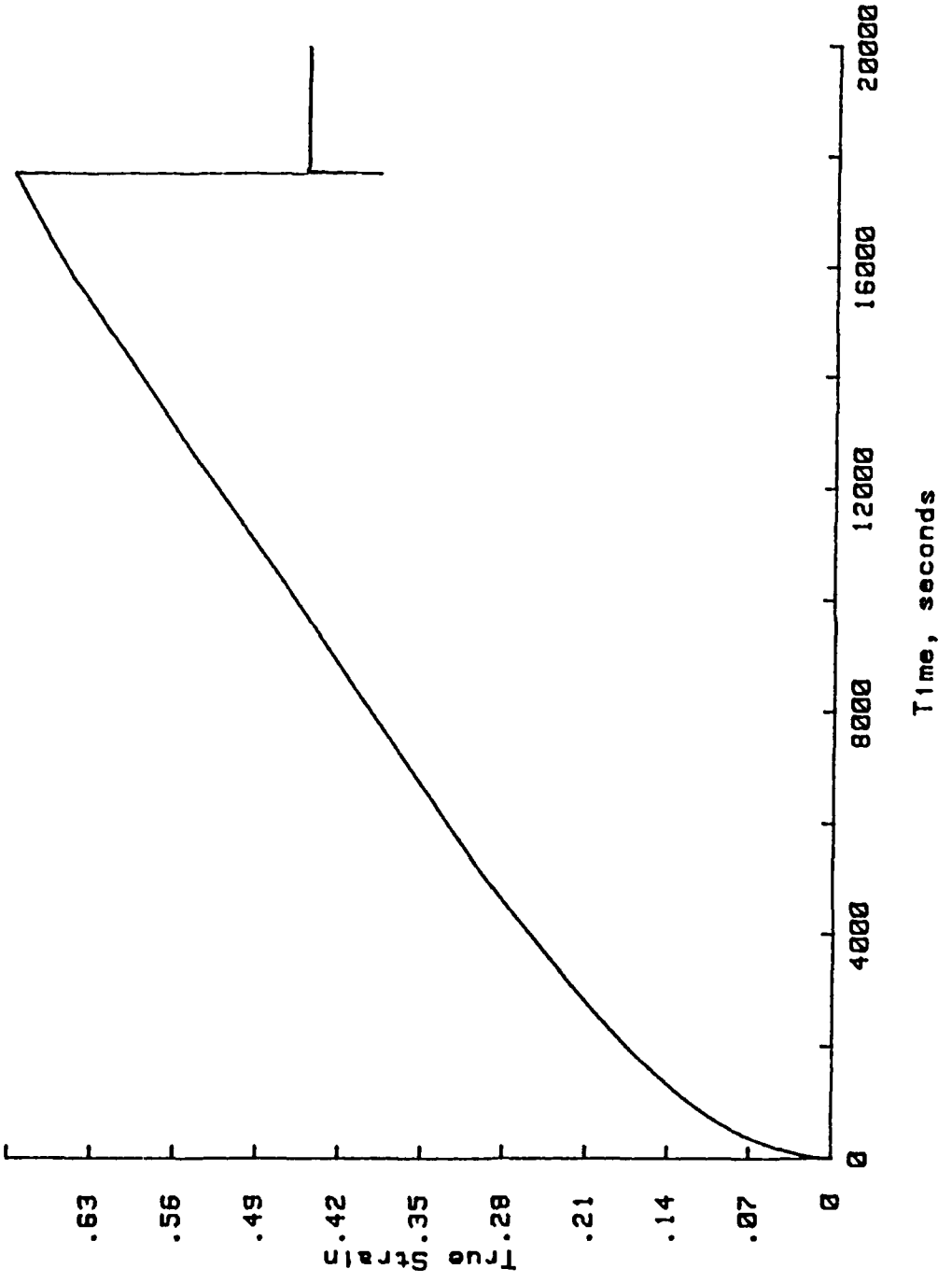

Figure 43. Creep Curve at 400°C for a stress of 5.32 MPa: $\dot{\epsilon}_{min} = 3.61 \times 10^{-6}$ sec^{-1}

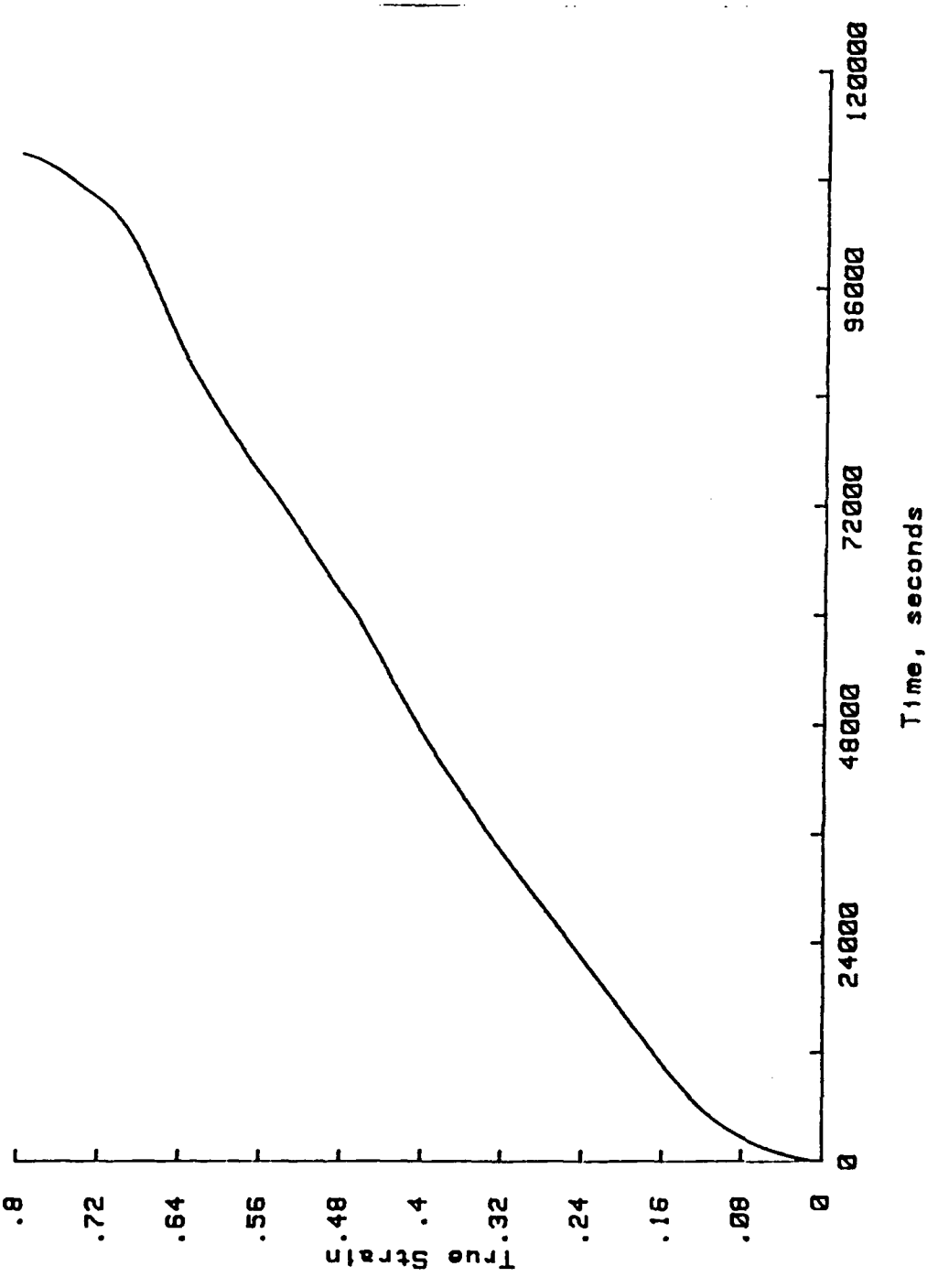

Figure 44. Creep Curve at 400°C for a stress of 3.68 MPa: $\dot{\epsilon}_{min}$ = 5.23 x 10^{-6} sec^{-1}

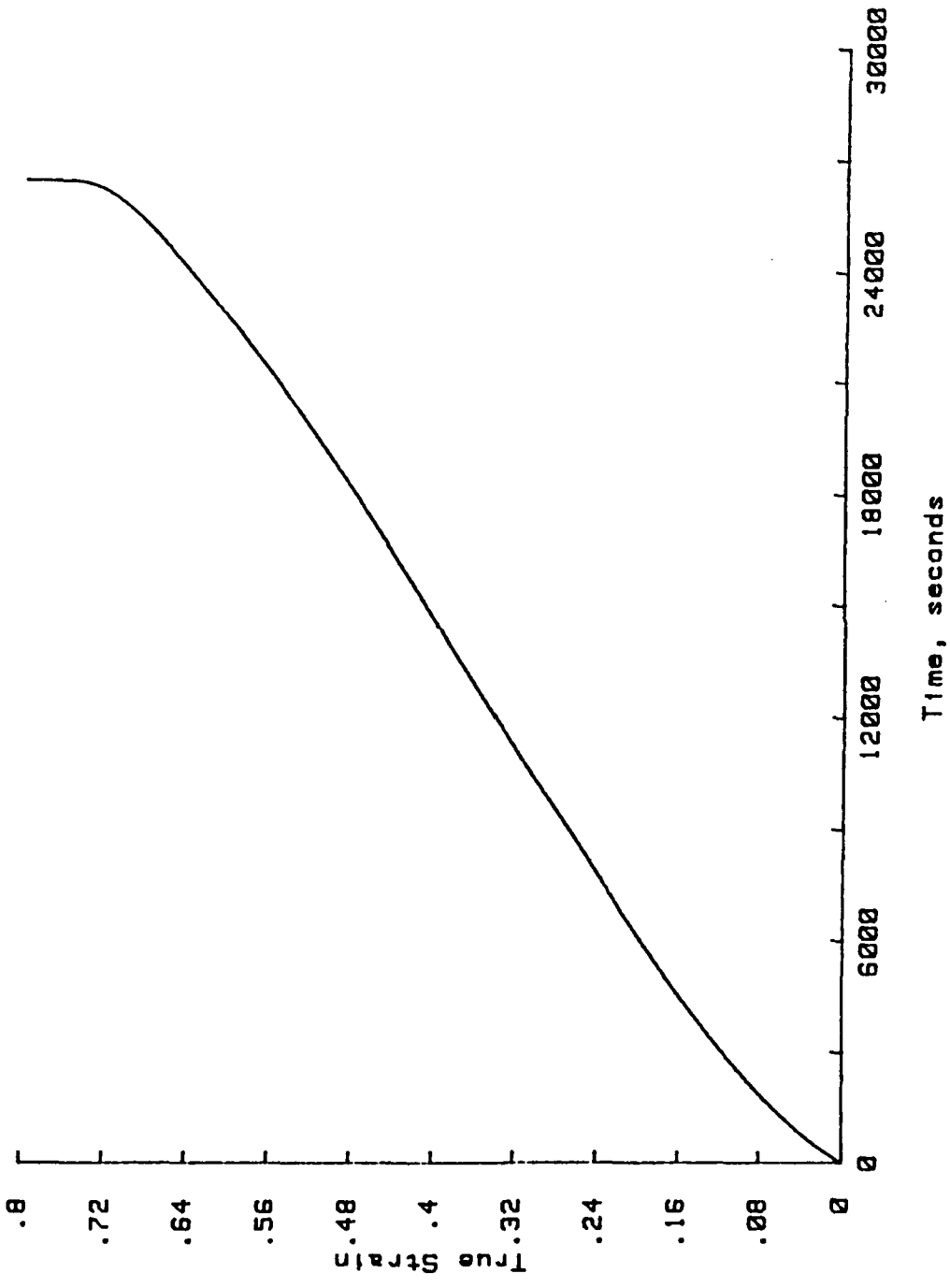

Figure 45. Creep Curve at 450°C for a stress of 2.65 MPa: $\dot{\epsilon}_{min} = 2.29 \times 10^{-5}$ sec^{-1}

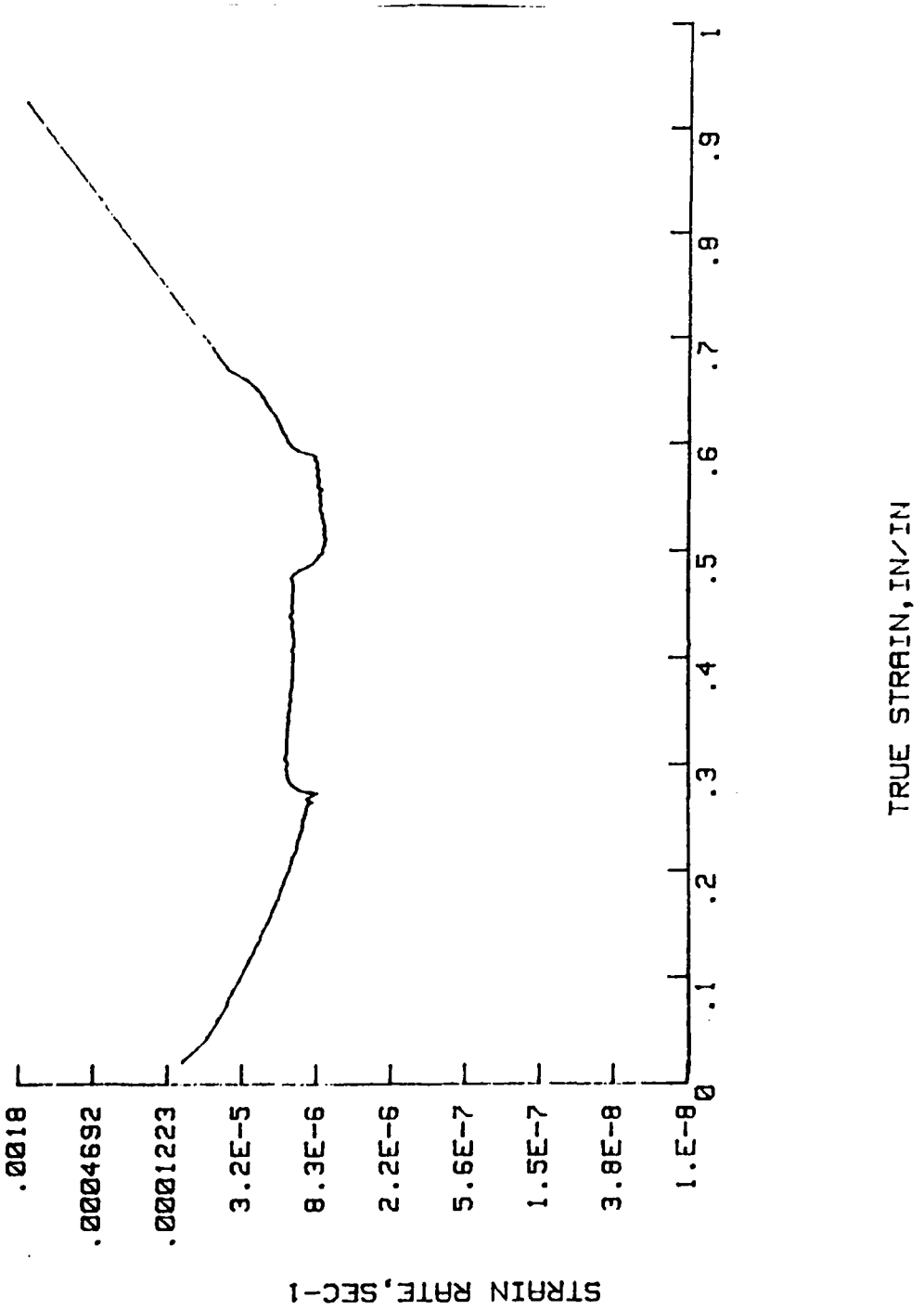

Figure 46. Creep Rate Curve at 300-310°C for a stress of 9.05 MPa: $\dot{\epsilon}_1$ = 1.32 x 10^{-5} sec^{-1} & $\dot{\epsilon}_2$ = 7.71 x 10^{-6} sec^{-1}

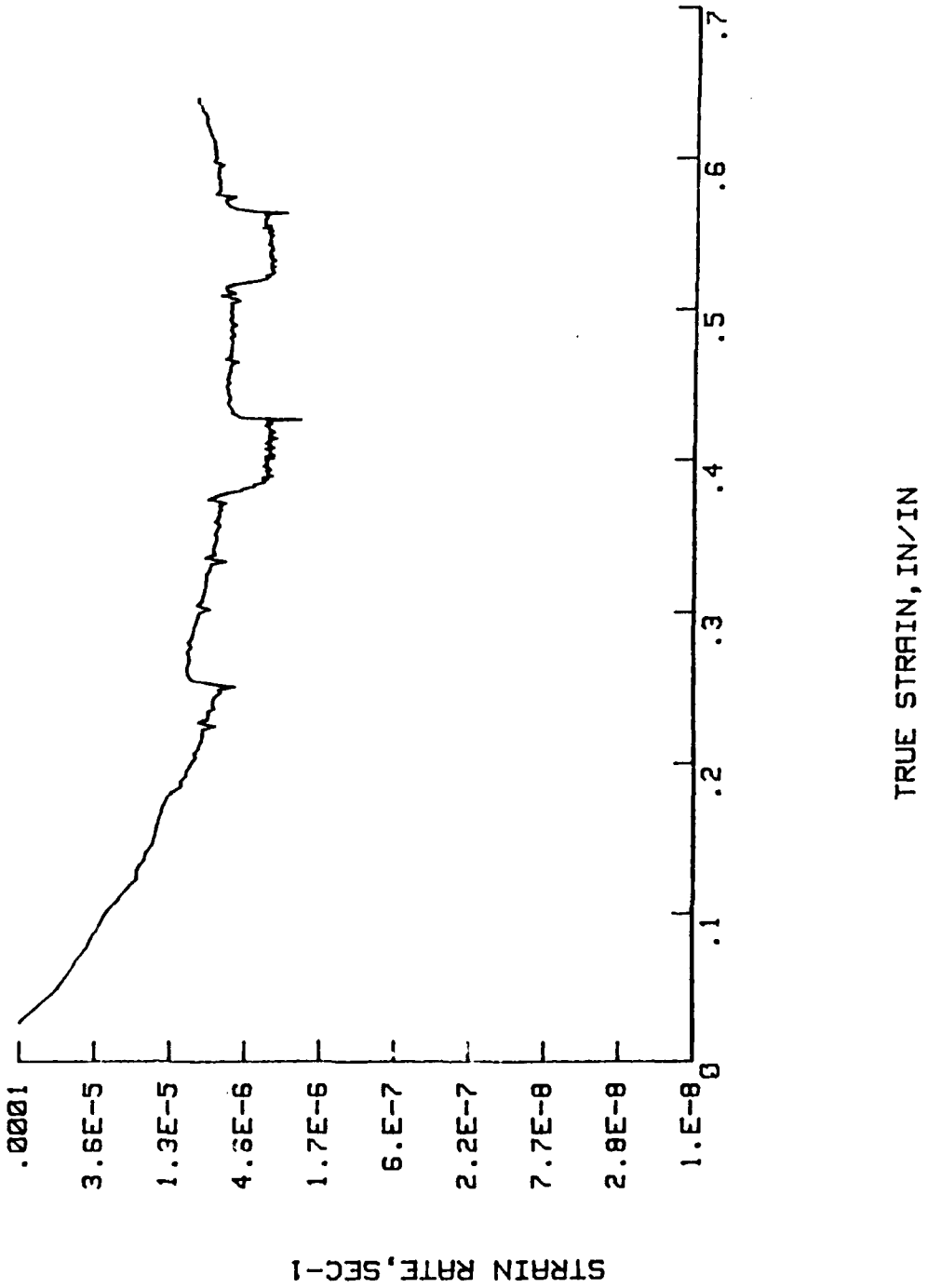

Figure 47. Creep Rate Curve at 300-310°C for a stress of 9.84 MPa: $\dot{\epsilon}_1$ = 6.47 x 10^{-6} sec^{-1} & $\dot{\epsilon}_2$ = 3.75 x 10^{-6} sec^{-1}

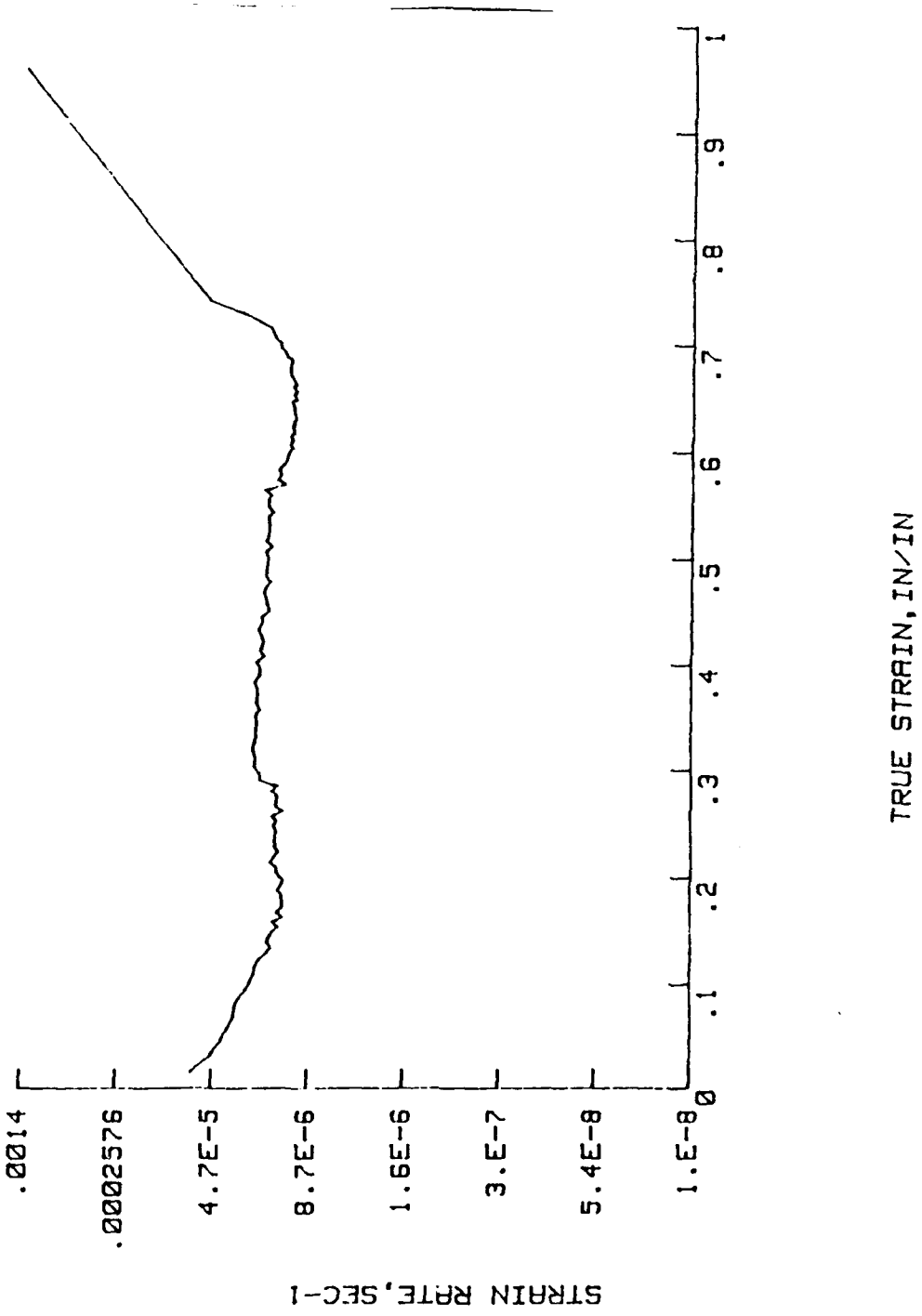

Figure 48. Creep Rate Curve at 350-360°C for a stress of 5.33 MPa: $\dot{\epsilon}_1$ = 1.81 x 10^{-5} sec^{-1} & $\dot{\epsilon}_2$ = 1.21 x 10^{-5} sec^{-1}

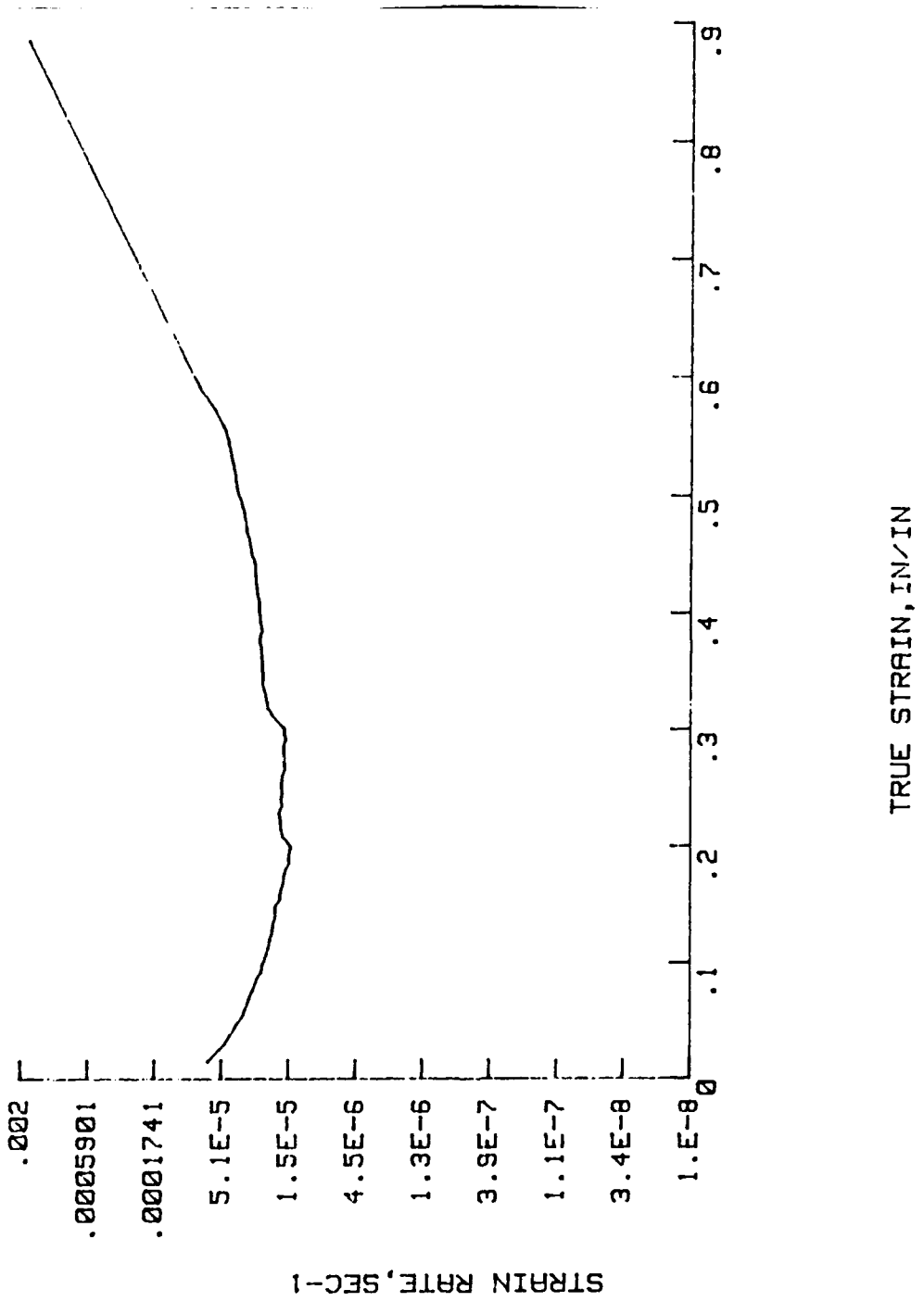

Figure 49. Creep Rate Curve at 400-410°C for a stress of 3.63 MPa: $\dot{\epsilon}_1$ = 2.49 x 10^{-3} sec^{-1} & $\dot{\epsilon}_2$ = 1.71 x 10^{-3} sec^{-1}

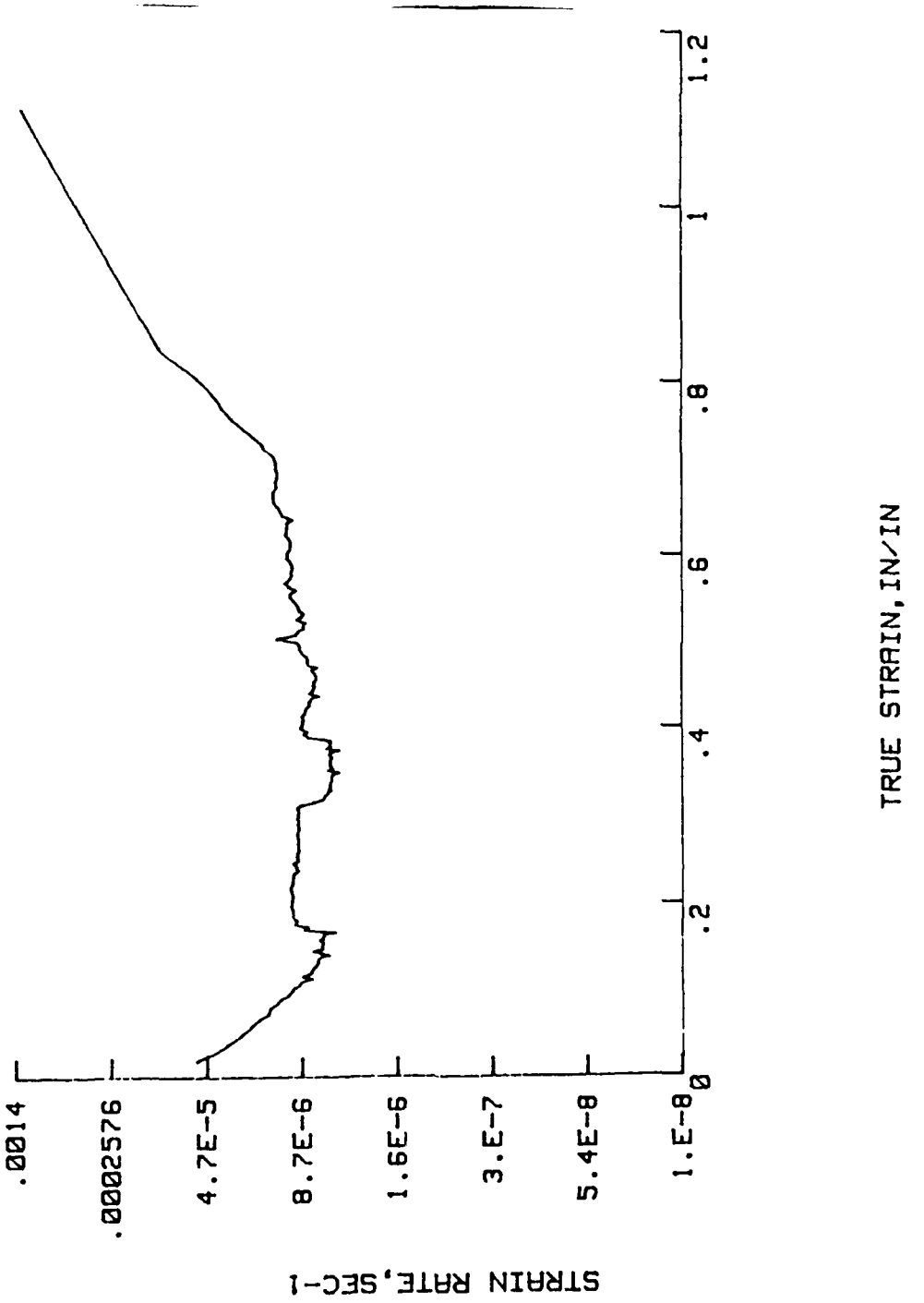

Figure 50. Creep Rate Curve at 400-410°C for a stress of 3.60 MPa: $\dot{\epsilon}_1 = 7.26 \times 10^{-6}$ sec^{-1} & $\dot{\epsilon}_2 = 5.04 \times 10^{-6}$ sec^{-1}

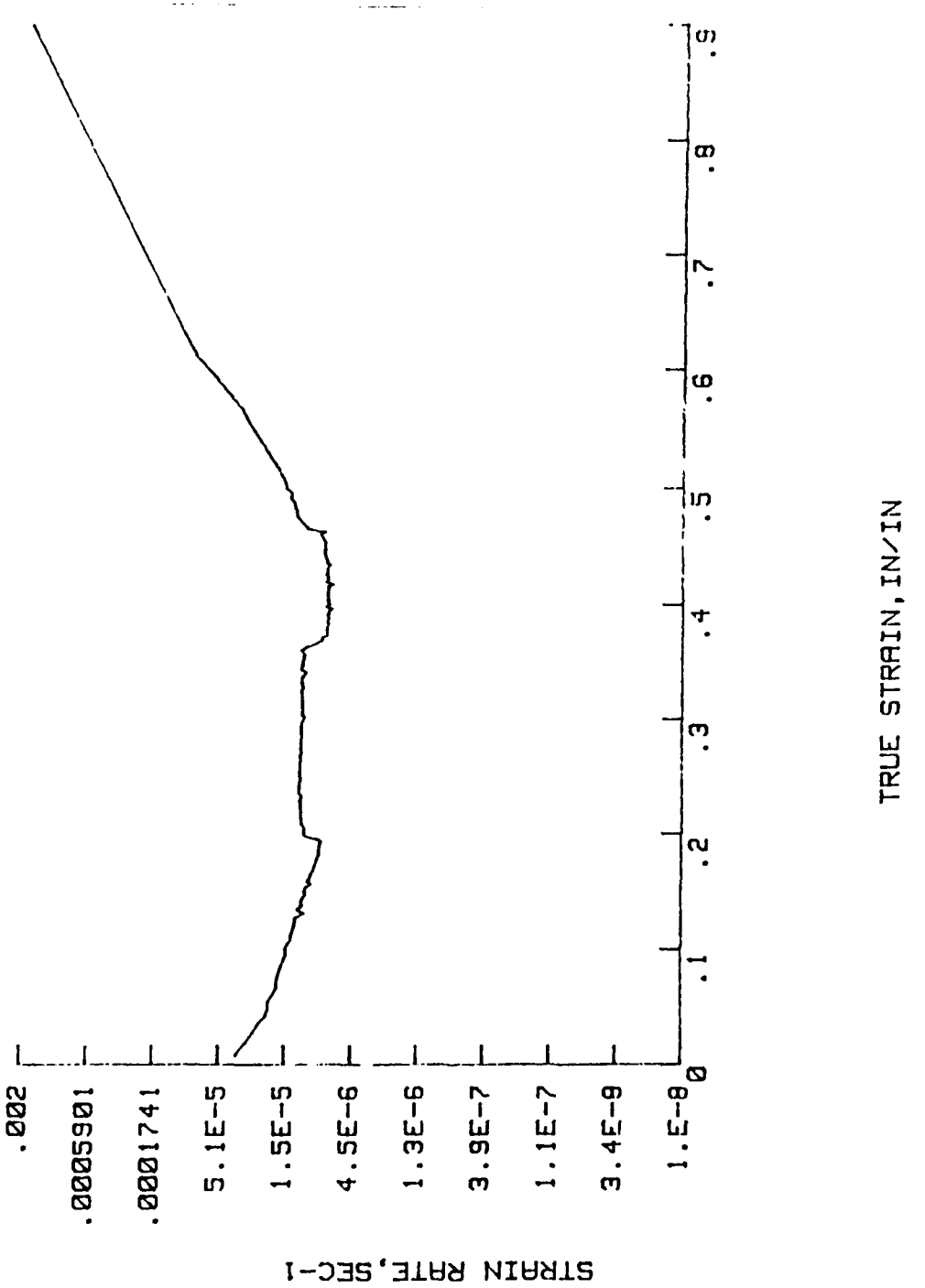

Figure 51. Creep Rate Curve at 400-410°C for a stress of 3.26 MPa: $\dot{\epsilon}_1$ = 1.24 x 10^{-5} sec^{-1} & $\dot{\epsilon}_2$ = 8.44 x 10^{-6} sec^{-1}

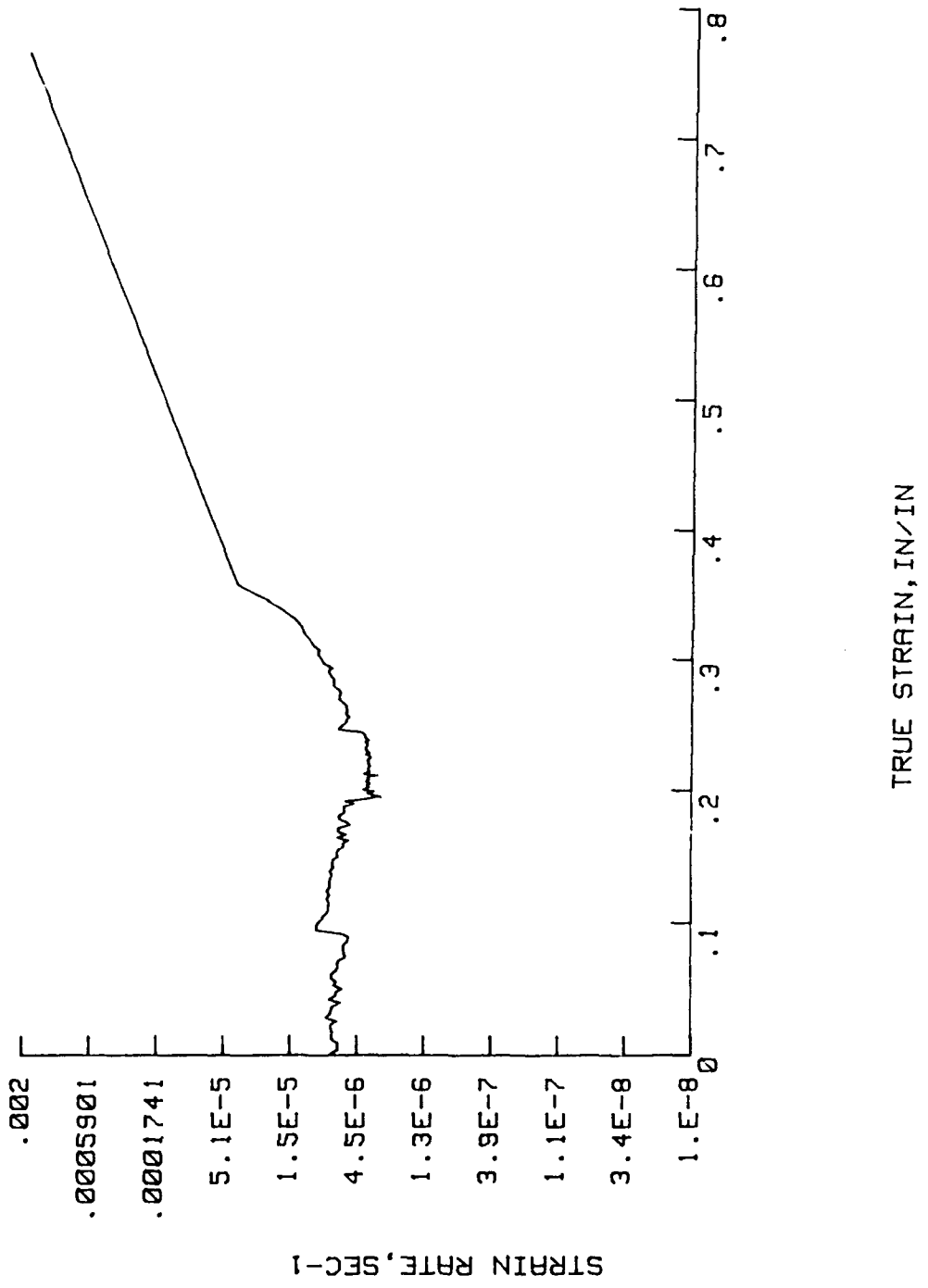

Figure 52. Creep Rate Curve at 450-460°C for a stress of 1.88 MPa: $\dot{\epsilon}_1$ = 5.37 x 10^{-6} sec^{-1} & $\dot{\epsilon}_2$ = 3.67 x 10^{-6} sec^{-1}

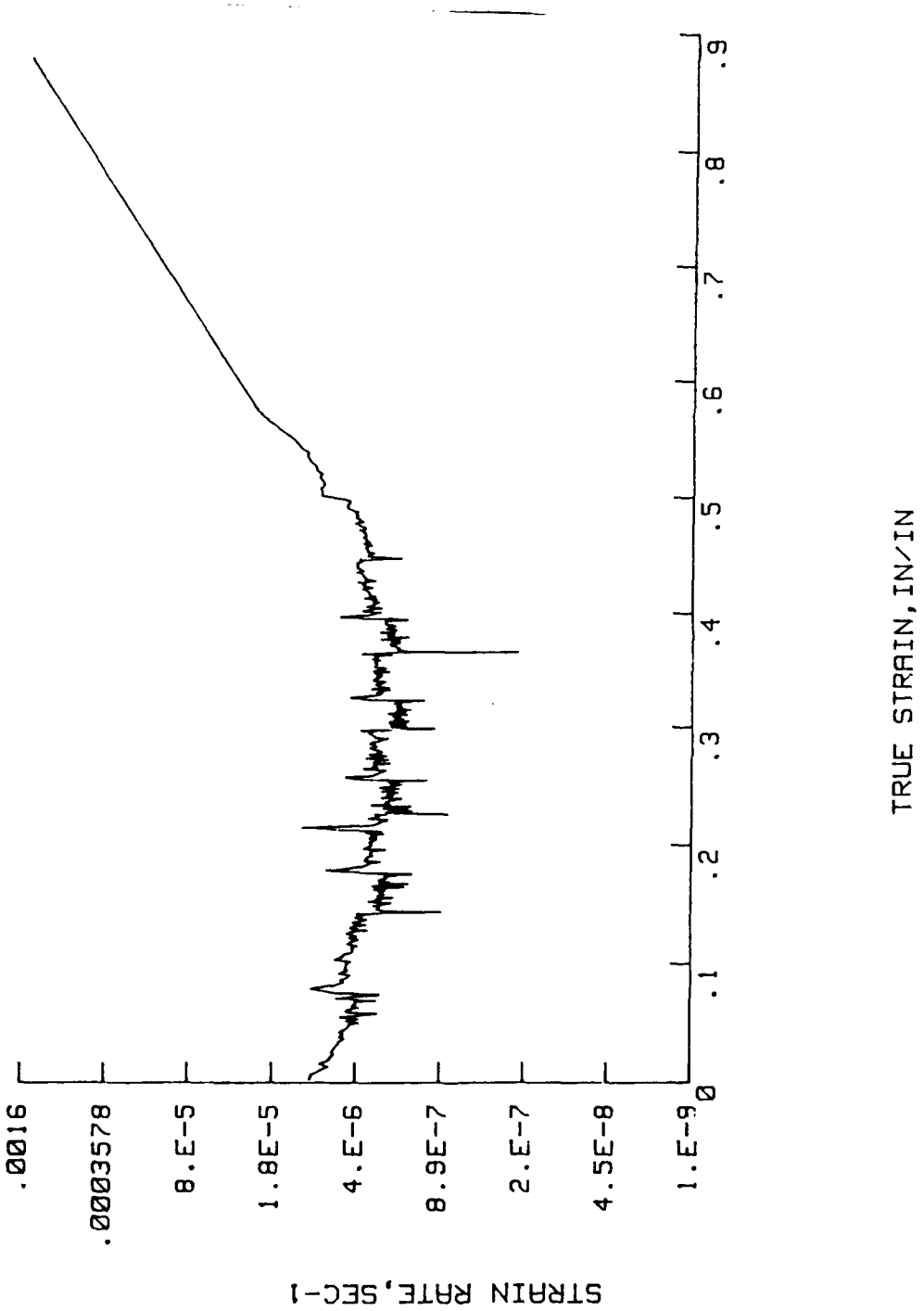

Figure 53. Creep Rate Curve at 450-460°C for a stress of 1.92 MPa: $\dot{\epsilon}_1$ = 2.79 x 10^{-6} sec^{-1} ? $\dot{\epsilon}_2$ = 2.00 x 10^{-6} sec^{-1}

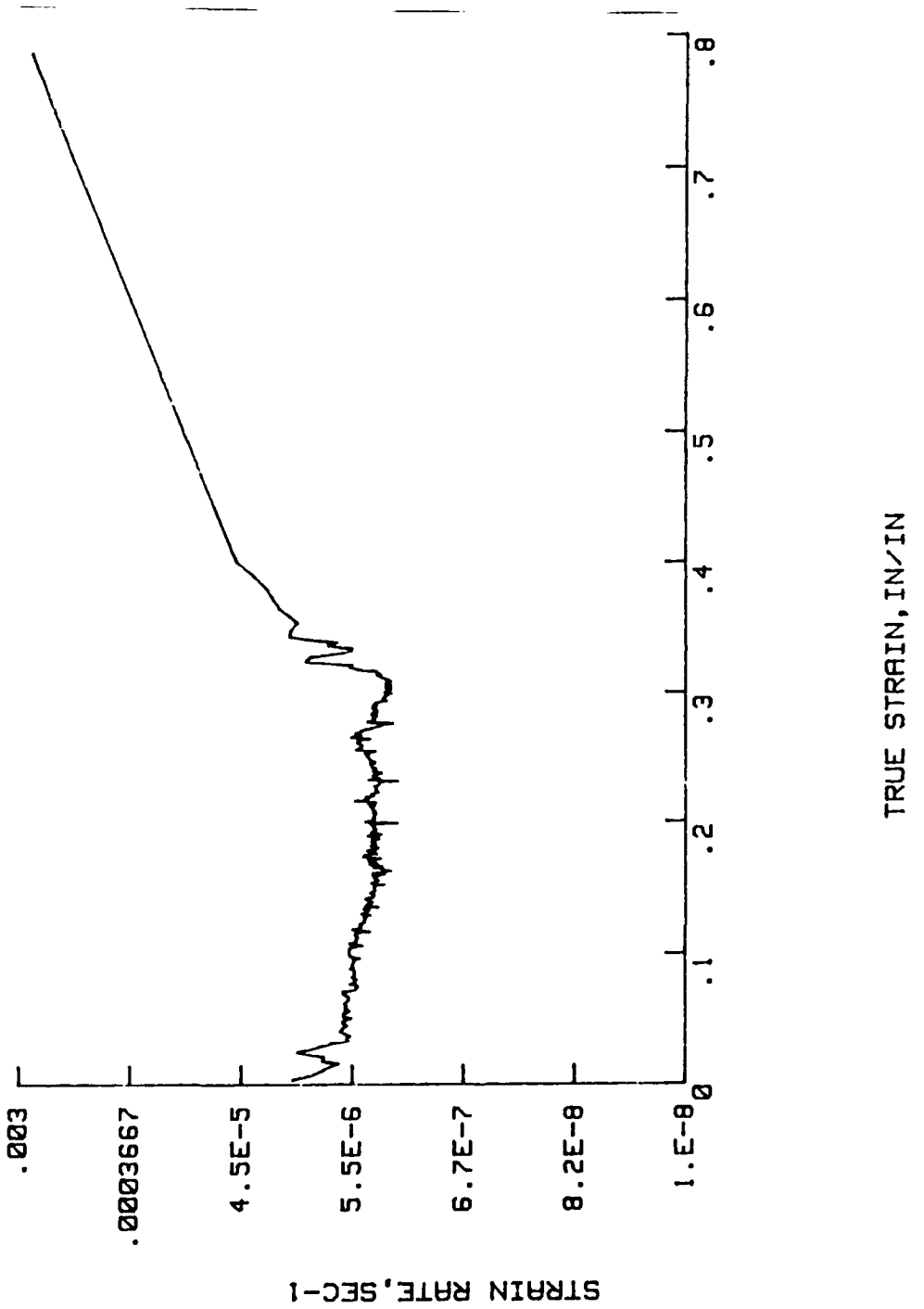

Figure 54. Creep Rate Curve at 500-510°C for a stress of 1.17 MPa: $\dot{\epsilon}_1$ = 4.55 x 10^{-6} sec^{-1} & $\dot{\epsilon}_2$ = 3.47 x 10^{-6} sec^{-1}

APPENDIX C. CREEP AND CREEP RATE CURVES FOR Al-2.0%Li

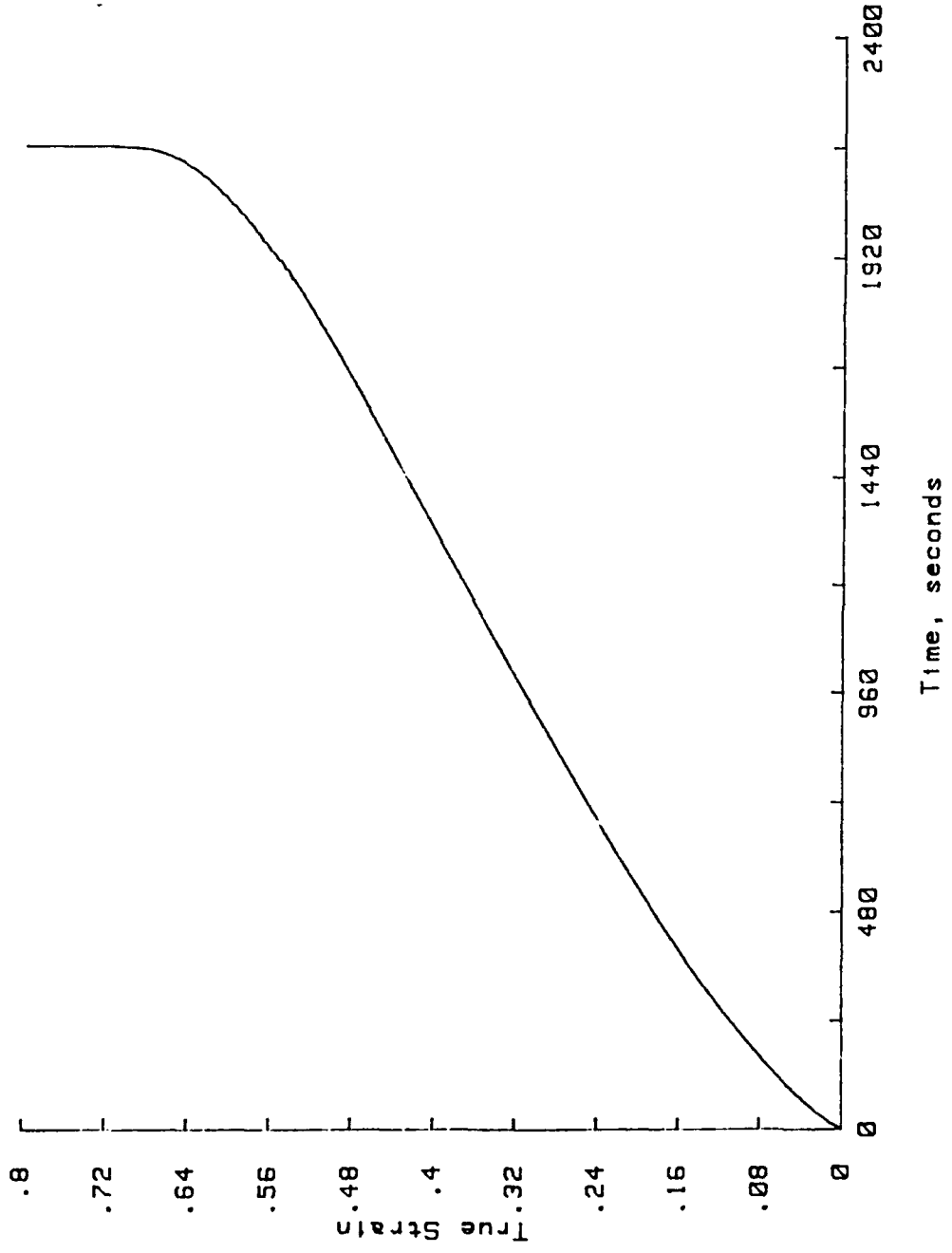

Figure 55. Creep Curve at 500°C for a stress of 3.03 MPa: $\dot{\epsilon}_{min} = 6.13 \times 10^{-4}$ sec^{-1}

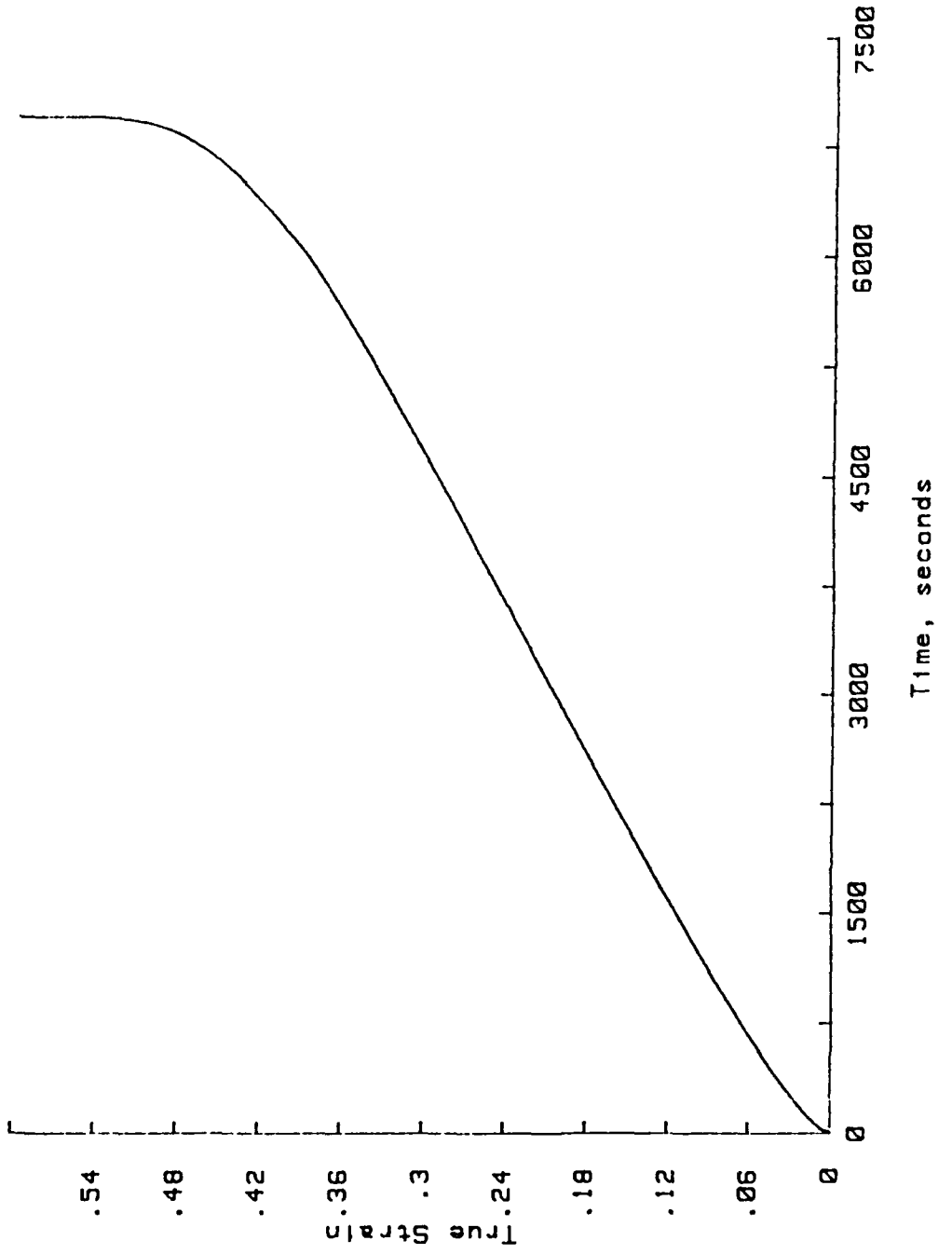

Figure 56. Creep Curve at 500°C for a stress of 2.34 MPa: $\dot{\epsilon}_{min}$ = 8.30 x 10^{-6} sec^{-1}

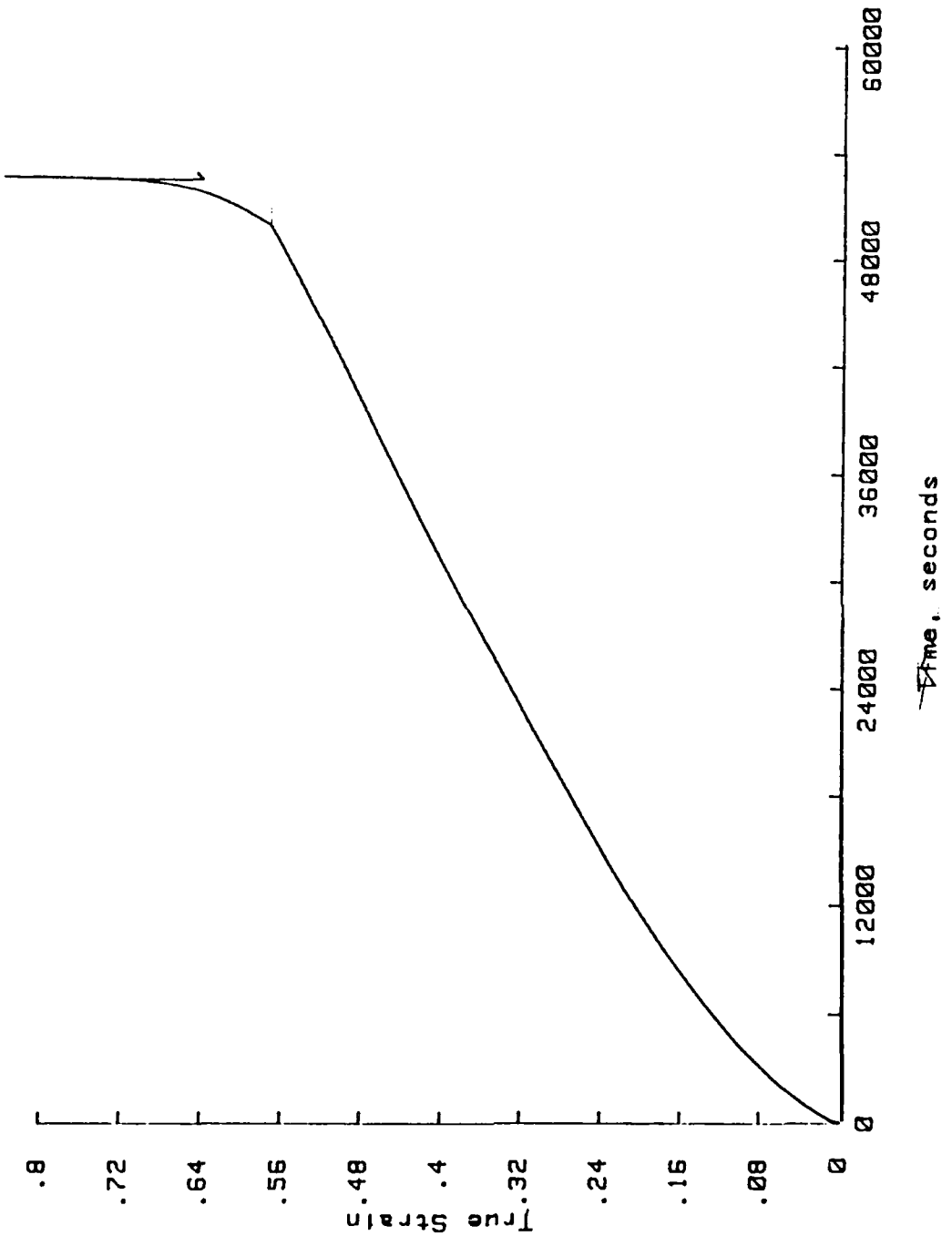

Figure 57. Creep Curve at 500°C for a stress of 1.74 MPa: $\dot{\epsilon}_{min}$ = 9.38 x 10^{-6} sec^{-1}

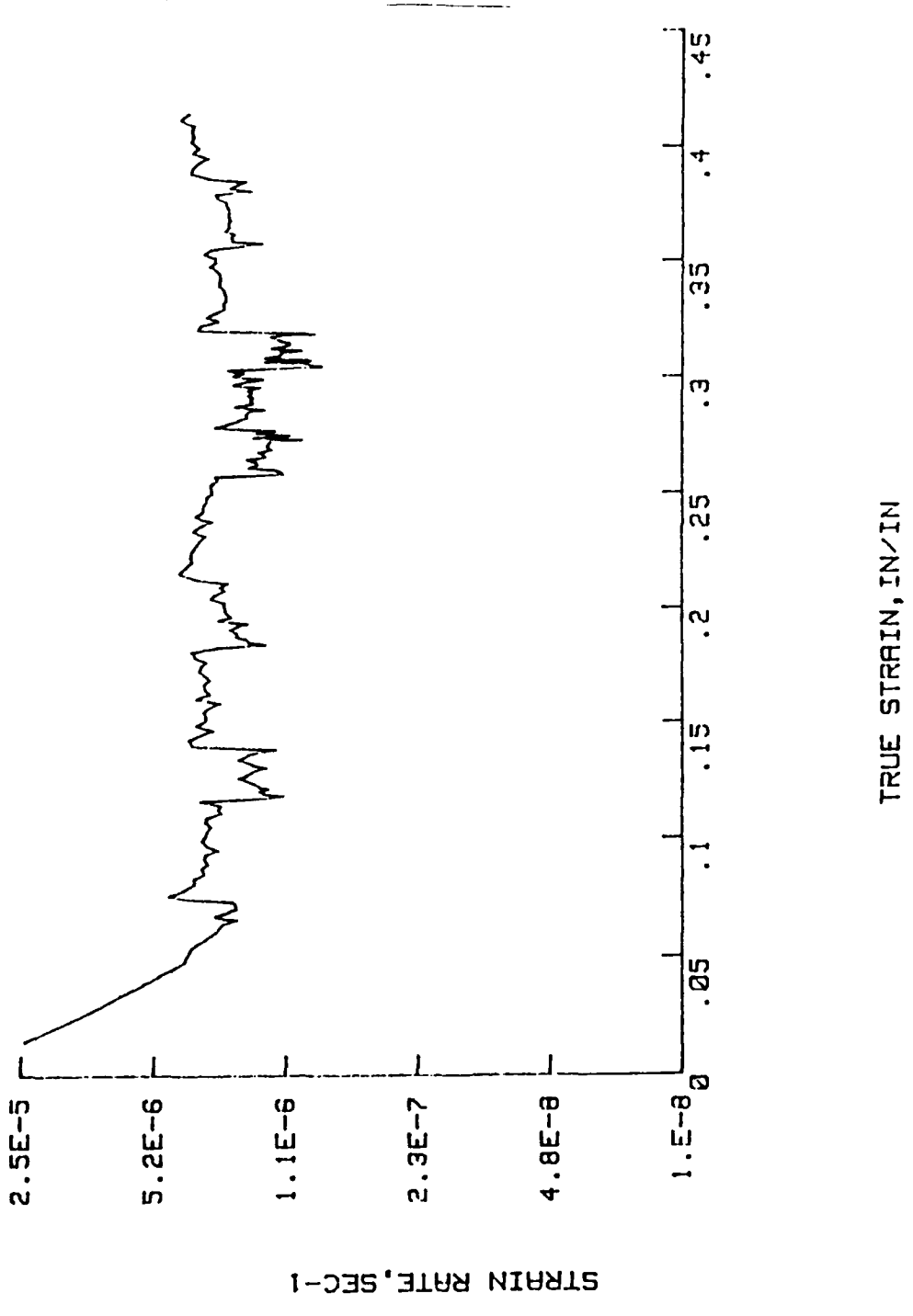

Figure 58. Creep Rate Curve at 500-510°C for a stress of 1.40 MPa: $\dot{\epsilon}_1$ = 9.14 x 10^{-7} sec^{-1} & $\dot{\epsilon}_2$ = 1.58 x 10^{-6} sec^{-1}

APPENDIX D. DATA FROM PREVIOUS WORK AT NPS

Table IV. SUMMARY OF STRESS EXPONENTS

Temp (°C)	Value of n		
	0.5%Li (1)	1.0%Li (1)	2.0%Li (2)
250	5.2	5.4	
300	7.1	6.1	6.7
350	5.2	4.9	6.0
400	4.4	5.6	5.0
450	4.5	4.3	4.8
500	4.3	4.3	4.9

(1). Data from work by Taylor [Ref. 8]
(2). Data from work by Goodson [Ref. 10]

Table V. SUMMARY OF ACTIVATION ENERGY AT CONSTANT STRESS [Ref. 8]

Temperature Interval(°C)	Log of Applied Stress	Activation Energy (Kcal/mole)	Lithium Concentration
250-300	1.4	30.6	5%
300-350	1.3	26.0	
	1.0	36.4	
	0.7	46.2	
350-400	1.0	38.3	
	0.6	45.9	
400-450	.06	48.8	
450-500	.06	50.7	
250-300	1.7	31.6	1.0%
	1.3	45.6	
300-350	1.46	40.4	
	0.84	39.7	
350-400	1.3	41.0	
	0.7	44.8	
400-450	1.0	38.1	
	0.6	53.8	
450-500	0.8	31.3	

Table VI. SUMMARY OF AL-2.0%LI ACTIVATION ENERGY RESULTS IN KCAL/MOLE [Ref. 10]

Temp(°C)	Mean Temp(°C)	Creep Curves	Creep Rate	Log-Log Curve
300-310	304.92	47.4	45.9	42.5
350-360	354.93	52.3	50.9	55.9
400-410	404.94	57.5	55.6	49.0
400-410	404.94	55.3	62.7	49.0
450-460	454.95	54.9	54.6	54.4
470-480	474.95	40.4	*	--
500-510	504.95	33.1	*	--

* Note: these values not obtained due to limits in the data acquisition system.

Table VII. SUMMARY OF AL-2.0%LI TEMPERATURE CYCLING RESULTS [Ref. 10]

Temp(°C)	Mean Temp(°C)	$\dot{\epsilon}_l$(sec^{-1})	$\dot{\epsilon}_h$(sec^{-1})	Q_c (kcal/mole)
300-310	305	2.10×10^{-6}	4.30×10^{-6}	47.4
350-360	355	1.28×10^{-6}	6.55×10^{-7}	52.3
400-410	405	1.18×10^{-6}	2.22×10^{-6}	57.5
400-410	405	3.98×10^{-7}	7.31×10^{-7}	55.3
450-460	455	5.51×10^{-6}	8.69×10^{-6}	54.9
470-480	475	1.75×10^{-6}	2.52×10^{-6}	40.4
500-510	505	1.51×10^{-6}	1.99×10^{-6}	33.1

LIST OF REFERENCES

1. Ashby, M. F., "Overview NO.80: On tne Engineering Properties of Materials," Acta Metallurgica, v. 37, pp. 1273-1293, May 1989.

2. Divecha, A. P., and Karmarker, S. D., "The Search for Al-Li Alloys," Advanced Materials and Processes, v.130, pp. 74-79, 1986.

3. McAlister, A. J., "Al-Li Phase Diagram," Binary Alloy Phase Diagrams, ed. Massalski, T. B., p.128, American Society for Metals, 1986.

4. Fox, A. G., and Fisher, R. M., "Structure and Debye Temperatures of Al-Li Solid Solution Alloys," Acta Crystallographa, v. A43, pp. 260-265, 1987.

5. Racmilovic, V., Fox, A. G., and Thomas, G., "Spinodal Decomposition of Al-Rich Al-Li Alloys," Acta Metallurgica, v. 34, pp. 2385-2394, 1989.

6. Sherby, O. D., and Burke, P. M., "Mechanical Behavior of Polycrystalline Solids at Elevated Temperature," Progress in Materials Science, pp. 325-386, 1967.

7. Myers, M. A. and Chawla, K. K., Mechanical Metallurgy Principles and Applications, pp. 659-687, Prentice Hall Inc., 1984.

8. Taylor, D. W., The Lithium Concentration Dependence of Creep in Binary Aluminum-Lithium Alloys, Master's Thesis, Naval Postgraduate School, Monterey, California, June 1989.

9. Ellison, K., The Elevated Temperature Creep Behavior of a Binary Al-Li Alloy Containing 2.0 Weight Percent Lithium, Master's Thesis, Colorado School of Mines, Golden, Colorado, May 1989.

10. Goodson, E., The Stress and Temperature Dependence of Creep in an Al-2.0wt%Li Alloy, Master's Thesis, Naval Postgraduate School, Monterey, California, December 1989.

11. Matlock, D. K., A Study of the Effects of Sample Size and Irradiation on the High Temperature Creep of Nickel-6 W/O Tungsten, Ph.D. Dissertation, Stanford University, Palo Alto, California, 1972.

12. Garafalo, F. and Richmond, W. F., "Design of Apparatus for Constant-Stress or Constant Load Creep Tests," Journal of Basic Engineering, pp. 287-293, 1962.

13. Coughlan, W. A., "Constant Stress Continuous Load Compression Creep Machine for Small Single Crystals," The Review of Scientific Instruments, pp. 464-467, 1971.

14. Hertzberg, R. W., Deformation and Fracture Mechanics Of Engineering Materials, 2nd edition, pp. 145-159, John Wiley & Sons Inc., 1983.

15. Lytton, J. C., Shepard, L. A. and Dorn, J. E., "The Activation Energies for Creep of Single Aluminum Crystals Favorably Oriented for (111)[101] Slip," Transactions of the American Institute of Mining, Metallurgical, and Petroleum Engineers, v. 212, pp. 220-225, 1958.